Universidad de Santiago de Compostela
Facultad de Medicina
Departamento de Medicina

"Structural studies of PrP^{Sc}"

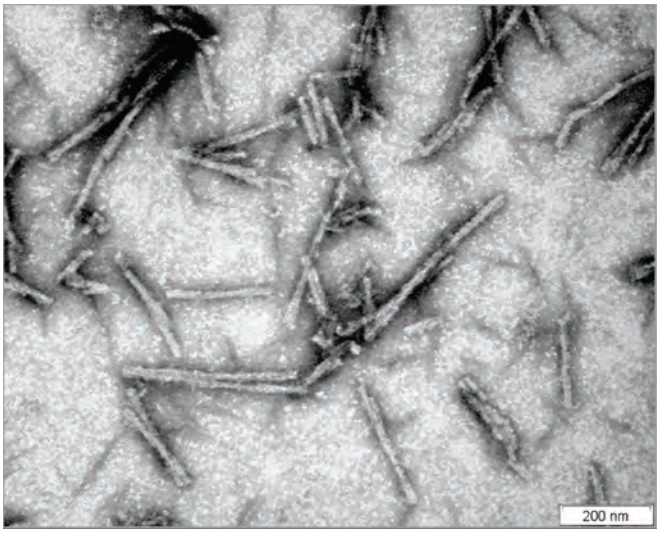

Tesis Doctoral / Doctoral Thesis
Director: Dr. Jesús Rodríguez Requena

Ester Vázquez Fernández
Santiago de Compostela, 2012

Este trabajo ha sido financiado a través de la subvención europea FP7 222887 “Priority”

Autora: Ester Vázquez Fernández
Director: Jesús R. Requena
Año: 2012

Facultad de Medicina
Departamento de Medicina

El Dr. JESÚS RODRÍGUEZ REQUENA, profesor contratado del Departamento de Medicina, de la Universidad de Santiago de Compostela,

INFORMA

Que la presente memoria titulada *"Structural studies of PrP^{Sc}"*, presentada por Dña. ESTER VÁZQUEZ FERNÁNDEZ, para optar al grado de doctor por la Universidad de Santiago de Compostela, ha sido realizada bajo su dirección en el Departamento de Medicina de la Facultad de Medicina de la Universidad de Santiago de Compostela y reúne los requisitos exigidos por la normativa vigente para ser valorada por el tribunal correspondiente,

Y para que así conste a los efectos oportunos, se firma el presente informe.

En Santiago de Compostela, a 4 de Septiembre de 2012.

Fdo.: Dr. Jesús Rodríguez Requena

Agradecimientos

"La gratitud no es solo la más grande de las virtudes, sino la madre de todas las demás"
Cicerón

Cuando un sueño se hace realidad, no siempre hay que atribuirle el mérito al empeño que uno pone en realizarlo. Detrás de cada sueño siempre hay personas que nos apoyan y que creen en nosotros. Son seres que han aparecido en nuestro camino, que nos animan a seguir adelante en nuestros proyectos, brindándonos de diferentes maneras, su solidaridad y conocimientos.

A todos vosotros gracias por enseñarme, entenderme, motivarme, hacerme reír, escuchar mis frustraciones y alegrías, no dejar que me rindiera, por vuestros consejos … En definitiva, gracias por hacerme feliz durante esta etapa de mi vida y porque sin vosotros esta tesis no hubiera visto la luz.

Estoy en deuda con vosotros y espero que sintáis parte de esta tesis como vuestra.

Aut inveniam viam aut faciam
"Encontraré un camino, o yo misma lo crearé"

Structural studies of PrP^{Sc}

Resumen en castellano

Resumo en galego

Summary in English

RESUMEN
Estudios estructurales de la PrP^{Sc}

Los priones son agentes responsables de un conjunto diverso de enfermedades neurodegenerativas transmisibles en humanos y animales, que se caracterizan por una acumulación anormal de la proteína priónica (PrP), principalmente en el cerebro. Las lesiones neuropatológicas que se pueden encontrar son atrofia generalizada, pérdida neuronal, vacuolación, cambios espongiformes, gliosis astrocitica y placas amiloides de PrP. Además dichas enfermedades tienen un amplio espectro de manifestaciones clínicas, caracterizadas por demencia, ataxia, insomnio, paraplejía, parestesia y comportamiento anormal.

La replicación de los priones se produce mediante la conversión de la PrP^{C}, que es la proteína normal no infecciosa, en PrP^{Sc}. Durante el proceso ocurre un cambio conformacional a través de una modificación post-traduccional, sin embargo, dicho proceso todavía no está completamente entendido.

La cadena polipeptídica de la PrP^{C} y la PrP^{Sc} son idénticas. En ratón, la PrP contiene 209 amino ácidos (numerado como 23-231, después de la escisión del péptidos señal de 22 amino ácidos) y tiene cuatro modificaciones post-traduccionales covalentes: dos aparaginas con glicanos unidos, en los residuos N_{180} y N_{196}; un puente disulfuro entre los residuos C_{178}-C_{213}; y un glicosilfosfatidilinositol (GPI) de anclaje a la membrana, en la región C-terminal de la proteína (residuo S_{231}). La PrP^{C} es un monómero, mientras la PrP^{Sc} es un multímetro heterogéneo. No se han demostrado diferencias covalentes entre ellas, la única diferencia entre la PrP^{C} y la PrP^{Sc} es conformacional, son isoformas.

La estructura de la PrP^{C} ha sido resuelta mediante resonancia magnética nuclear (RMN) y cristalografía de rayos X, en grandes rasgos contiene tres hélices-α y dos tramos de hojas-β antiparalelas. En contraste, la estructura de la PrP^{Sc} todavía no está resuelta, debido a que la insolubilidad de la PrP^{Sc} y la incapacidad de cristalizar de los multímetros heterogéneos de PrP^{Sc} impiden la aplicación de las mencionadas técnicas analíticas de alta resolución. Sin embargo, una variedad de técnicas instrumentales de baja resolución han proporcionado alguna información sobre la estructura de la PrP^{Sc}. A diferencia de la PrP^{C}, la PrP^{Sc} es parcialmente resistente a la digestión con la enzima proteinasa K (PK). Estudios de espectroscopía infrarroja de transformada de Fourier (FTIR) han mostrado que la estructura secundaria de la PrP^{C} se compone, en gran parte, de regiones no estructuradas y hélices-α, mientras que la PrP^{Sc} está compuesta, en gran medida, por hojas-β con alguna, si hay, hélice-α. La estructura de la PrP^{Sc} también ha sido estudiada usando microscopía electrónica basada en el análisis de cristales bidimensionales del núcleo resistente a PK de la PrP^{Sc} de hámster sirio (PrP27-30) y por espectrometría de masas (MS) acoplada al análisis de intercambio hidrogeno/deuterio. Durante estos últimos años, varios modelos teóricos para la estructura de la PrP^{Sc} han sido propuestos, pero hay insuficientes datos experimentales para alcanzar un consenso definitivo.

La elucidación de la estructura de la PrP^{Sc} sigue siendo uno de los mayores retos en la investigación sobre priones. Las bases moleculares de la biología de la proteína priónica (PrP), tal

como el mecanismo molecular de replicación y agregación, la barrera de especie y la patogénesis de la neurodegeneración, no serán entendidos hasta que la estructura este resuelta.

La proteolisis limitada es una técnica muy útil para elucidar características estructurales de la PrP^{Sc}. Parámetros conformacionales como la exposición de los amino ácidos a la superficie, flexibilidad e interacciones locales correlacionan muy bien con la proteolisis limitada. Los enlaces peptídicos localizados dentro de hojas-β son resistentes a la digestión proteolítica, mientras que los enlaces peptídicos localizados dentro de lazos, y mas raramente, en hélices-α, pueden ser cortados. Por lo tanto esta técnica proporciona información exhaustiva del enlace peptídico con respecto al plegamiento de la proteína, permitiendo localizar las áreas mas flexibles y las posibles hélices-α y hojas-β.

En la literatura hay numerosos estudios que utilizan la proteolisis limitada para averiguar información sobre la proteína priónica. El tratamiento con la enzima no específica PK muestra que la PrP^{C} es completamente sensible a proteolisis y la PrP^{Sc} es parcialmente resistente, produciendo un núcleo resistente a PK de diferente longitud. La longitud de este núcleo depende de la especie, en hámster Sirio, consiste de los residuos amino acídicos ~90-231. Esta región resistente, llamada PrPres o PrP27-30 debido a su peso molecular, continua siendo infecciosa y tiene las características básicas de un prión. Por lo tanto puede ser concluido que la PrP^{Sc} consiste de dos dominios: una área N-terminal lábil y desestructurada y una región globular estructurada resistente a proteasas. Otros estudios utilizando esta técnica han demostrado la existencia de una fracción de PrP^{Sc} sensible a la digestión con PK, llamada $sPrP^{Sc}$. Esta fracción también es infecciosa y comparte las características básicas estructurales con la PrPres. Otros experimentos basados en proteolisis limitada han visto que la resistencia a la digestión proteolitica es ligeramente diferente en las distintas cepas de la PrP^{Sc}. Por lo tanto, es compartida una arquitectura básica entre las diferentes cepas, con diferencias menores. Otros análisis de la PrP^{Sc} resistente a PK han informado de otros fragmentos más pequeños resistentes, detectados con anticuerpos que reconocen la región C-terminal de la proteína.

Además, en el estudio (Sajnani *et al*. (2008)) que precede a los experimentos realizados en esta tesis se demostró la utilidad de combinar proteolisis limitada y espectrometría de masas (MS) para obtener información estructural sobre dos cepas de PrP^{Sc} de hámster. En este estudio se llegó a la conclusión de que la mitad amino terminal de la PrP^{Sc} está caracterizada por una serie de tramos cortos resistente a PK, presumiblemente son hebras-β, intercaladas con tramos sensible a PK, probablemente formados por lazos y giros. Desafortunadamente, la información estructural se limitó a la región N-terminal de la proteína; ya que la presencia del glicosilfosfatidilinositol (GPI) de anclaje a la membrana y los heterogéneos azucares unidos a los amino ácidos asparagina, en la zona C-terminal de la molécula, impiden el análisis de espectrometría de masas (MS) en esta región.

Con la finalidad de vencer estas dificultades en el análisis de la proteína, se usó la PrP^{Sc} de ratones transgénicos que expresan la proteína priónica (PrP) sin el GPI de anclaje a la membrana. Estos animales, producen PrP^{Sc} que está desprovista del anclaje GPI y de los carbohidratos, por lo tanto, se elimina la heterogeneidad, permitiendo la detección y la localización de regiones

flexibles, susceptibles a la enzima proteinasa K (PK), mediante Western Plot y espectrometría de masas. Por primera vez, ha sido posible obtener un estudio de la estructura completa de la PrP^{Sc}, teniendo en cuenta su susceptibilidad a la proteolisis.

Los ratones transgénicos homocigotos para la PrP sin GPI fueron inoculados con RML, que es una cepa de ratón adaptada desde scrapie, los animales fueron sacrificados 365 días después de la inoculación. Como ha sido descrito en la literatura (Chesebro B *et al.* (2005)), los ratones infectados no mostraron signos de enfermedad, sus cerebros tenían características patológicas y había PrP resistente a la enzima PK. Además, diez ratones de tipo salvaje para la PrP fueron inoculados con homogenado de cerebro infectado de ratones con PrP sin GPI. Todos los animales desarrollaron la enfermedad a los 154±15 días después de la inoculación, demostrando la infectividad de la PrP^{Sc} sin GPI.

Las muestras de PrP^{Sc} sin GPI fueron digeridas con PK, sometidas a una electroforesis llamada Tricina-SDS-PAGE, especial para resolver proteínas de bajo peso molecular, y fueron hibridadas con un anticuerpo específico C-terminal (R1). Siete bandas fueron detectadas mediante Western blot, con pesos moleculares de aproximadamente 17, 14.6, 13, 12, 10.2, 8 y 6.7 kDa. A continuación, fueron llevados a cabo los estudios de espectrometría de masas. En primer lugar la muestra purificada de PrP^{Sc} sin GPI fue analizada por ESI-TOF, esta técnica proporciona una elevada exactitud de las masas, dos picos fueron identificados con masas moleculares exactas: 17148 Da y 16371 Da, que corresponden con los péptidos G_{81}-S_{232} y G_{89}-S_{232}, respectivamente. Sin embargo, después de varios intentos los péptidos más pequeños no se ionizaban bien bajo las condiciones del ESI-TOF. Por lo tanto, la proteína fue analizada mediante MALDI-TOF como método analítico alternativo. Dado que el rango de masas de los péptidos resistentes a PK es muy amplio, entre 17 y 6 kDa, se desarrolló un complejo método de calibración que cubre el rango entero, proporcionando una aceptable exactitud. Primero, la insulina (m/z= 5733), ribonucleasa A (m/z= 13682) y lisozima (m/z= 14395) fueron mezcladas con la muestra, como calibrantes internos, sin embargo, suprimen algunos de lo picos menos abundantes del espectro, por lo que con estos calibrantes se calibró un único pico con una masa de 9573 Da, con este pico no existen interferencias, y corresponde con el péptido M_{152}-S_{232}. A continuación, los picos de 9573, 16371 y 17148 fueron usados para calibrar el resto de los picos del espectro. Fueron detectados 13 péptidos diferentes, con un peso molecular exacto de: 17148, 16726, 16371, 13606, 13463, 12173, 12041, 11171, 9687, 9573, 8358, 7436 y 6274; lo que coincide bien con las bandas resistentes a PK, identificadas en el Western blot. Estos péptidos corresponden a moléculas cortadas en las posiciones 81, 85, 89, 116, 118, 133, 134, 141, 152, 153, 162, 169 o 179, respectivamente. Los resultados observados, coinciden con las áreas susceptibles identificadas en la PrP^{Sc} natural de hámster, en el estudio anterior (Sajnani *et al.* (2008)): 23-101, 117-119, 131-142, y la región alrededor del residuo 154 (los números corresponden con la secuencia de la PrP de hámster). Aunque en el presente estudio, tres puntos de corte adicionales fueron encontrados mas allá de la posición 154, en los residuos 162, 169 y 179.

Por lo tanto, el mapa de susceptibilidad a PK, de la PrP^{Sc} de ratón sin GPI, que engloba a las regiones 116-118, 133-134, 141, 152-153, 162, 169 y 179, sugiere que estas regiones corresponden a lazos y giros, mientras que los cortes en las posiciones 81, 85 y 89 señalan la

frontera entre los dominios C-terminal estructurado y el N-terminal desestructurado de la PrP^{Sc}. Dada la proporción de hoja-β, proporcionada por los estudios de FTIR, es lógico concluir que las zonas resistentes a la PK que están flanqueando estas regiones susceptibles, probablemente corresponden a hebras de hojas-β.

Además, es importante tener en cuenta que no se ha encontrado ningún péptido N-terminal, resistente a PK mas allá de la posición 179. Esto significa que la región C-terminal es completamente resistente a la proteinasa K, o por el contrario, que ninguna región PK resistente permanece después de la digestión con PK. Otro detalle a señalar, es que tampoco hay péptidos truncados en la región C-terminal. Esta evidente ausencia sugiere dos posibilidades. La PK, al igual que todas las proteasas, corta en regiones flexibles y accesibles, particularmente en áreas que no tienen abundantes puentes de hidrógeno, por ejemplo lazos. Por lo tanto, después de que la mella se ha producido en un región flexible, el lado N-terminal se hace inestable y como se desenrolla, es degradado por la PK; o mas probablemente, toda la región N-terminal, hasta la posición en la que comienza la resistencia, está en un momento dado en un estado parcialmente desplegado en una fracción de las subunidades de PrP^{Sc}. En consecuencia, los extremos N-terminales de los péptidos resistentes a PK probablemente indican el comienzo de los tramos rígidos, fuertemente empaquetados y con muchos puentes de hidrógeno (probablemente segmentos ricos en hojas-β), mientras el tramo de secuencia inmediatamente anterior a dichos extremos probablemente corresponden a tramos flexibles (giros y lazos) conectándolos.

Los estudios con proteolisis limitada fueron ampliados con dos estudios: tratando la PrP^{Sc} sin GPI con PK, a tiempos crecientes de incubación de la enzima y desplegando parcialmente e la PrP^{Sc} con diferentes concentraciones de guanidina. En ambos experimentos se puede observar un sucesivo decrecimiento den la intensidad de las bandas, aunque no todas se comportan igual y no aparece ningún nuevo punto de corte. Por lo tanto, ambos estudios sugieren que los fragmentos resistente a PK no provienen de diferentes subpoblaciones de PrP^{Sc} sin GPI, por el contrario derivan de un péptido común de PrP^{Sc} mas largo.

En resumen, se presentan datos que expanden el conocimiento sobre la estructura de la PrP^{Sc}, en la forma de un completo mapa de susceptibilidad a PK de la proteína priónica. Estos estudios apoyan la hipótesis de que la estructura de la PrP^{Sc} consiste en una serie de tramos de hojas-β cortos, extremadamente resistentes a PK, conectados por lazos y giros cortos y flexibles, muy sensibles a PK. El mapa de susceptibilidad a PK presentado aquí permite la identificación de posible tramos de hebras-β, que constituyen la columna vertebral "cross-β" de la $PrP^{Sc.}$. Además, los datos sugieren que el considerable tramo C-terminal de PrP^{Sc} es altamente resistente a PK y por lo tanto está constituido por hojas-β.

Al mismo tiempo, aprovechando la propiedad de la PrP^{Sc} de polimerizar en fibras amiloides y los avances tecnológicos que han permito mejorar la resolución de las diferentes técnicas de microscopia electrónica, la ultraestructura del prion fue estudiada usando técnicas desde baja resolución hasta la reconstrucción tridimensional. Para llevar acabo estos exhaustivos estudios, la proteína usada fue la PrP^{Sc} sin anclaje a la membrana, ya que esta proteína ha permitido la mejora en el proceso de purificación, de modo que proporciona la muestra mas limpia y adecuada para

ser analizada mediante estas técnicas, sin perder las propiedades naturales de la PrP^{Sc}.

Se ha encontrado que las fibras individuales tienen una anchura de 3-5 nm, un patrón helicoidal irregular y que están formadas por dos protofilamentos entrelazados, con una distancia no regular entre cada entrecruzamiento. La reconstrucción tridimensional de las imágenes bidimensionales de las fibras, obtenidas mediante criomicroscopía también muestran dos protofilamentos enroscándose, alrededor de un eje común. Además, existen unas densidades de 2-2,5 nm que se repiten a lo largo del eje, sugiriendo que cada una de estas repeticiones es un monómero de PrP^{Sc} apilado. Estas densidades axiales son también evidentes en los tomogramas de las fibras, reconstruidos mediante tomografía electrónica. Otra medida importante, es la presencia de una reflexión de 4,8 Å en la transformada rápida de Fourier (FFT), característica de una estructura "cross-β". Una de las imágenes de alta resolución obtenidas durante la criomicroscopía, también muestra claramente la reflexión de 4,8 Å en la separación entre las repeticiones de hebras-β que se apilan como si fuera una escalera.

Los priones de mamíferos resultan ser muy similares a la proteína priónica HET-s, que proviene del hongo filamentoso *Podospora anserina*, ya que los dos muestran densidades a lo largo de su "columna". Las densidades de HET-s están espaciadas por ~1 nm, mientras que las densidades de PrP^{Sc} son del doble de longitud (2-2,5 nm). Además los monómeros apilados del prion HET-s consisten en un solenoide caracterizado por dos "pisos" compuestos de hebras-β. Por lo tanto, PrP^{Sc} tiene que estar probablemente compuesta por cuatro "pisos". La fibra de HET-s es simple, mientras que la fibra de PrP^{Sc} está casi exclusivamente constituida por dos protofilamentos. Al igual que HET-s, la fibra individual está torsionada en la forma de una cinta retorcida. Para la estructura de la PrP^{Sc} dos de esas cintas están entrelazadas.

Aunando todos los datos obtenidos durante esta investigación, el conjunto sugiere que cada monómero de PrP^{Sc} debe de estar enrollado en un estructura "cross-β", de modo que aproximadamente 144 residuos (~G_{89}-S_{232}) encajen dentro de una anchura de 3-5 nm, mientras se mantiene la elevada proporción de hoja-β. Por lo tanto, los monómeros de PrP^{Sc} deben necesariamente adoptar una arquitectura de multicapas. Dicha arquitectura es observada en las fibras de SH3 o en el dominio de prion del hongo HET-s. Este dominio del prion de HET-s empaqueta 72 residuos (218-289) en dos pisos de tres hebras-β cada uno, alternando con giros y lazos. Específicamente los resultados encajan perfectamente con las arquitectura de cuatro peldaños de hebras-β, propuesto por Wille H *et al.* (2009), basado en sus interpretaciones de los patrones de difracción de rayos X. Por consiguiente, cada peldaño de monómero de PrP^{Sc} sin GPI estaría constituido por ~36-37 residuos.

La información que proviene de la proteolisis limitada indica que, las posiciones N_{152}-M_{153} se encuentran ubicadas cerca de la mitad de la secuencia G_{85}-S_{232}, y por lo tanto, es tentador especular que esta región podría estar localizada en un área expuesta en la frontera entre los dos "pisos". Esto podría explicar porque los fragmentos N_{152}-S_{232} and/or M_{153}-S_{232} se perfilan como los más destacados fragmentos resistentes a PK después del prolongado tratamiento con PK o del despliegue parcial de la proteína con la guanidina. Los residuos A_{116}-G_{118} podrían estar en la frontera entre los "pisos" más amino terminales (aproximadamente G_{85}-A_{115} y A_{119}-E_{151}). Por otro

lado, los resultados presentados son parcialmente inconsistentes con las localizaciones específicas asignadas por Govaerts *et al*. (2004), donde los residuos K_{100}-P_{104} y E_{145}-R_{163} están ubicados en lazos, no en hebras-β. Mis datos experimentales sugieren que los tramos formados por los residuos K_{100}-P_{104}, N_{142}-E_{151} y Y_{154}-Y_{161} son resistentes a la enzima PK, probablemente son parte de tramos de hebras-β que son estabilizados por numerosos puentes de hidrogeno. Sin embargo, debido a las limitaciones de las técnicas, no es posible describir cuantas hojas-β están formando cada vuelta. Sin embargo, lo mas probable es que cada "piso" esté compuesto como mínimo por tres hojas-β, pero podría haber más o incluso que sea imposible detectar otros puntos de corte debido a la conformación existente entre los tramos.

Para concluir, los resultados apoyan la noción de que la estructura de la PrP^{Sc} consiste en un solenoide de cuatro pisos, con un núcleo central rico en hebras-β; donde las hebras de hoja-β muy resistente a PK, están intercaladas con cortos y flexible lazos y giros, sensibles a PK. Además, la región que comprende $\sim V_{179}$ hasta la posición mas C-terminal de la PrP^{Sc} está probablemente compuesta de hoja-β, debido a su elevada resistencia a la digestión con PK. Los datos obtenidos a partir de esta PrP^{Sc} desprovista del GPI son consecuentes con el anterior estudio de Sajnani *et al.* (2008), donde PrP^{Sc} de hámster fue estudiada (cepas 263K y Dy). Además, los resultados son concordantes con los observados en la PrP^{Sc} de CJD, lo cual sugiere que el gran número de priones de humano, hámster y ratón comparten una estructura básica común.

RESUMO
Estudos estructurais da PrP^{Sc}

A elucidación da estructura da PrP^{Sc} sigue sendo un dos maiores retos na investigación sobre os prions. As bases moleculares da bioloxía da proteina priónica (PrP), tal como o mecanismo molecular de replicación e agregación, a barreira de especie e a patoxénese da neurodexeneración, non serán entendidos ata que a estructura estea resolta. Dado que as técnicas de alta resolución como RMN ou cristalografía de raios X non poden ser usadas, foron levadas a cabo outras técnicas de baixa resolución.

A proteólise limitada foi utilizada para identificar rexións flexibles no interior dos multímeros da PrP^{Sc}. Nembargantes, a presenza de carbohidratos covalentemente unidos e do glicosilfosfatidilinositol (GPI) para a ancoraxe á membrana, fan imposible o estudio por espectrometría de masas. Co fin de superar estas dificultades, foi usada a PrP^{Sc} de ratos transxénicos que expresan a proteína priónica (PrP) sen a ancoraxe á membrana. Estes animais producen PrP^{Sc} que carece do GPI e dos carbohidratos e, polo tanto, permite a detección e localización de rexións flexibles sensibles á enzima Proteinasa K (PK), a través do Western blot e a espectrometría de masas. Por primeira vez se puido obter un estudo da estrutura completa da PrP^{Sc}, tendo en conta a súa susceptibilidade á proteólise.

As mostras de PrP^{Sc} sen GPI foron dixeridas con PK, sometidas á electroforese de Tricina-SDS-PAGE e hibridizado cun anticorpo C-terminal específico (R1). Sete bandas foron detectadas pola análise mediante Western blot, con pesos moleculares sobre 17, 14,6, 13, 12, 10,2, 8 e 6,7 kDa. A continuación, os estudos de espectrometría de masas detectaron 13 péptidos diferentes, cun peso molecular exacto de: 17148, 16726, 16371, 13606, 13463, 12173, 12041, 11171, 9687, 9573, 8358, 7436 e 6274; coincidindo ben coas bandas resistentes a PK identificadas no Western blot. Estes péptidos corresponden a moléculas cortadas nas posicións 81, 85, 89, 116, 118, 133, 134, 141, 152, 153, 162, 169 ou 179, respectivamente. Os primeiros 9 péptidos (ata a posición 153), coinciden cos puntos de corte previamente identificados na PrP^{Sc} natural (Sajnani et al. (2008)). Polo tanto, o mapa de susceptibilidade á PK, que comprende a rexión 116-118, 133-134, 141, 152-153, 162, 169 e 179, suxire que estas rexións corresponden a lazos e xiros, mentres que os cortes nas posicións 81, 85 e 89 indican a fronteira entre os dominios C-terminal estruturado e o N-terminal non estruturado da PrP^{Sc}. Dada a proporción de follas-β, obtida por estudos de FTIR, é lóxico concluír que as zonas resistentes á PK que están flanqueando esas rexións susceptibles, probablemente corresponden a cadeas de follas-β. Ademais, unha porción substancial da rexión C-terminal da PrP^{Sc} é moi resistente á PK, e polo tanto, pode estar completamente formada por folla-β.

Ao mesmo tempo, aproveitando a propiedade de polimerización en fibras amiloides da PrP^{Sc}, diferentes técnicas de microscopia electrónica, dende baixa resolución ata a reconstrución tridimensional, foron utilizadas para estudar a ultraestrutura do prion. Para levar a cabo estes estudos, a proteína empregada foi a PrP^{Sc} sen a ancoraxe á membrana, xa que esta proteína permitiu a mellora do proceso de purificación, proporcionado a mostra máis limpa e adecuada, sen a perda das propiedades naturais da PrP^{Sc}.

Verificouse que as fibras individuais teñen un ancho de 3-5 nm, un patrón helicoidal irregular e que están formadas por dous protofilamentos entrelazados, cunha distancia non regular entre cada entrecruzamento. A reconstrución tridimensional das imaxes bidimensionais das fibras, obtidas a través da criomicroscopía, tamén mostra dous protofilamentos torsionados en torno a un eixe común. Ademais, hai unhas densidades de 2-2,5 nm que se repiten ao longo do eixe, o que suxire que cada unha destas repeticións é un monómero de PrP^{Sc} apilado. Estas densidades axiais son tamén evidentes nos tomogramas das fibras reconstruídos por tomografía electrónica. Outra medida importante, é a presenza dun reflexo de 4,8 Å na transformada rápida de Fourier (FFT), característica dunha estrutura "cross-β". Unha das imaxes de alta resolución obtidas durante a criomicroscopía, tamén demostra claramente a reflexión de 4,8 Å, na separación entre as repeticións das cadeas-β que están apiladas como si foran unha escaleira.

Todos os datos recollidos durante o estudo, suxiren que cada monómero de PrP^{Sc} debe de estar enrolado nunha estrutura "cross-β", de xeito que os ~144 residuos ($\sim G_{89}$-S_{232}) encaixen dentro dunha anchura de 3-5 nm, mantendo a elevada porcentaxe de follas-β. Polo tanto, os monómeros PrP^{Sc} deben necesariamente ter unha arquitectura de múltiples capas; os resultados encaixan perfectamente coa arquitectura de catro chanzos de cadeas-β, proposto por Wille H *et al.* (2009), en base ás súas interpretacións dos patróns de difracción de raios X. Consecuentemente, cada chanzo do monómero de PrP^{Sc} sen GPI estará composto por ~36-37 residuos.

En resumo, os resultados sosteñen a idea de que a estructura da PrP^{Sc} consiste nun solenoide de catro chanzos, cun núcleo rico en cadeas-β; onde as cadeas de follas-β altamente resistente á PK, son intercaladas con curtos e flexibles lazos e xiros, sensibles á PK. Ademais, a rexión que comprende $\sim V_{179}$ ata a posición máis C-terminal da PrP^{Sc} está probablemente composta de folla-β, debido á súa elevada resistencia á dixestión coa PK. Os datos obtidos a partir desta PrP^{Sc} sin o GPI son consistentes co anterior estudo de Sajnani *et al.* (2008), onde foi estudada a PrP^{Sc} do hamster (cepas 263K e Dy). Ademais, os resultados son consistentes cos observados na PrP^{Sc} de CJD, suxerindo que o gran número de prions do humano, hamster e rato comparten unha estrutura básica común.

SUMMARY
Structural studies of PrP^{Sc}

Elucidation of the structure of PrP^{Sc} continues to be one major challenge in prion research. Molecular basis of the biology of prion protein, such as the molecular mechanism of prion replication and aggregation, the species barrier and the pathogenesis of neurodegeneration will not be understood until the structure is solved. Given that high-resolution techniques such as NMR or X-ray crystallography cannot be used, a number of lower resolution analytical approaches have been attempted.

Limited proteolysis has been successfully used to pinpoint flexible regions within prion multimers (PrP^{Sc}). However, the presence of covalently attached carbohydrates and glycosylphosphatidylinositol (GPI) membrane anchor makes mass spectrometry-based analysis impractical. In order to surmount these difficulties it was analyzed PrP^{Sc} from transgenic mice expressing prion protein (PrP) lacking the GPI membrane anchor. Such animals produce prions that are devoid of the GPI anchor and carbohydrates, and, thereby, permit the detection and location of flexible, proteinase K (PK) susceptible regions by Western blot and mass spectrometry-based analysis. Then, these properties have allowed to obtain, for the first time, a complete survey of the whole PrP^{Sc} sequence, regarding its susceptibility to proteolysis.

PrP^{Sc} samples were digested with PK, subjected to Tricine-SDS-PAGE, and probed with a C-terminal specific antibody (R1). Seven bands were detected by Western blot analysis, with apparent MWs of approximately 17, 14.6, 13, 12, 10.2, 8 and 6.7 kDa. Subsequently, mass spectrometry-based analysis detected 13 different peptides with exact MWs: 17148, 16726, 16371, 13606, 13463, 12173, 12041, 11171, 9687, 9573, 8358, 7436 and 6274, which match quite well with PK-resistant bands identified by Western blot analysis. These peptides correspond to molecules cleaved at positions 81, 85, 89, 116, 118, 133, 134, 141, 152, 153, 162, 169 or 179, respectively. The first 9 peptides (to position 153), match very well with PK cleavage sites previously identified in wild type PrP^{Sc} (Sajnani *et al*. (2008)). Then, the map of PK-susceptible spots, namely 116-118, 133-134, 141, 152-153, 162, 169, and 179, strongly suggests regions corresponding to loops and turns, while nicks at 81, 85, and 89 signal the frontier between the structured C-terminal and unstructured N-terminal domains of PrP^{Sc}. Given the high proportion of β-sheet secondary structure derived from FTIR analyses, it is logical to conclude that PK-resistant sequence stretches flanking these spots most likely corresponds to strands of β-sheet. Furthermore, the sizeable C-terminal stretch of PrP^{Sc} is highly resistant to PK and therefore perhaps constituted by β-sheet secondary structure.

At the same time, taking advantage of the property of prion protein to polymerize into amyloid fibers, different electron microscopy (EM) techniques, from low-resolution to three-dimensional reconstruction were used to study the ultrastructure of the PrP^{Sc}. To perform these comprehensive studies, GPI-anchorless PrP^{Sc} was used, because this protein has allowed the improvement of the isolation method, so it provides the adequate cleanest sample, without losing the natural properties of the wild-type PrP^{Sc}.

It was found out that the single fibers have a width of 3-5 nm, no regular helical pitch and are made up for two protofilaments intertwined, with no regular crossover distance. Three-dimensional reconstruction of 2D cryomicroscopy (cryo-EM) images of the fibers also shows two protofilaments coiling around a common axis. Moreover, there are 2-2.5 nm repetition densities along the axis, suggesting each of these is a stacked monomer of PrP^{Sc}. These axial densities are also evident in reconstructed tomograms obtained by cryo-EM tomography of fiber sample. Another important measure is a 4.8 Å reflection presents in the Fast Fourier Transform (FFT), characteristic of the cross-β structure. A high-resolution image of cryo-EM also shows clearly the 4.8 Å reflection of the spacing between the beta repeat strands that are stacked like a "ladder".

All of the data, obtained during this research, suggest that, each PrP^{Sc} monomer must be coiled in a cross-β along the fiber, as to fit approximately 144 residues ($\sim G_{89}$-S_{232}) into the 3-5 nm width while maintaining the observed high proportion of β-sheet secondary structure. In order to do so, the PrP^{Sc} monomers must necessarily adopt a multi-layer architecture, specifically the results fit perfectly with the four-rung β-strands architecture proposed by Wille H *et al.* (2009), based on their interpretation of X-ray diffraction patterns. Accordingly, each rung of the GPI-anchorless PrP^{Sc} monomer would be comprised of ~36-37 residues.

In summary, the data support a PrP^{Sc} structure consisting of a four-rung solenoid with a central β-strand-rich core; from which a series of highly PK-resistant β-sheet strands intersperse with PK-sensitive short flexible loops and turns. Furthermore, the region comprising $\sim V_{179}$ to the C-terminus of PrP^{Sc} is probably composed primarily of β-sheet, as it is highly resistant to PK. The data obtained from this GPI-anchorless PrP^{Sc} work is consistent with the previous study of Sajnani *et al.* (2008) using $SHaPrP^{Sc}$ (263K and Dy strains). Besides, the results are consistent with those observed for human CJD PrP^{Sc}, which suggests that the myriad human, hamster and mouse prions share a common basic structure.

Table of contents

1. Introduction **1**

1.1 Historical background 2

1.2 Prion protein structure 5

1.3 Structural insights on the architecture of PrP^{Sc} 8

1.3.1 Limited proteolysis 8

1.3.2 Fourier transform infrared spectroscopy (FTIR) 9

1.3.3 Transmission electron microscopy (TEM) 10

1.3.4 Fiber X-ray diffraction 11

1.3.5 Electron crystallography 12

1.3.6 Antibody mapping studies 13

1.3.7 Chemical cross-linking 13

1.3.8 Chemical surface labeling 14

1.3.9 Hydrogen-deuterium exchange (H/D) 15

1.4 Structural models of PrP^{Sc} 15

1.4.1 β-helical model 15

1.4.2 Spiral model 16

1.5 Aim of the thesis 18

1.6 Outline of the thesis 18

1.7 References 19

2. Generation of PrP^{Sc} **27**

2.1 Introduction 28

2.2 Animal model 28

2.2.1 Syrian hamsters 28

2.2.2 GPI-anchorless PrP transgenic mice 29

2.3 Isolation of PrP^{Sc} 33

2.3.1 Brain homogenate 33

2.3.2 Isolation of GPI-anchorless PrP^{Sc} 33

2.4 Concluding remarks 36

2.5 References 37

3. Limited proteolysis **41**

3.1 Introduction 42

3.1.1 Limited proteolysis 42

3.1.2 Tricine-SDS-PAGE 46

3.1.3 Outline of experimental approach 47

3.2 Studies on GPI-anchorless PrP^{Sc} 48

3.2.1 Identification of PK cleavage sites by Western blot (WB) 48

3.2.2 Identification of PK cleavage sites by mass spectrometric detection 49

3.2.3 Kinetics of PK digestion 51

3.2.4 PK cleavage analysis after partial unfolding 52

3.3 Studies on Syrian hamster PrP^{Sc} ($SHaPrP^{Sc}$) 53

3.3.1 Identification of PK cleavage sites in two strains of $SHaPrP^{Sc}$ by WB 53

3.3.2 Identification of PK cleavage sites in PK-sensitive $SHaPrP^{Sc}$ by WB 55

3.4 Conclusions 57

3.5 Experimental 60

3.6 References 62

4. Electron Microscopy **67**

4.1 Introduction 68

4.1.1 Outline of experimental approach 69

4.2 Transmission electron microscopy (TEM) 70

4.2.1 Results of TEM 71

4.3 Cryo-transmission electron microscopy (Cryo-TEM) 73

4.3.1 Results of cryo-TEM 73

4.4 Cryo-TEM tomography (Cryo-ET) 76

4.4.1 Results of cryo-ET 77

4.5 Helical reconstruction 79

4.5.1 Results of helical reconstruction 80

4.6 Conclusions 81

4.7 Experimental 83

4.8 References 84

5. Discussion **89**

6. Appendices **95**

Appendix I. Explanation of the GPI-anchorless tg mice sequence (23-232) 96

Appendix II. Calibration of the GPI-anchorless PrP^{Sc} MALDI-TOF spectrum 97

Appendix III. List of abbreviations 101

Appendix IV. List of publications / Participation in conferences 103

1

Introduction

Abstract

This chapter is a general introduction and describes the thesis background and outline. A brief description of the prion field is presented and divided into four different blocks: historical background, prion protein structure, structural insights on the architecture of PrP^{Ss} and structural models of PrP^{Sc}. Due to the complexity of the issues in the study of the structure of PrP^{Sc}, most data available in the literature come from low-resolution biophysical techniques; this information has permitted the development of some structural models in the last decade, but there are many pros an cons to each of the models. Therefore, until know, the structure of mammalian prions has remained unknown. With the support of the research group to which I belong, and collaborators from different fields, I have been capable to present new constraints and a new model of the structure of PrP^{Sc}. This thesis has numerous implications for understanding the etiology and pathogenesis of prions and other neurodegenerative diseases.

1.1 Historical background

Prion diseases or transmissible spongiform encephalopathies (TSE) are a wide group of fatal neurodegenerative diseases that affect humans and animals, associated with the accumulation of aggregates of misfolded conformers of the host-encoded cellular prion protein (PrP^{C}), primarily in the brain [1]. Prion diseases have a broad spectrum of clinical manifestations: dementia, ataxia, insomnia, paraplegia, paresthesia and abnormal behaviour. The neuropathologycal findings range from widespread atrophy, neuronal loss, vacuolation, spongiform changes, astrocytic gliosis and PrP amyloid plaques (Figure 1.1) [1].

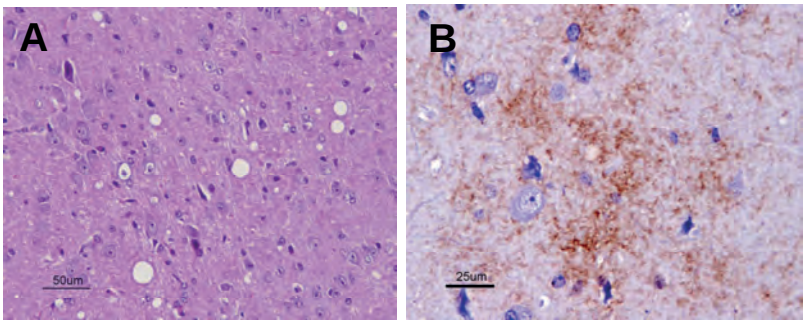

Figure 1.1. *Neuropathological features of TSEs. The images represent histopathological and immunohistochemical studies in scrapie-infected mice with RML strain.* ***A.*** *This panel shows spongiform degeneration in the thalamus, the vacuoles are the unstained globular structures (Haematoxyllin eosin staining). Bar 50 µm.* ***B.*** *PrP deposits in the thalamus, stained in brown. Bar 25 µm.*

The earliest description of scrapie, a natural TSE affecting sheep and goats exhibiting a strong scraping and ataxia, was made in the 18th century. More recently, other animal TSEs were recognized, including chronic wasting disease (CWD) of deer and elk [2] described in captive and wild animals, bovine spongiform encephalopathy (BSE) or "mad cow disease", in cattle [3] and transmissible mink encephalopathy (TME) [4]. TSEs were also discovered in domestic cats and in other zoo animals [5]. The natural routes of transmission are unclear; some TSEs are endemic, with a low but stable incidence, however it is known that some epizootics have resulted via contaminated feed, like meat and bone meal (MBM) prepared from carcasses. BSE epizootic caused the infectious agent to spread, transmitting the disease to human beings (vCJD).

In humans, prion diseases can arise spontaneously, be inherited or acquired through transmission. The first cases of a TSE in humans were described in 1920; it was termed Creutzfeldt-Jakob disease (CJD). It was discovered that CJD could be caused by the three vias, such as the variant CJD that was transmitted to humans by eating food contaminated. Furthermore, an infectious human prion disease, called kuru, was discovered in the highlanders of Papua New Guinea [6]. Other typical diseases are Gerstmann-Sträussler syndrome (GSS) [7] and fatal familial insomnia (FFI), they are mainly associated to a number of mutations in the prion protein gene, although there are sporadic cases of FFI.

Table 1.I. *Prion diseases of human and animals. (Modified from Colby DW et al. (2011)* [8]*)*

Disease	Host	Mechanism of pathogenesis
Kuru	humans (Fore people)	infection through ritualistic cannibalism
Iatrogenic CJD	humans	infection from prion-contaminated HGH, medical equipment, etc.
Variant CJD	humans	infection from bobine prions
Familial CJD	humans	germline mutation in the Prnp gene
GSS	humans	germline mutation in the Prnp gene
FFI	humans	germline mutation in the Prnp gene
Sporadic CJD	humans	somatic mutation or spontaneous conversion of PrP^{C} to PrP^{Sc}
Sporadic FI	humans	somatic mutation or spontaneous conversion of PrP^{C} to PrP^{Sc}
Scrapie	sheep	infection
BSE	cattle	infection or sporadic
TME	mink	infection with prions from sheep or cattle
CWD	deer, elk	infection
FSE	cats	infection with prion-contaminated bovine tissues or MBM
Exotic ungulate encephalopathy	greater kudu, nyala, oryx	infection with prion-contaminated bovine tissues or MBM

CJD: Creutzfeldt-Jakob disease; GSS: Gerstmann-Sträussler-Scheinker; FFI: fatal familial insomnia; BSE: bovine spongiform encephalopathy; TME: transmissible mink encephalopathy; CWD: chronic wasting disease; FSE: feline spongiform encephalopathy; HGH: human growth hormone; MBM: meat and bone meal.

Scrapie was demonstrated to be transmissible by inoculation between sheep (and goats) with characteristic prolonged incubation periods. It was concluded that some kind of virus must be the infectious agent, and it was defined by the term "slow virus". Kuru, characterized by a progressive ataxia, probably was transmitted during ritual funeral cannibalistic ceremonies. Researchers observed similarities between kuru and scrapie at the neuropathological, clinical and epidemiologic levels, and transmissibility of kuru and CJD was proved by intracerebral inoculation into chimpanzees. More recently, humans have contracted a new variant CJD (vCJD) from prion-tainted beef products [9].

However, the transmissible agent in these diseases was not clear and the concept of "slow virus" was defeated because the specific virus was never found. There was not immunological response and this agent was resistant to treatment for inactivate nucleic acids, such as ultraviolet radiation or treatment with nucleases [10]. Thus, it was suggested that the transmissible agent might be a self-replicating protein [11]. Successive studies with substantially purified preparations of the scrapie agent showed that a protein is required for infectivity and a protease-resistant protein associated with a glycosylphosphatidylinositol (GPI) anchored membrane, termed prion protein (PrP), was isolated from infected brains [12][13]. Then, the term prion: "small proteinaceous infectious particles that resist inactivation by procedures which modify nucleic acids" was established [14].

The protease-resistant form of the PrP was the major constituent of infective brain fractions, extremely resistant to physical and chemical treatments and hydrophobic. Its molecular size is 27 to 30 kDa and was called PrP27-30 or PrPres. But this form derives from a total protein of 33-35 kDa named PrP^{Sc} (infectious scrapie isoform) (Figure 1.2). It was discovered that PrP27-30 is encoded by single copy chromosomal gene, nevertheless the normal product of PrP gene (Prnp) is a protease-sensible protein called PrP^{C} (normal non-infectious cellular isoform) [15][16]. Therefore scrapie and cellular PrP isoforms are encoded by the same chromosomal gene [17], then the cellular protein is converted into PrP^{Sc} through a posttranslational process, consisting of a conformational transformation [18]. This is the core of the "protein only" hypothesis, according to which the infectious agent (PrP^{Sc}) is a misfolded form of the cellular prion protein (PrP^{C}) [1].

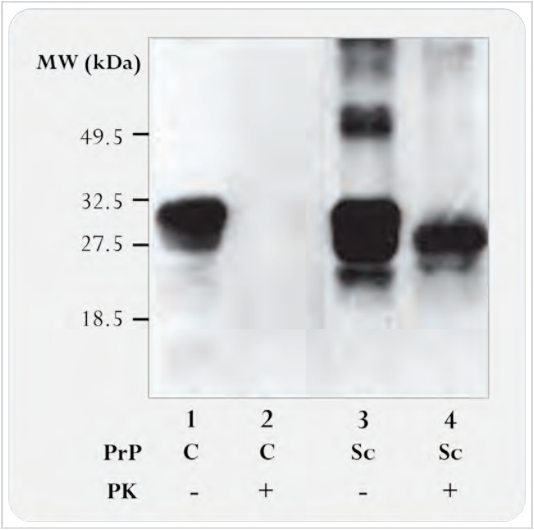

Figure 1.2. *Western blot of the prion protein isoforms. Brain homogenates from uninfected (lane 1 and 2) and prion-infected hamster (lane 3 and 4). Samples in lane 2 and 4 were digested with 50 µg/ml of proteinase K (PK) for 30 min at 37 °C. PrP^{C} in lane 2 and 4 was completely hydrolyzed, whereas approximately 67 amino acids were digested from the NH_2 terminus of PrP^{Sc} to generate PrP27-30. The blot was developed with anti-PrP R073 polyclonal rabbit antiserum. (Adapted from Prusiner SB (1998) [1])*

Although the prion replication comes about by a self-propagating conversion of PrP^{C} to the pathogenic isoform, the mechanism is still unknown. Two replication models could be considered (Figure 1.3): "template-directed model", it proposes that monomeric PrP^{C} is the most stable conformer and PrP^{Sc} monomer can bind to PrP^{C} molecule generating a heterodimer. Hence PrP^{Sc} acts as a template, inducing a conformational transition of PrP^{C}. In this mechanism, the formation of oligomers occurs after the conversion. The other model is the "seeded nucleation model", it postulates that the PrP^{C} converts spontaneously to PrP^{Sc}, but PrP^{Sc} is unstable unless it is "protected" or "stabilized" by being part of an oligomer bigger that a critical size [19]. Both mechanisms are theoretically plausible, however, the most probably is the seeded nucleation model because prion infectivity is associated with small PrP^{Sc} oligomers with 14-28 PrP monomers [20][21]. However, recent studies where transmissible prion disease is generated

de novo by non-infectious recombinant amyloid fibrils suggested a new replication mechanism termed "deformed templating", showing that replication could be induced by PrP structures different from that of PrP^{Sc} [22][23]. Actually, the deformed templating hypothesis is not competing with the other hypotheses, because it only refers to the case of recombinant PrP fibers transforming into PrP^{Sc} through a "promiscuous" molecular process; thus, a simple propagation of PrP^{Sc} cannot be by deformed templating.

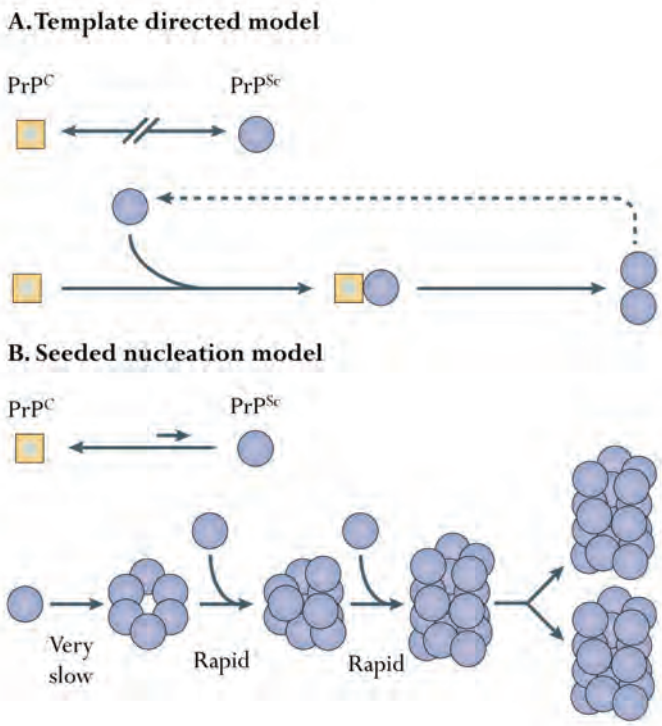

Figure 1.3. *Models for the conversion of PrP^C to PrP^{Sc}.* ***A.*** *The template-directed model. The conformational change is kinetically controlled, a high activation energy barrier preventing spontaneous conversion at detectable rates. Interaction with PrP^{Sc} (blue sphere) causes PrP^C (yellow square) to undergo an induced conformational change to yield PrP^{Sc}. In the case of certain mutations in PrP^C, spontaneous conversion to PrP^{Sc} can occur as a rare event.* ***B.*** *The seeded nucleation model. PrP^C (yellow square) and PrP^{Sc} (blue sphere) are in equilibrium, with PrP^C strongly favoured. PrP^{Sc} is only stabilized when it adds onto a crystal-like seed or aggregate of PrP^{Sc}. Seed formation is rare; however, once a seed is present, monomer addition ensues rapidly. (Weissman C. 2004) [24])*

1.2 Prion protein structure

The polypeptide chains of the PrP^C and PrP^{Sc} are identical in composition. The primary sequence is composed of approximately 254 amino acids (aa), depending on the species. It has an amino-terminal signal peptide and in the N-terminal region there are five copies of an octarepeat PHGGGWGQ (residues 51-90, in mouse sequence). There is a single disulphide bond between

cysteines 178 and 213 and two N-glycosylation sites at asparagines 180 and 196 (mouse numbering). Furthermore, in the residue 231 it has a hydrophobic carboxy-terminal domain to be attached to the cell membrane by a glycosylphosphatidylinositol (GPI) anchor. PrP polypeptide is posttranslationally processed, and is shortened to 209 residues (numbered 23-231) removing the 22 aa of the signal peptide and 23 C-terminal aa that are replaced by a GPI anchor. Proteinase K (PK) digestion of the PrP^{Sc} produces a smaller, protease-resistant form of approximately 147 aa, termed PrP27-30 (Figure 1.4).

To assess what is happening during the conformational transition from PrP^{C} to PrP^{Sc}, secondary structural studies by Fourier-transform infrared spectroscopy (FTIR) were performed under nondenaturing conditions. It was estimated that PrP^{C} has a high content of α-helix (42 %), only a 3 % of β-sheet content and 32 % and 23 % of turn and random coil. In contrast, PrP^{Sc} appeared to have, by these studies (but see further comments) a β-sheet content of 43 %, 30 % of α-helix and lower content of turn and random coil [18]. Other FTIR-based secondary structure analysis of the PrP27-30, derived of PrP^{Sc} by limited proteolysis, showed that this fraction is composed predominantly of β-sheet (47 %) [25]. These studies suggested that the fundamental event in the transition to PrP^{Sc} is the conversion of the α-helices in PrP^{C} into β-sheets.

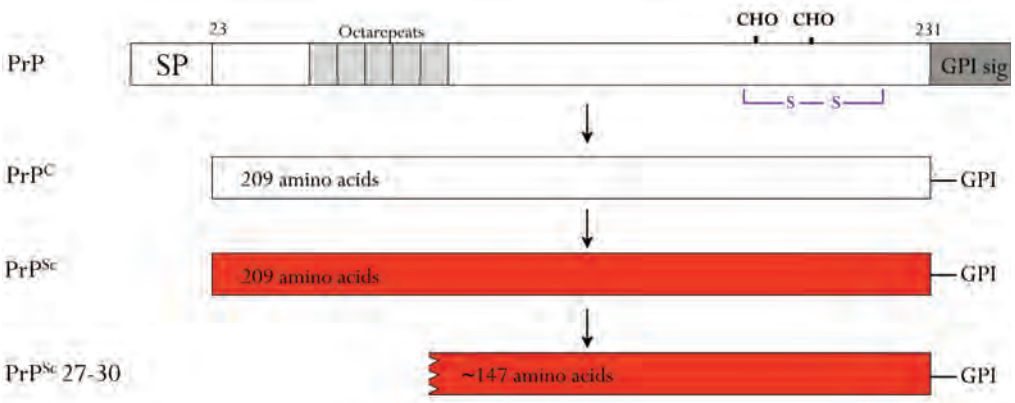

Figure 1.4. *Prion protein isoforms. The primary sequence of mouse prion protein is represented; SP is the signal peptide, S-S the disulfide bond, CHO the N-linked glycosylation sites and GPI sig. is the signal sequence to be substituted by the GPI (glycosylphosphatidylinositol anchor). Mouse PrP^{C} has 254 residues, which is shortened to 209 amino acids during posttranslational process. PrP^{Sc} has the identical primary structure of PrP^{C}. The protease-resistant form of the PrP is PrP27-30; it is composed of approximately 147 residues. Although glycans and the disulfide bond are not drawn in the three last schemes, they are part of the protein.*

The elucidation of the cellular prion protein (PrP^{C}) structure was possible because of the improvements in the expression of recombinant PrP, in sufficient amount to permit nuclear magnetic resonance (NMR) studies. The first determination of the structure was in mouse recombinant PrP comprising the residues 121-231, NMR showed that moPrP(121-231) is a globular region that contains three α-helices and two-stranded antiparallel β-sheet [26].

Subsequently, this study was completed characterizing the full-lengh mouse prion protein, moPrP(23-231) and it was determined that the N-terminal region 23-120 is flexible and disordered (Figure 1.5) [27]. Three-dimensional studies were also conducted in Syrian hamster recombinant PrP (90-231). SHaPrP(90-231) is constituted by three α-helices: A (residues 144-154), B (residues 172-193) and C (residues 200-227); and two short antiparallel β-strands: S1 (residues 129-131) and S2 (residue 161-163) [28]. The N-terminal region (90-119) is unstructured and there are turns or loops in the structure.

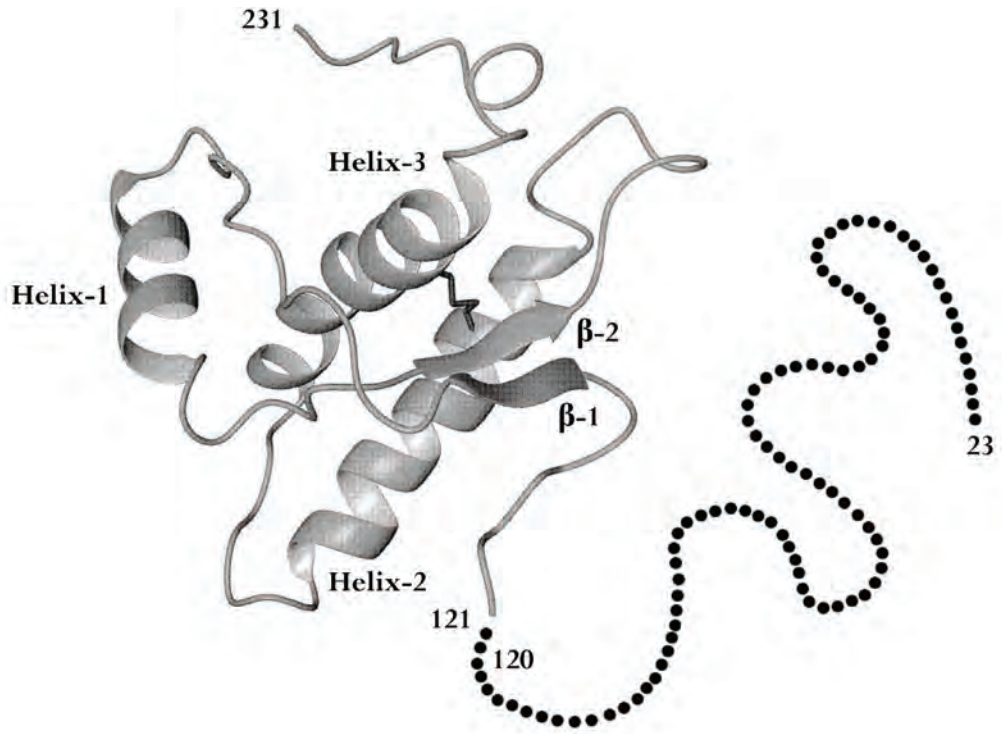

Figure 1.5. *NMR structure of mouse PrP23-231. The three α-helices (Helix-1, Helix-2 and Helix-3) and two antiparallel β-sheets (β-1 and β-2) are labelled. The disulphide bond joining Helix-2 and Helix-3 is represented by the "black line". The 23-120 N-terminal segment represented by dots is unstructured. (Adapted from Riek R. et al. (1997) [27])*

Other mammalian prion protein structures of different species such as human prion protein (hPrP(23-230) [29][30] and bovine prion protein (bPrP(23-230)) [31] were resolved. When compared with the previous studies of the mouse and Syrian hamster PrP, it can be observed they are essentially identical, except that there are small local differences relative to the conformations like the length of the helices or loops, then a highly conserved structure of PrP^{C} exists from different mammals.

Also, the structure of the PrP^{C} was determined by X-ray crystallography [30], which agree very well with NMR studies. However, the crystal structure of the human PrP is a dimmer form and it was revealed a domain-swap mechanism for the assembly of PrP.

The tertiary structure of PrP^{Sc} remains unknown due to its properties such as the polymerization into heterogeneous amyloid fibrils during its purification, in part as a consequence of its high quantity β-sheet. It forms insoluble aggregates that resist the solubilisation in nondenaturing detergents hampering the obtaining of suitable preparations from brains of infected animals for high-resolution techniques like NMR spectroscopy and X-ray crystallography. Furthermore, PrP^{Sc} has high heterogeneity derived from the glycophosphatidylinositol (GPI) anchor and the carbohydrates contained in its C-terminal region, which make very difficult the interpretation of data.

1.3 Structural insights on the architecture of PrP^{Sc}

Although it is impossible to characterize the protein by highly-resolution methods, several structural characteristics and constraints of PrP^{Sc} have been determined using low-resolution techniques, providing useful knowledge to built potential structural models.

1.3.1 Limited proteolysis

One of these indirect methods is the limited proteolysis, a good tool to find out conformational features of PrP^{Sc}. It provides information about the peptide bonds with respect to the fold of the protein.

Treatment with the nonspecific protease proteinase K (PK) showed that whereas PrP^{C} is completely sensitive to proteolysis, PrP^{Sc} is partially resistant, yielding PK-resistant cores of variable length. It depends on the species, in Syrian hamster, the most abundant of which consists of amino acid residues ~90-231. This resistant region, called PrPres or PrP27-30 due to its molecular size, continues to be infectious and retains the basic characteristics of a prion. Therefore, it can be concluded that PrP^{Sc} consists of two domains: an N-terminal unstructured labile area and a highly structured globular protease-resistant region [12][13].

Nonetheless, more recent studies have shown the existence of a fraction of PrP^{Sc} sensitive to digestion by PK ($sPrP^{Sc}$) [32][33]. Indeed it was demonstrated that this PK-sensitive PrP^{Sc} is infectious and shares basic structural features with PK-resistant PrP^{Sc} [34]. PK resistance of PrP^{Sc} shows a strong dependence on the quaternary structure, so $sPrP^{Sc}$ is sensitive because is made up for the smaller multimers, however PrPres is formed by weight aggregates.

Other limited proteolysis experiments have shown that the size of the PK-resistant core and the resistance to proteolytic digestion are slightly different between distinct strains of PrP^{Sc} [35]. So, perhaps a basic architecture between strains is shared, with minor differences.

Further analyses of the PK-resistant PrP^{Sc} have reported other minor PK-resistant fragments, detected with monoclonal antibodies specific for C-terminal region [36][37][38][39][40]; knowing that proteolitic cleavage in native state proteins occurs preferentially within loops, more rarely within α-helix, and with much higher difficulty within β-strands [41]; it is possible to conclude that there are other flexible regions within the structure of the PrP^{Sc}. These studies led other studies of the PrPres analyzed by mass spectrometry and sequencing, increasing the resolution and locating the exact position of the predominant PK cleavage sites in different species of PrP^{Sc} [1][35][40][42]. The study carried out by Sajnani *et al*. [40] with two different $SHaPrP^{Sc}$ strains showed four regions sensitive to PK digestion: 23-86 (263K strain), 23-101 (Dy strain), 117-119, 131-142, and the region around 154. Then, this study suggests that the N-terminal of the PrP^{Sc} is formed by β-sheets interspersed with loops and/or turns, although there is no information available beyond the position 154 because of GPI anchor and the carbohydrates in the C-terminal portion of the protein hamper the analysis.

1.3.2 Fourier transform infrared spectroscopy (FTIR)

Fourier transform infrared (FTIR) spectroscopy provides the relative amounts, as percentages, of secondary structure composition for proteins.

Table 1.II. *Secondary structure determination from FTIR [18][25].*

Content of secondary structure, %			
Structure	PrP^{C}	PrP^{Sc}	PrP27-30
α-helix	42	30	14
β-sheet	3	43	48
Turn	32	11	34
Coil	23	16	4

FTIR studies have indicated that the transition from PrP^{C} to PrP^{Sc} is associated with a loss of α-helix and a large increase of β-sheet structure [18][25][43]. More specifically, data from FTIR of PrP27-30 have shown a specific content of secondary structures of 14 % α-helix, 48 % β-sheet, 34 % turn, and 4 % random coil [25]. Specific FTIR analysis of PrP^{Sc} from 23-231 residues presented a 30 % α-helix, 43 % β-sheet, 11 % turn, and 16 % random coil [18]. However very recent FTIR studies, comparing GPI-less PrP^{Sc} and recombinant PrP amyloid fibris, contend that there is no presence of α-helices in PrP^{Sc} [44]. This last study suggests that the assignments in the previous FTIR studies are uncertain, since besides the α-helices, other structures like turns and loops give a infrared band in the same frequency range, then the amount of α-helix is overestimate.

Moreover, infrared (IR) spectroscopy studies have indicated a strain-dependent differences in β-sheet amount of PrP^{Sc}, showing that the strain diversity in the prion diseases is determined by variations in the conformation of PrP27-30 form [43][45]. More recently, it was observed that the glycans and the GPI anchor do not affect to the secondary structure of PrPres of a specific strain [43].

1.3.3 Transmission electron microscopy (TEM)

Transmission electron microscopy (TEM) enables to study the ultrastructural characteristic of prion aggregates.

In early TEM studies, scrapie associated fibrils (SAFs), derived from mice and hamsters infected with different scrapie strains, were described [46][47]. Other studies on purified hamster PrP^{Sc} observed a polymerization into heterogeneous rod particles, termed prion rods [48][49]. Despite such differences in nomenclature, it is almost certain that rods and SAFs are the same kind of structures, this is, fibrils that associate laterally to form thicker, intertwined, fibrilar structures.

A comprehensive study, comparing PrP27-30 fibers from GPI-anchorless and wild type mice infected with different scrapie strains, has observed that fibers are typically formed by twisted or straight pairs of two protofilaments variably intertwined. These fibers have generally 100-150 nm in length, and 4-5 nm in width (Figure 1.6). Also it is revealed that there are basic structural differences between strains of PrP^{Sc}, such as differences in periodicity of twisting and protofilament width. Although, the morphology between strains is similar [50].

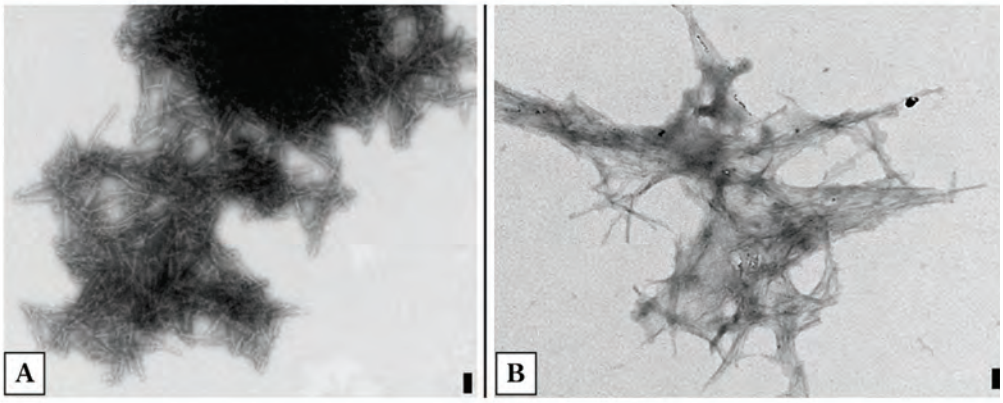

Figure 1.6. *TEM image comparison of PrP27-30 fibers.* ***A.*** *Wild-type 22L fibers.* ***B.*** *Anchorless 22L fibers. Samples were stained with methylamine tungstate. Scale bar are 100 nm. (Sim VL. et al. (2009) [50])*

However, it is worth noting that brains of scrapie-infected animals do not always present PrP^{Sc} fibers *in vivo* [51]. Then it was discovered that, the aggregation into prion rods structures and their visualization by electron microscopy are dependent of the method of isolation [52][53], which generally involves consecutive steps of ultracentrifugation, protease and detergent

treatment. GPI-anchorless PrP^{Sc}, produced in mice expressing PrP lacking the GPI anchor, is deposited as amyloid plaques into the brain [54], however they look similar to wild-type fibers [50], which are less prone to form deposits.

All these studies suggest that PrP^{Sc} is capable of fibrilization, a property shared with other known prions [55][56] and with amyloids [57][58].

1.3.4 Fiber X-ray diffraction

The fiber formation property of PrP^{Sc} makes possible to determine additional information about the three-dimensional structure of PrP27-30 molecule by fiber X-ray diffraction technique.

In early studies, X-ray diffraction pattern of mammalian prions has shown a meridional diffraction at 4.72 Å, that is a measure characteristic of amyloid structure [59], indicating a cross β-structure, and corresponding to the distance between β-sheets parallel to the fiber axis. Furthermore, the intersheet distance was 8.82 Å, meaning a uniform geometric distribution in the H-bonding direction [60].

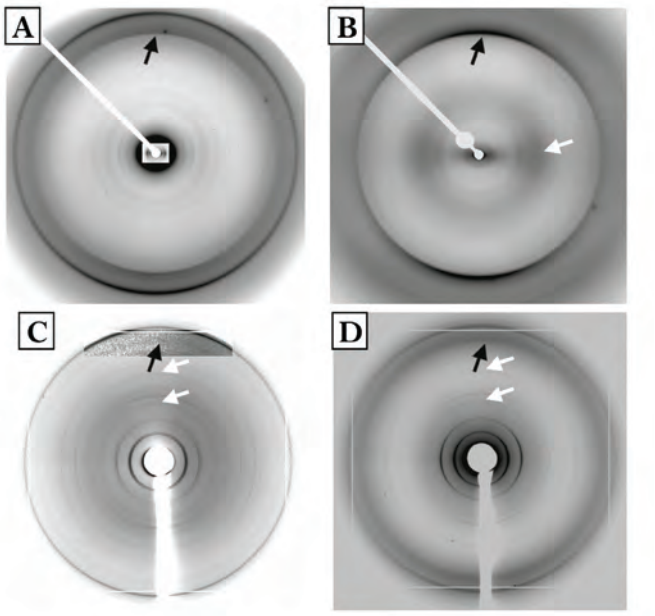

Figure 1.7. *Fiber diffraction patterns. Black arrows indicate cross-β meridional diffraction at close 4.8 Å resolution. The equatorial reflections do not identified are characteristic of lipids present in the preparations.* ***A.*** *SHaPrP27-30.* ***B.*** *RecSHaPrP(90-231) amyloid. White arrow indicates a broad equatorial diffraction at 10.5 Å, absent in A.* ***C.*** *MoPrP27-30 (RML strain). White arrows (also in D) show second and third orders of meridional 19.2 Å diffraction.* ***D.*** *Synthetic prion strain, MoSP1, derived from recPrP(89-230) amyloid, passaged twice through Tg9949 mice. (Modified from Wille H. et al. (2009)* [61]*)*

More recent studies [61] have obtained diffraction pattern from infectious prions that show cross-β diffraction (meridional intensity 4.8 Å). In MoPrP27-30 appears a pattern (meridional reflection of 19.2 Å, and its second, third and fourth order: 4.8 Å, 6.4 Å and 9.6 Å) which has been interpreted by the author as indicating the presence of a repeating unit that correspond to four β-strands. Further, it was found that recPrP amyloid differs from highly infectious PrP^{Sc} fibers from infected brains; also presents a strong equatorial intensity (approximately 10.5 Å) very typical of an amyloid structure, showing the existence of flat, parallel stacks β-strands separated by this distance. Such equatorial reflection is absent in PrP^{Sc} preparations. This difference suggests that PrP^{Sc} from brain-derived prions could have a cross-β structure different from the classic amyloid-β conformation; the most plausible structure would be a β-helical architecture. However, there are different equatorial intensities characteristic of diffraction from lipids or lipid-detergent assemblies due to the isolation process, which cast some doubts on the assignment of other reflections to the protein component of preparations (Figure 1.7).

1.3.5 Electron crystallography

The ultrastructure of PrP^{Sc} has also been analyzed using electron microscopy-based analysis of two-dimensional crystals of PrP27-30 [62][63]. These 2D crystals were discovered in some purified fractions of the PrP^{Sc}, showing a hexagonal lattice with dimensions of α and β= 6.9 nm and γ=120º, as determined by electron diffraction. The obtained data were analyzed by digital processing using a single particle analysis approach.

Through labelling with a sugar-specific nanogold derivative, the authors were able to localize the sugars in the periphery of the crystal subunit (Figure 1.8). Furthermore, in this study the 2D crystals of PrP^{Sc}106 (lacks residues 23-89 and 141-176) were also analyzed, it is the minimum sequence able to sustain conversion to PrP^{Sc} and is called miniprion [1]. PrP^{Sc}106 was obtained from PrP106-expressing transgenic mice infected with scrapie prions. PrP^{Sc}106 2D crystals are isomorphous to PrP27-30 ones and it was observed that the last 36 deleted residues, associated to a β-sheet structure are located at the inside of the oligomer. The authors concluded that PrP^{Sc} is formed by a parallel β-helix, since such structure would be the only one to fit to the hexagonal lattice dimensions.

They also observed interactions of heavy metal cations with the centre of the hexagons, providing a positive stain; it could be related with the presence of negative charges of the protein in that region. Furthermore, subsequent studies, analyzing the binding and interaction of different heavy metal salts with the protein revealed three different negative densities into the crystal subunit [63]. In essence, threefold symmetry seems to exist, coinciding with the location of the proposed parallel β-helix. The resolution of this technique is about 2 nm, which is just the diameter of the proposed β-helix. Therefore, it is not possible to provide any detail of higher resolution, just that their architecture might correspond to a solenoid.

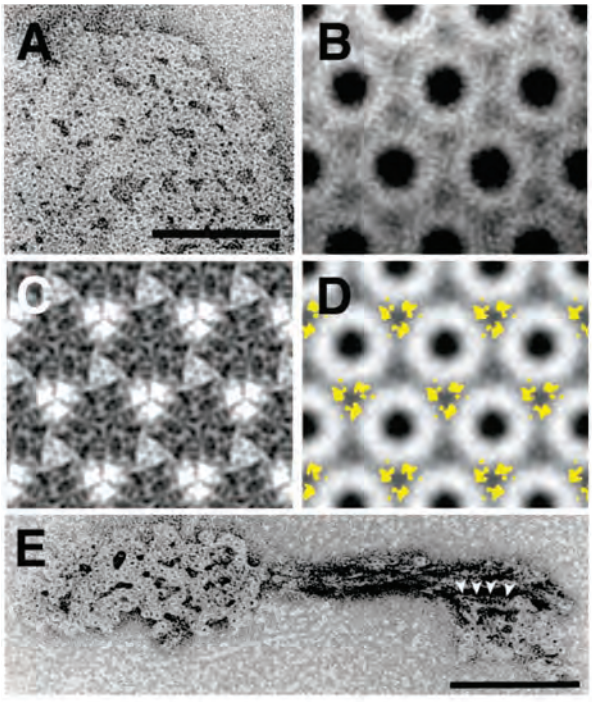

Figure 1.8. *2D crystals of PrP27-30.* ***A.*** *2D crystal of PrP27-30 stained with uranyl acetate showing an apparent hexagonal lattice.* ***B.*** *High view of a crystal after contrast transfer function and correlation-mapping and averaging.* ***C.*** *Subtraction map between unlabelled and labelled with nanogold (labelling the N-linked sugars) crystals, showing differences in lighter shades.* ***D.*** *Projection map of PrP27-30 with the sugars labelled outside (yellow).* ***E.*** *Typical rod with an aggregate of crystal subunits at each end. The scale bars are 100 nm. (Wille H. et al (2002) [62])*

1.3.6 Antibody mapping studies

With the aim to prove conformational transition in the formation of PrP^{Sc}, monoclonal antibodies and Fab fragments to several epitopes of PrP^{C} and PrP^{Sc} have been used [64][65].

In these antibody mapping studies, PrP^{C} and PrP27-20 in its native conformation and in denaturing conditions were studied to find out the exposure of the epitopes within the protein. The authors observed that epitopes in the N-terminal region (residues 90-120) were accessible in PrP^{C}, but stayed hidden in native PrP27-30. However, denaturation of PrP27-30 rendered accessible the epitopes of that region. The extreme C-terminal region of the prion protein is exposed on both PrP^{C} and PrP^{Sc}.

1.3.7 Chemical cross-linking

Chemical cross-linking, in combination with proteolytic digestion and mass spectrometric analysis is a good tool to obtain valuable information regarding the three-dimensional structure of proteins [66]. This technique is based on chemical modification process where a bifunctional

cross-linking reagent (cross-linker) reacts with specific groups in the protein, resulting in the formation of a covalent bond. Moreover, the cross-linker has a specific spacer length between its functional groups [66]. Then, the length of the spacer arm provides a maximum distance constraint between the two reacting residues.

A cross-linking study probing Syrian hamster PrP27-30 and using bis(sulfosuccinimidyl) suberate (BS^3), an agent that reacts with amino groups, showed that PrP27-30 is easily cross-linked with formation of dimers, trimers, and higher-order oligomers. Furthermore the study showed that that BS^3 reacted preferentially with G_{90} and a cross-link involving two G_{90} was found in cross-linked PrP27-30 dimers. These results indicated that in PrP27-30 aggregate exists a spatial proximity of G_{90} amino termini. The maximum possible spacer distance of this cross-linker (1.14 nm) between consecutive G_{90} amino termini suggested a two/three layer architecture in the PrP27-30 (note that one rung is 0.47 nm) [67]. However, four layers could also be a possibility if G_{90} are not "flush and rigid" but rather in short but flexible mini-tails.

1.3.8 Chemical surface labeling

A useful method to study the surface accessibility of the PrP^{Sc} is the chemical surface labeling. The relative reactivity of amino acids to a specific chemical, in native conformation of the protein, reflects the surface accessibility of the residues.

In a recent study, this approach was applied to find out locations of conformational change. Recombinant Syrian hamster PrP(90-231) and Syrian hamster PrP27-30 were treated with two chemical modifiers, tetranitromethane (TNM) and acetic anhydride (Ac_2O), which specifically target accessible tyrosine and lysine residues, respectively. Several differences in chemical reactivity were observed in specific locations within the common sequence of both isoforms of PrP. With TNM, the most conspicuous reactivity difference seen involves peptide E_{221}-R_{229} (containing Y_{225} and Y_{226}), which it was much more modified in recSHaPrP(90-231). Instead, peptides Y_{149}-R_{151}, Y_{157}-R_{164}, and R_{151}-Y_{162} suffered more extensive modifications in SHaPrP27-30. Ac_2O modified extensively peptide G_{90}-K_{106} and the amino terminus in both isoforms of PrP. These results suggested that the C-terminal region of the SHaPrP27-30 has lost part of the solvent accessibility of the residue Y_{225} and Y_{226}, which can means that the two C-terminal helices are tightly packed in this isoform, but, alternatively, that these C-terminal helices have disappeared in PrP^{Sc}, transformed into β-sheet. On the other hand, the stretch spanning approximately Y_{149}-R_{164} is also more accessible in SHaPrP27-30, suggesting rearrangements in α-helix H1 and the short β-sheet of recSHaPrP(90-231). The last conclusion is the N-terminal region of SHaPrP27-30 is very accessible [68].

Besides, this method can be combined with antibody-based detection, to identify accessible amino acids and differentiate between PrP isoforms or even prion strains, without the use of PK [69].

1.3.9 Hydrogen-deuterium exchange (H/D)

H/D exchange is a chemical reaction in which a covalently bonded hydrogen atom is replaced by a deuterium atom. This reaction is the basis of a method that provides information about the solvent accessibility and tertiary structure of proteins. Backbone amide hydrogens located within the unstructured region of PrP^{Sc} exchange quickly with solvent deuterium, whereas in those placed in α-helices the hydrogen exchange rate decrease, and in those located in β-sheets it becomes exceedingly slow, as such hydrogen atoms are tightly held in place by bonding to N and O (CO) atoms.

Different surveys of H/D exchange coupled to mass spectrometry, in the structure of amyloid fibrils formed by the recombinant PrP, have been performed [70][71]. However, recently it was published a study on GPI-less PrP^{Sc} [44]. It was showed that the C-terminal half of GPI-less PrP^{Sc} exhibits extremely low rates of H/D exchange, which is typical of stretches with extensive H-bonding (β-sheet) and the whole 90-215 stretch is relatively resistant to exchange. Some stretches exhibiting a somewhat higher exchange rate, suggested to partially overlap with loops/turns, such as 133-148 or 81-118. Therefore, it was concluded that GPI-less PrP^{Sc} consists of a series of β-sheet stretches connected by short loops and/or turns.

1.4 Structural models of PrP^{Sc}

The above data and other structural experiments have been used to develop structural models of PrP^{Sc}. In the last decade, two models of a prion protofibril have been suggested: β-helix model [72] and β-spiral model [73].

1.4.1 β-helical model

The discovery of 2D crystals of PrP27–30 and PrP^{Sc}106 [62][63] along with threading the PrP sequence through a known β-helix fold have allowed the development of a plausible model termed β-helical model [72]. This model suggests that PrP27-30 displays a central parallel left-handed β-helix formed by the residues 89-175, the C-terminal region (residues 176-227) retains the α-helical conformation and is located on the outside together with the sugars moieties. Furthermore, the segment encompassing residues 141-176 is a long unstructured loop. The symmetry of this model is based on trimeric arrangement, where three of such β-helical subunits pack tightly through lateral associations to form a trimer. The vertical stacking of these trimers occurs by hydrogen bonds, through head-to-tail-arrangement.

Nonetheless, there is also evidence that the β-helix model cannot be fully correct. Three parallel left-handed β-helices trimerize at the level of their β-helix, providing a natural template to assemble three monomers, but the electron microscopy data disagree with this feature, because the width of PrP^{Sc} is 3-5 nm and the trimer is wider [50]. Furthermore, from limited proteolysis

studies it is possible to observe which residues participate in the β-strand formation, and in currently studies new cleavage points have been found, so that it is possible that PrP^{Sc} may have more loops or/and these are located in different places that in the β-helix model [40]. Also, treatment with BS^3 [67] and Ac_2O [68] show that the amino termini of PrP27-30 are very solvent exposed, in contrast with their internal location in the model. Also, other problem is that the threading, based on the structure of the β-helical part of trimeric carbonic anhydrase from *Methanosarcina thermophila* is very arbitrary

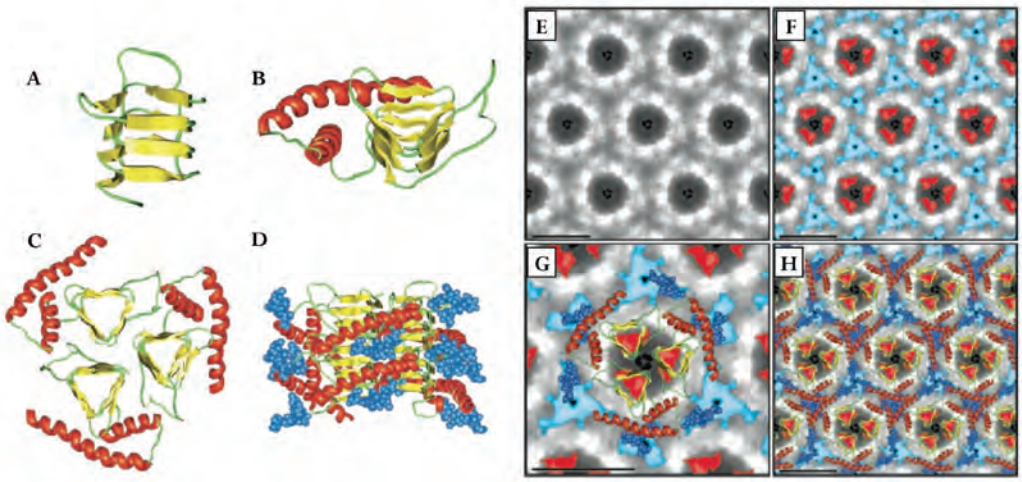

Figure 1.9. *β-helical structural model of PrP^{Sc}.* ***A.*** *Residues 89-174 of PrP are threaded onto a left-handed β-helical fold (yellow).* ***B.*** *Model of the monomer of PrP27-30. The α-helices (residues 177-227) are shown in red.* ***C.*** *Trimeric model of PrP27-30 built by superimposing three monomeric models.* ***D.*** *Fibrilization. Two trimers of PrP27-30 are assembling through polar backbone interactions between the lower β-helical rung of the top trimer disc and the upper rung of the bottom trimer. The sugars linked to N180 and N196 are shown like blue spheres and they are extended away from the centre of the structure.* ***E.*** *Projection map of 2D crystals of PrP27-30.* ***F.*** *Differences between PrP27-30 and PrP^{Sc}106. The differences attributed to the internal deletion of PrP^{Sc}106 (residues 141-176) are depicted in red; the differences in glycosylation are shown in blue.* ***G.*** *Superimposition of the trimeric left-handed β-helical model with the electron microscopy map of the PrP27-30 2D crystals. Scale bar is 50 Å.* ***H.*** *The scaled trimeric model was copied onto the neighbouring units of the crystals to show the crystallographic packing suggested by the model. Scale bar is 50 Å. (Adapted from Govaerts et al. (2004) [72])*

In summary, while the solenoid-like basic architecture of individual PrP^{Sc} monomers seems very reasonable, the trimeric arrangement is very likely to be the result of tight packing to form the 2D crystals from individual PrP^{Sc} monomers that are in equilibrium with the fibers.

1.4.2 Spiral model

This model derives from a molecular dynamics simulation of the prion protein under amyloidogenic conditions. The spiral model proposes a spiralling core of extended β-sheets formed by three parallel stranded sheets, spanning through the following regions: residues 116-

119, 129-132 and 160-164; and one isolated one, comprising the residues 135-140, although this last one is connected to the three-stranded sheet, forming a continuous four-stranded sheet. Then, a spiraling protofibril with a three-fold symmetry is formed. Furthermore, the glycosylation sites are exposed, the N and C-terminal regions are accessible with a protected core of more tightly packed β-strands [73].

The spiral model is consistent with a wide variety of low-resolution experimental data; but there is a critical constraint that makes it impossible; TEM (this thesis, Chapter 4) and fiber X-ray diffraction data [61] show that PrP^{Sc} fibers contain a cross-β stack of β-strands, that means β-strands are completely parallel to the axis of fiber growth.

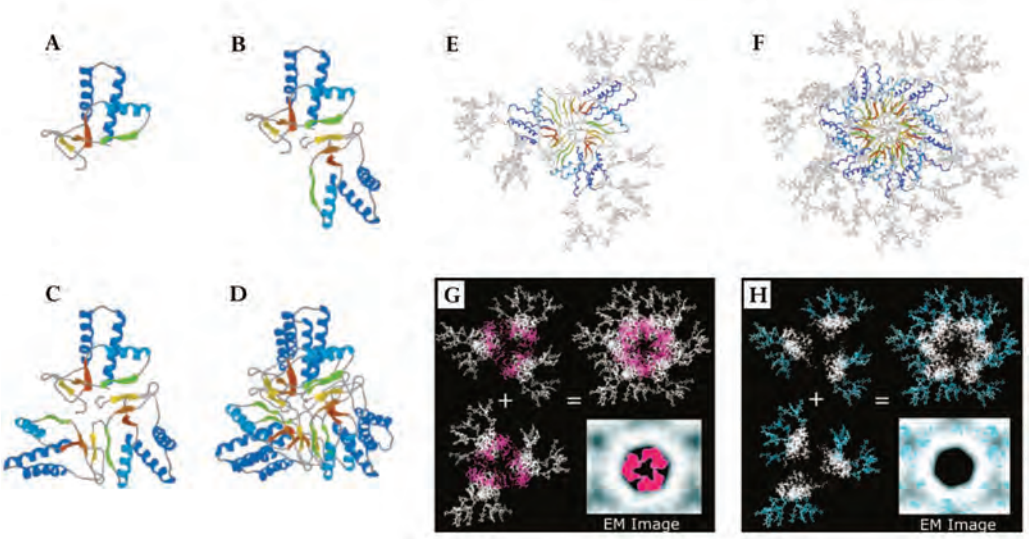

Figure 1.10. *Spiral model of the structure of PrP^{Sc}.* ***A-B.*** *Building of a protofibril with a three-fold symmetry. The oligomerization occurs between the isolated β-sheet (fourth) and the first β-sheet of the adjacent monomer.* ***C-D.*** *Views of hexameric representation of protofibril showing the maintenance of symmetry on oligomerization and forming a spiralling core of extended sheets.* ***E.*** *Modeled protofibril (hexamer) with the diglycosylated subunits.* ***F.*** *Superimposition of two hexamers rotated 60° from one another around the fiber axis replicates the 6-fold symmetry of the crystals.* ***G.*** *Representation of a superimposing of two hexamers as in figure F. Residues 142-176 (magenta) represent the residues deleted from PrP27-30 to form PrP^{Sc}106. α-helices and sugar groups are shown in white. The EM image is a difference map between PrP^{Sc}106 and PrP27-30 with differences shown in magenta.* ***H.*** *The same figure as G, but in this case the EM image is a difference map between PrP^{Sc}106 and PrP27-30 with differences in the glycosylation. Sugars are shown in cyan colour. (Adapted from DeMarco ML. et al. (2004) [73])*

As it can be seen from the above discussion, although theoretical models for PrP^{Sc} have been proposed, there is an insufficient amount of experimental data to reach a definitive consensus.

It should be noted that there is a structural model that could help to understand the structure of mammalian prions. HET-s is a protein of the filamentous fungus *Podospora anserina*, which forms a prion that plays a role in heterokaryon incompatibility and it has some similarities with PrP^{Sc}. It

has a PK-resistant core like PrP^{Sc} and its structure, derived from NMR, forms a left-handed β-solenoid, with each molecule forming two helical windings, a triangular hydrophobic core, at least 23 hydrogen bonds, three salt bridges and two asparagine ladders. Furthermore HET-s protofibrils are also approximately 5 nm wide [55]. It is likely that the structure of PrP^{Sc} might have a lot of common with this one, as will be discussed later.

1.5 Aim of this thesis

Elucidation of the structure of the mammalian prions continues to be one the major and difficult challenges in prion research due to their insoluble nature and heterogeneity. Molecular basis of the biology of PrP^{Sc}, such as the molecular mechanism of prion replication and aggregation, the species barrier and the pathogenesis of neurodegeneration will not be understood until the structure is solved. No less crucial is the fact that the knowledge of the structure of PrP^{Sc} will provide the essential clues to develop therapies for the treatment of prion diseases.

For this reason, the aim of the thesis is focused on the pursuit of conformational constraints through the study of the GPI-anchorless PrP^{Sc}, mainly, and wild type PrP^{Sc} by different techniques such as limited proteolysis coupled with high-resolution electrophoresis and mass spectrometry, electron microscopy and computational 3D reconstruction, in order to find out the real structure of the scrapie prion protein.

1.6 Outline of the thesis

In chapter 1 some background information, and the aim and outline of the thesis have been presented. As described in the introduction of this thesis, because of the insolubility of PrP^{Sc} and the failure to crystallize the heterogeneous PrP^{Sc} multimers, the application of high-resolution analytical techniques has not been possible, so that only lower resolution instrumental techniques have provided some information about the structure of PrP^{Sc}. Furthermore the high heterogeneity derived from the GPI moiety and the carbohydrates contained in its C-terminal region hamper such analysis.

To solve the presented problem and extend my studies of the structure of PrP^{Sc}, I have used transgenic (tg) mice expressing PrP^{C} lacking the GPI anchor; they were provided by Bruce Chesebro from the Rocky Mountain Laboratories, NIH, Montana, USA [54]. GPI-less PrP^{Sc} produced by these mice, when infected with wt prions, is infectious, lacks the GPI anchor, and is largely unglycosylated, which reduces the heterogeneity in the C-terminal portion of the molecule. The description of these mice, the generation of the PrP^{Sc} and the method of isolation are given in great detail in chapter 2. In this chapter, it is also described the generation of wild-type PrP^{Sc} from Syrian hamster.

Chapter 3 briefly explain the basis of the limited proteolysis technique [41] that it is combined with high-resolution electrophoresis, called Tricine-SDS-PAGE [74] and two different methods of mass spectrometry, MALDI (matrix-assisted laser desorption/ionization)–TOF (time of flight) and nano-LC-ESI (electrospray ionization)-Qq (double quadrupole)-TOF , to allow an accurate detection an location of flexible, proteinase K susceptible regions. The obtained results are presented and discussed meticulously. It is worth noting that I have been able to survey the whole structure of PrP^{Sc} thanks to the GPI-less tg mice.

Chapter 4 introduces the general principles of the different electron microscopy techniques. These techniques were used to study the ultrastructure of PrP^{Sc}. As the previous chapter and continuing the thread of my studies, the experiments were realized with the fibers of GPI-less PrP^{Sc}. This protein has allowed the improvement of the isolation method, so I have got the adequate sample, without any artefacts, to be analyzed by microscopy and subsequently to use computational 3D reconstruction. It is very important to mention that these studies were made possible by the collaboration of different research groups from many diverse fields of knowledge: Dr. Matthijn Vos, from the FEI Company, Eindhoven, The Netherlands; and Dr. Howard S. Young, Dr. Ludovic Renault and Dr. Holger Wille, from the University of Alberta, Edmonton, Canada.

In the chapter 5 is presented a common discussion, taken together all the results obtaining during this research. Furthermore, it is described an approach to a new model of the PrP^{Sc} structure.

Four appendices are enclosed in the chapter 6. The first appendix explain an inconsistency, founded during the experiments by mass spectrometry (MS), in the sequence of the GPI-anchorless PrP described previously by Chesebro B. *et al.* [54]. The second appendix shows the different peaks obtained by MS techniques, subsequently used to calibrate the GPI-less PrP^{Sc} MALDI-TOF spectrum. Abbreviations used in this document and a compilation of the publications and participation in conferences during the thesis are also annexed in this last chapter.

1.7 References

1. Prusiner SB (1998) Prions. Proc. Natl. Acad. Sci. U.S.A. 95: 13363–13383.

2. Williams ES, Young S (1980) Chronic wasting disease of captive mule deer: a spongiform encephalopathy. J. Wildl. Dis. 16: 89–98.

3. Wells GA, Scott AC, Johnson CT, Gunning RF, Hancock RD, et al. (1987) A novel progressive spongiform encephalopathy in cattle. Vet. Rec. 121: 419–420.

4. Marsh RF, Hadlow WJ (1992) Transmissible mink encephalopathy. Rev. Sci. Tech 11: 539–550.

5. Jeffrey M, Wells GAH (1988) Spongiform Encephalopathy in a Nyala (Tragelaphus angusi). Veterinary Pathology 25: 398–399.

6. Gajdusek DC, ZIGAS V (1957) Degenerative disease of the central nervous system in New Guinea; the endemic occurrence of kuru in the native population. N. Engl. J. Med. 257: 974–978.

7. Masters CL, Gajdusek DC, Gibbs CJ (1981) Creutzfeldt-Jakob disease virus isolations from the Gerstmann-Sträussler syndrome with an analysis of the various forms of amyloid plaque deposition in the virus-induced spongiform encephalopathies. Brain 104: 559–588.

8. Colby DW, Prusiner SB (2011) Prions. Cold Spring Harb Perspect Biol 3: a006833.

9. Will RG, Ironside JW, Zeidler M, Cousens SN, Estibeiro K, et al. (1996) A new variant of Creutzfeldt-Jakob disease in the UK. Lancet 347: 921–925.

10. Alper T, Cramp WA, Haig DA, Clarke MC (1967) Does the agent of scrapie replicate without nucleic acid? Nature 214: 764–766.

11. Griffith JS (1967) Self-replication and scrapie. Nature 215: 1043–1044.

12. Bolton DC, McKinley MP, Prusiner SB (1982) Identification of a protein that purifies with the scrapie prion. Science 218: 1309–1311.

13. McKinley MP, Bolton DC, Prusiner SB (1983) A protease-resistant protein is a structural component of the scrapie prion. Cell 35: 57–62.

14. Prusiner SB (1982) Novel proteinaceous infectious particles cause scrapie. Science 216: 136–144.

15. Oesch B, Westaway D, Wälchli M, McKinley MP, Kent SB, et al. (1985) A cellular gene encodes scrapie PrP 27-30 protein. Cell 40: 735–746.

16. Chesebro B, Race R, Wehrly K, Nishio J, Bloom M, et al. (1985) Identification of scrapie prion protein-specific mRNA in scrapie-infected and uninfected brain. Nature 315: 331–333.

17. Basler K, Oesch B, Scott M, Westaway D, Wälchli M, et al. (1986) Scrapie and cellular PrP isoforms are encoded by the same chromosomal gene. Cell 46: 417–428.

18. Pan KM, Baldwin M, Nguyen J, Gasset M, Serban A, et al. (1993) Conversion of alpha-helices into beta-sheets features in the formation of the scrapie prion proteins. Proc. Natl. Acad. Sci. U.S.A. 90: 10962–10966.

19. Jarrett JT, Lansbury PT (1993) Seeding "one-dimensional crystallization" of amyloid: a pathogenic mechanism in Alzheimer's disease and scrapie? Cell 73: 1055–1058.

20. Silveira JR, Raymond GJ, Hughson AG, Race RE, Sim VL, et al. (2005) The most infectious prion protein particles. Nature 437: 257–261.

21. Tixador P, Herzog L, Reine F, Jaumain E, Chapuis J, et al. (2010) The physical relationship between infectivity and prion protein aggregates is strain-dependent. PLoS Pathog. 6: e1000859.

22. Makarava N, Kovacs GG, Savtchenko R, Alexeeva I, Budka H, et al. (2011) Genesis of mammalian prions: from non-infectious amyloid fibrils to a transmissible prion disease. PLoS Pathog. 7: e1002419.

23. Makarava N, Kovacs GG, Savtchenko R, Alexeeva I, Ostapchenko VG, et al. (2012) A new mechanism for transmissible prion diseases. J. Neurosci. 32: 7345–7355.

24. Weissmann C (2004) The state of the prion. Nat. Rev. Microbiol. 2: 861–871.

25. Caughey BW, Dong A, Bhat KS, Ernst D, Hayes SF, et al. (1991) Secondary structure analysis of the scrapie-associated protein PrP 27-30 in water by infrared spectroscopy. Biochemistry 30: 7672–7680.

26. Riek R, Hornemann S, Wider G, Billeter M, Glockshuber R, et al. (1996) NMR structure of the mouse prion protein domain PrP(121-231). Nature 382: 180–182.

27. Riek R, Hornemann S, Wider G, Glockshuber R, Wüthrich K (1997) NMR characterization of the full-length recombinant murine prion protein, mPrP(23-231). FEBS Lett. 413: 282–288.

28. Liu H, Farr-Jones S, Ulyanov NB, Llinas M, Marqusee S, et al. (1999) Solution structure of Syrian hamster prion protein rPrP(90-231). Biochemistry 38: 5362–5377.

29. Zahn R, Liu A, Lührs T, Riek R, Schroetter von C, et al. (2000) NMR solution structure of the human prion protein. Proc. Natl. Acad. Sci. U.S.A. 97: 145–150.

30. Knaus KJ, Morillas M, Swietnicki W, Malone M, Surewicz WK, et al. (2001) Crystal structure of the human prion protein reveals a mechanism for oligomerization. Nat. Struct. Biol. 8: 770–774.

31. López Garcia F, Zahn R, Riek R, Wüthrich K (2000) NMR structure of the bovine prion protein. Proc. Natl. Acad. Sci. U.S.A. 97: 8334–8339.

32. Safar J, Wille H, Itri V, Groth D, Serban H, et al. (1998) Eight prion strains have PrP(Sc) molecules with different conformations. Nat. Med. 4: 1157–1165.

33. Pastrana MA, Sajnani G, Onisko B, Castilla J, Morales R, et al. (2006) Isolation and characterization of a proteinase K-sensitive PrPSc fraction. Biochemistry 45: 15710–15717.

34. Sajnani G, Silva CJ, Ramos A, Pastrana MA, Onisko BC, et al. (2012) PK-sensitive PrP Is Infectious and Shares Basic Structural Features with PK-resistant PrP. PLoS Pathog. 8: e1002547.

35. Bessen RA, Marsh RF (1994) Distinct PrP properties suggest the molecular basis of strain variation in transmissible mink encephalopathy. Journal of Virology 68: 7859–7868.

36. Kocisko DA, Lansbury PT, Caughey B (1996) Partial unfolding and refolding of scrapie-associated prion protein: evidence for a critical 16-kDa C-terminal domain. Biochemistry 35: 13434–13442.

37. Bartz JC, Bessen RA, McKenzie D, Marsh RF, Aiken JM (2000) Adaptation and selection of prion protein strain conformations following interspecies transmission of transmissible mink encephalopathy. Journal of Virology 74: 5542–5547.

38. Zou W-Q, Capellari S, Parchi P, Sy M-S, Gambetti P, et al. (2003) Identification of novel proteinase K-resistant C-terminal fragments of PrP in Creutzfeldt-Jakob disease. J. Biol. Chem. 278: 40429–40436.

39. Zanusso G, Farinazzo A, Prelli F, Fiorini M, Gelati M, et al. (2004) Identification of distinct N-terminal truncated forms of prion protein in different Creutzfeldt-Jakob disease subtypes. J. Biol. Chem. 279: 38936–38942.

40. Sajnani G, Pastrana MA, Dynin I, Onisko B, Requena JR (2008) Scrapie prion protein structural constraints obtained by limited proteolysis and mass spectrometry. J. Mol. Biol. 382: 88–98.

41. Hubbard SJ (1998) The structural aspects of limited proteolysis of native proteins. Biochim. Biophys. Acta 1382: 191–206.

42. Parchi P, Zou W, Wang W, Brown P, Capellari S, et al. (2000) Genetic influence on the structural variations of the abnormal prion protein. Proc. Natl. Acad. Sci. U.S.A. 97: 10168–10172.

43. Baron GS, Hughson AG, Raymond GJ, Offerdahl DK, Barton KA, et al. (2011) Effect of glycans and the glycophosphatidylinositol anchor on strain dependent conformations of scrapie prion protein: improved purifications and infrared spectra. Biochemistry 50: 4479–4490.

44. Smirnovas V, Baron GS, Offerdahl DK, Raymond GJ, Caughey B, et al. (2011) Structural organization of brain-derived mammalian prions examined by hydrogen-deuterium exchange. Nat. Struct. Mol. Biol. 18: 504–506.

45. Caughey B, Raymond GJ, Bessen RA (1998) Strain-dependent differences in beta-sheet conformations of abnormal prion protein. J. Biol. Chem. 273: 32230–32235.

46. Merz PA, Somerville RA, Wisniewski HM, Iqbal K (1981) Abnormal fibrils from scrapie-infected brain. Acta Neuropathol. 54: 63–74.

47. Merz PA, Somerville RA, Wisniewski HM, Manuelidis L, Manuelidis EE (1983) Scrapie-associated fibrils in Creutzfeldt-Jakob disease. Nature 306: 474–476.

48. Prusiner SB, McKinley MP, Bowman KA, Bolton DC, Bendheim PE, et al. (1983) Scrapie prions aggregate to form amyloid-like birefringent rods. Cell 35: 349–358.

49. McKinley MP, Braunfeld MB, Bellinger CG, Prusiner SB (1986) Molecular characteristics of prion rods purified from scrapie-infected hamster brains. J. Infect. Dis. 154: 110–120.

50. Sim VL, Caughey B (2009) Ultrastructures and strain comparison of under-glycosylated scrapie prion fibrils. Neurobiol. Aging 30: 2031–2042.

51. Godsave SF, Wille H, Kujala P, Latawiec D, DeArmond SJ, et al. (2008) Cryo-immunogold electron microscopy for prions: toward identification of a conversion site. J. Neurosci. 28: 12489–12499.

52. Meyer RK, McKinley MP, Bowman KA, Braunfeld MB, Barry RA, et al. (1986) Separation and properties of cellular and scrapie prion proteins. Proc. Natl. Acad. Sci. U.S.A. 83: 2310–2314.

53. McKinley MP, Meyer RK, Kenaga L, Rahbar F, Cotter R, et al. (1991) Scrapie prion rod formation in vitro requires both detergent extraction and limited proteolysis. Journal of Virology 65: 1340–1351.

54. Chesebro B, Trifilo M, Race R, Meade-White K, Teng C, et al. (2005) Anchorless prion protein results in infectious amyloid disease without clinical scrapie. Science 308: 1435–1439.

55. Wasmer C, Lange A, Van Melckebeke H, Siemer AB, Riek R, et al. (2008) Amyloid fibrils of the HET-s(218-289) prion form a beta solenoid with a triangular hydrophobic core. Science 319: 1523–1526.

56. Jiménez JL, Guijarro JI, Orlova E, Zurdo J, Dobson CM, et al. (1999) Cryo-electron microscopy structure of an SH3 amyloid fibril and model of the molecular packing. EMBO J. 18: 815–821.

57. Pepys MB (2006) Amyloidosis. Annu. Rev. Med. 57: 223–241.

58. Chiti F, Dobson CM (2006) Protein misfolding, functional amyloid, and human disease. Annu. Rev. Biochem. 75: 333–366.

59. Eanes ED, Glenner GG (1968) X-ray diffraction studies on amyloid filaments. J. Histochem. Cytochem. 16: 673–677.

60. Nguyen JT, Inouye H, Baldwin MA, Fletterick RJ, Cohen FE, et al. (1995) X-ray diffraction of scrapie prion rods and PrP peptides. J. Mol. Biol. 252: 412–422.

61. Wille H, Bian W, McDonald M, Kendall A, Colby DW, et al. (2009) Natural and synthetic prion structure from X-ray fiber diffraction. Proc. Natl. Acad. Sci. U.S.A. 106: 16990–16995.

62. Wille H, Michelitsch MD, Guenebaut V, Supattapone S, Serban A, et al. (2002) Structural studies of the scrapie prion protein by electron crystallography. Proc. Natl. Acad. Sci. U.S.A. 99: 3563–3568.

63. Wille H, Govaerts C, Borovinskiy A, Latawiec D, Downing KH, et al. (2007) Electron crystallography of the scrapie prion protein complexed with heavy metals. Arch. Biochem. Biophys. 467: 239–248.

64. Peretz D, Williamson RA, Matsunaga Y, Serban H, Pinilla C, et al. (1997) A conformational transition at the N terminus of the prion protein features in formation of the scrapie isoform. J. Mol. Biol. 273: 614–622.

65. Williamson RA, Peretz D, Pinilla C, Ball H, Bastidas RB, et al. (1998) Mapping the prion protein using recombinant antibodies. Journal of Virology 72: 9413–9418.

66. Sinz A (2003) Chemical cross-linking and mass spectrometry for mapping three-dimensional structures of proteins and protein complexes. J Mass Spectrom 38: 1225–1237.

67. Onisko B, Fernández EG, Freire ML, Schwarz A, Baier M, et al. (2005) Probing PrPSc structure using chemical cross-linking and mass spectrometry: evidence of the proximity of Gly90 amino termini in the PrP 27-30 aggregate. Biochemistry 44: 10100–10109.

68. Gong B, Ramos A, Vázquez-Fernández E, Silva CJ, Alonso J, et al. (2011) Probing structural differences between PrP(C) and PrP(Sc) by surface nitration and acetylation: evidence of conformational change in the C-terminus. Biochemistry 50: 4963–4972.

69. Silva CJ (2012) Using small molecule reagents to selectively modify epitopes based on their conformation. Prion 6: 163–173.

70. Lu X, Wintrode PL, Surewicz WK (2007) Beta-sheet core of human prion protein amyloid fibrils as determined by hydrogen/deuterium exchange. Proc. Natl. Acad. Sci. U.S.A. 104: 1510–1515.

71. Nazabal A, Hornemann S, Aguzzi A, Zenobi R (2009) Hydrogen/deuterium exchange mass spectrometry identifies two highly protected regions in recombinant full-length prion protein amyloid fibrils. J Mass Spectrom 44: 965–977.

72. Govaerts C, Wille H, Prusiner SB, Cohen FE (2004) Evidence for assembly of prions with left-handed beta-helices into trimers. Proc. Natl. Acad. Sci. U.S.A. 101: 8342–8347.

73. DeMarco ML, Daggett V (2004) From conversion to aggregation: protofibril formation of the prion protein. Proc. Natl. Acad. Sci. U.S.A. 101: 2293–2298.

74. Schägger H (2006) Tricine-SDS-PAGE. Nat Protoc 1: 16–22.

2

Generation of PrP^{Sc}

Abstract

In this chapter the animal models used for the generation of PrP^{Sc} and the techniques to obtain the prion protein are presented. Prion disease was caused in two animal models, Syrian hamsters and GPI-anchorless PrP transgenic mice, with the aim of removing the scrapie-infected brain to obtain the PrP^{Sc}. Two different manners of working with the prion protein are described, such as brain homogenate or purified protein. With all of these remarks, it is worth noting that this chapter is very important for understanding of the following studies, because of this material will be used in different sort of experiments, applying from low to higher resolution techniques, with the purpose to obtain new insights on the PrP^{Sc} structure.

2.1 Introduction

Prion PrP^{Sc} has to be generated from the brains of infected laboratory animals, typically mice and hamsters, it is obtained as an insoluble aggregate and sufficient amounts for structural studies are required.

In the last years, there have been great advances in the generation of PrP^{Sc} *in vitro*. Infectious recombinant PrP fibers have been produced, nevertheless their infectivity was, for initial preparations, orders of magnitude lower than that of PrP^{Sc} [1][2][3][4][5]. Other studies have used Protein Misfolding Cyclic Amplification (PMCA) technique to induce the formation of prion infectivity *in vitro* [6][7], in these studies transmissible diseases were generated after long incubation time.

Hitherto, it was impossible to prepare recombinant PrP^{Sc} *in vitro* with the same properties of naturally occurring PrP^{Sc}. This suggests that the structure of these molecules is significantly different to the PrP^{Sc}, a suspicion that is further supported by the observation of key differences in sensitivity to proteases and infrared spectra. However, during the course of my thesis, it was published the most interesting survey in the generation of recombinant PrP^{Sc} [8], the authors were capable of synthesizing a highly infectious prion protein from recombinant PrP using PMCA in the presence of lipids and RNA, with the same features of the PrP^{Sc}: aggregated, protease-resistant, self-perpetuating and with the same incubation times of the disease. But this material has only been obtained in small amounts, which are not enough to structural studies.

It should be noted that the demonstration of infectivity of recombinant PrP^{Sc}, even if modest or in small amount, is a very important advance in its own right. To date, it has been disappointing from the perspective of facilitating structural studies. Nevertheless, thanks to the last studies, the future is very encouraging, because with the development of new technologies and strategies, we may get a recombinant PrP that mimic the characteristic of the PrP^{Sc}, in large amounts.

2.2 Animal model

All animal studies were authorized by the University of Santiago Ethical Committee, and complied with EU regulation 2003/65/CE.

2.2.1 Syrian hamsters

The Syrian hamster (*Mesocricetus auratus*) is a useful model for biochemical studies because it has two particular advantages, the incubation period of the disease is shorter and the infectivity titre in brain is higher that those found in mouse [9].

Hamsters were inoculated intracerebrally or intraperitoneally, depending on the strain to be inoculated. All inocula were prepared to 2 % in phosphate buffered saline (PBS) from brains taken from clinically affected hamsters, infected with Drowsy (Dy) or 263K. The intracerebral incoculation was carried out in animals of 4 weeks of age under anesthesia; the anesthetic solution was Xylazine-Ketamine (1.5 µg/µl-13.5 µg/µl respectively; 10-14 µl/g hamster) via intraperitoneal injection. Then, 20 µl of inoculum were injected in the frontal lobe of brain. Hamsters started to develop clinical signs and were culled within 70-90 days. The intraperitoneal inoculation was in animals with more than one month of age. By this via 100 µl of inoculum were injected, but only 263K strain can be inoculated in this way, because Dy strain does not lead to development of the disease when is inoculated intraperitoneally. Hamsters started to have clinical signs and were euthanized within 90-110 days.

The disease has two phases, latency phase where the hamster is incubating the disease, without clinical signs; and the clinical phase when the hamster exhibits different signs such as aggressiveness, ataxia, reactivity, head bobbing and tremor, until dead unless it is humanely culled. In the terminal phase, there is enough protein accumulated in the brain and hamster is killed with CO_2 euthanasia method, and dissected for the brain extraction. Hamster brains were collected and kept frozen at -80 ºC until use.

2.2.2 GPI-anchorless PrP transgenic mice

To study the GPI (glycosylphosphatidylinositol) function on pathogenesis of prion disease, GPI-anchorless PrP transgenic mice were generated. These mice were built using PrP (-/-) mice and their level of PrP mRNA expression in the brain in the heterozygous lines, was half that in C57BL/6 control mice [10]. PrP encoded by the transgene lacks the GPI anchor and contains the amino acids (23-232), like wild-type PrP after removal of the signal peptide and the C-terminal sequence, but with one amino acid serine (S) more in its sequence (see Chapter 6, appendix I). After scrapie infection, heterozygous mice expressing only anchorless PrP developed high titres of prion infectivity, however clinical signs were not seen after more than 600 days of incubation. Homozygous anchorless PrP transgenic mice expressed two-fold more anchorless PrP than heterozygous and scrapie infection induced a fatal disease after 300 to 480 days post-infection [11].

For my study, these transgenic mice expressing PrP lacking the GPI membrane anchor are very interesting because in the absence of the GPI anchor, PrP is not properly glycosylated by the cell machinery and therefore the PrP^{C} protein is mainly in the unglycosylated form. Thereby, I can work without the peptide heterogeneity resulting from the GPI and the carbohydrates, and I can use techniques previously impossible to implement due to this feature of the PrP.

Transgenic heterozygous GPI-anchorless PrP mice (tg44+/-) were generously provided by Bruce Chesebro, from the Rocky Mountain Laboratories, NIH, Montana, USA. Unfortunately, due to logistical problems, the females provided did not breed and that as they grew too old, we decided to cross the heterozygous GPI-anchorless PrP males with wild-type PrP (+/+) females

on the C57BL/10 background, in order to obtain homozygous GPI-less PrP line. From this crossing, two genotypes were obtained with or without the transgene and the endogenous mouse PrP gene. Then, the mice with the transgene (GPI-less) and the endogenous PrP allele were crossed to obtain homozygous GPI-anchorless mice. These mice express two anchorless PrP transgene alleles and no wild-type mouse PrP allele. Homozygous GPI-less mice were interbred to create additional mice for experimentation and to maintain the transgenic homozygous GP-anchorless line (Figure 2.1 A).

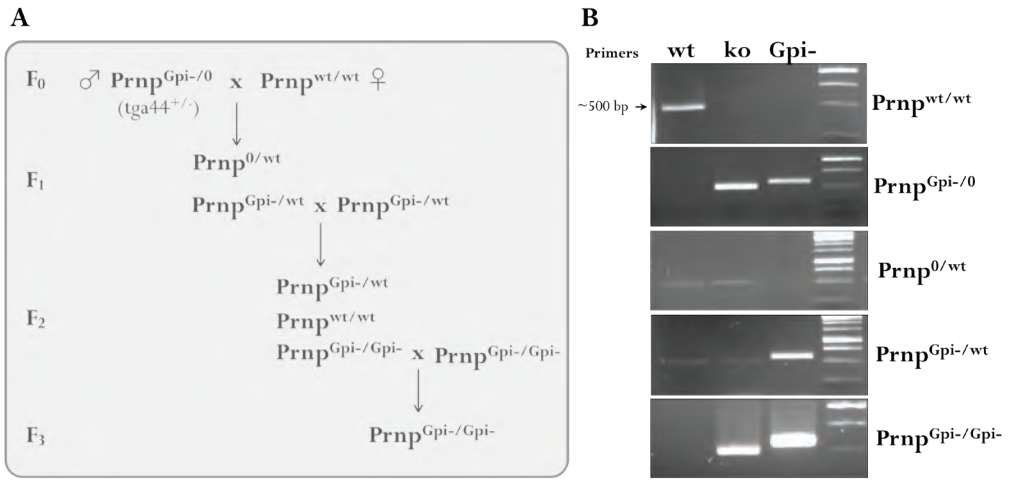

Figure 2.1. A. *GPI-anchorless transgenic mice family tree. The different generations and crossbreeds to obtain the homozygous GPI-less mice are represented.* ***B.*** *Mice genotyping corresponding to the each different cross, images of the PCR are shown with the three sets of primers.*

Mice were genotyped using three DNA PCR test on tail DNA. The DNA was extracted by using the Realpure DNA genomic extraction kit (Durviz, s.l.u, Valencia, Spain), according to the manufacturer's instructions. Primers for GPI-anchorless transgene: upper oligo 624 (5'AACCGTTACCCACCTCAGGGT3'), lower oligo 2037 (5'CAGGGCGCCTCGAGACGC GTCA3'). The set of oligonucleotide primers for PrP null allele specific for a portion of the neomycin resistance gene: upper oligo 1179 (5'GATGGATTGCACGCAGGTTC3') and lower oligo 1180 (5'TTGAGCCTGGCGAACAGTTC3'). Endogenous mouse PrP was amplified using: upper oligo 2057 (5'CCAAGGAGGGGGTACCCAT3'), lower oligo 2038 (5'TCCCACGATCAGGAAGATGAG3') [10]. The PCR reactions were performed following to the manufacturer's instructions, in a volume of 10 µl containing 0.1 units of PrimeSTAR HS DNA Polymerase (Takara Bio Inc., Otsu, Japan) and 100 ng of DNA. Amplification was carried out by cycling 27 times for 1 min at 94 ºC, 30 sec at 60 ºC and 1 min at 72 ºC. The PCR products were separated in agarose gels to 1.2 % in 1X TAE buffer (Figure 2.1 B). It is worth noting that I have had overlap problems between primers, as can be seen in figure 2.1 B; the primer set of null allele (ko) is able to amplify the GPI-anchorless transgene ($Prnp^{Gpi-}$). I have not found a satisfactory explanation for this and I have tried to solve that problem without

success. However, due to the kind of crossbreeds, after the F_0 generation it is not necessary to differentiate the null allele and the GPI-less trangene in the same mouse, on any occasion. Then, I decided to continue the safe crossings without confusion.

Only female mice were chosen for inoculation to avoid fighting problems leading to premature deaths. Mice at the age of six weeks, were anesthetized, via intraperitoneal injection, with Avertin (2,2,2 tribromoethanol 99 % (12.7 mg/ml) and tert-amyl alcohol (7.8 µl/ml); 15-17 µl/g mouse) and subsequently intracerebrally inoculated in the right temporal lobe, with 20 µl of 2 % RML-infected brain homogenate (RML [12] is a mouse-adapted scrapie isolate which was passaged in Swiss CD-1 mice obtained from Charles River Laboratories), kindly provided by Juan Maria Torres, CISA, Madrid, Spain. At 365 days post inoculation, mice, which did not show any scrapie-associated signs, were euthanized and their brains immediately were harvested and stored at -80 ºC until use.

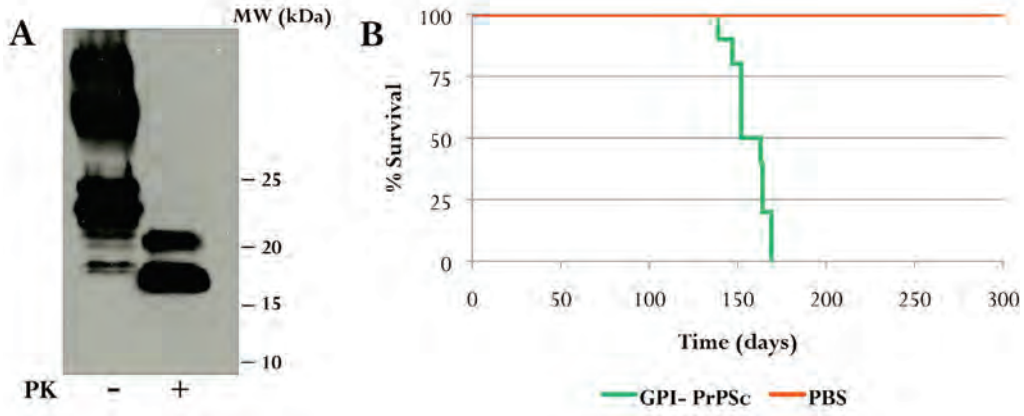

Figure 2.2. *Accumulation of PrP^{Sc} in the GPI-anchorless mice.* ***A.*** *Western blot of brain homogenate from scrapie-infected GPI-anchorless PrP mouse before and after digestion with proteinase K (25 µg/ml.). Samples were detected with a SAF83 antibody, which epitope is unknown. The two bands in the PrP^{Sc} treated with PK correspond with the mono and no- glycosylated form (from higher to lower size).* ***B.*** *Mortality curves of wild-type mice (C57BL/6) inoculated with 2 % of infected GPI-less brain homogenate (green line) and a negative control of wild-type mice inoculated with PBS (red line).*

Due to lack of scrapie signs, which on the other hand agrees with what has been previously described [10][11], I decided to determine whether PrP^{Sc} had been accumulated in the mice brains. Brain homogenate to 10 % of infected GPI-less mouse was analyzed by inmunoblotting, after digestion with 25 µg/ml of proteinase K (PK), for 1 h at 37 ºC; and PrPres was detected in these transgenic mice inoculated with RML scrapie (Figure 2.2 A). At the same time I tried to detect PrPres depositions in brain tissue. Thus immediately after sacrifice of infected GPI-less mouse, the brain was extracted and formalin fixed. Fixed brains were shipped to CRESA, Barcelona, and a histopathology study performed by Enric Vidal. Transversal sections of the brain were obtained at the level of the optic chiasm, piriform cortex and medulla oblongata. Samples were dehydrated through increasing alcohol concentrations, through xylene and then

paraffin-embedded. Four micrometer sections were obtained and haematoxylin-eosin stained for morphological evaluation. Further slides were mounted in 3-trietoxysilil-propilamine-coated glass slides for immunohistochemical (IHC) studies against PrP^{Sc}. Briefly, deparaffinised sections were immersed in formic acid and boiled at low pH in a pressure cooker, with endogenous peroxidases blocked. After pre-treatment with PK, the sections were incubated overnight with the primary antibody, which was the anti-PrP mAb 6H4 (1:2000, kindly provided by Prionics AG), and, finally, developed using DAKO EnVision system and 3,3'diaminobenzidine as the chromogen substrate. Then, hyaline deposits were observed arranged radially around blood vessels. Those deposits were strongly immunoreactive to PrP monoclonal 6H4 antibody. Deposits were also located submeningeally, subventricularly and scattered in the neuropil (Figure 2.3 A).

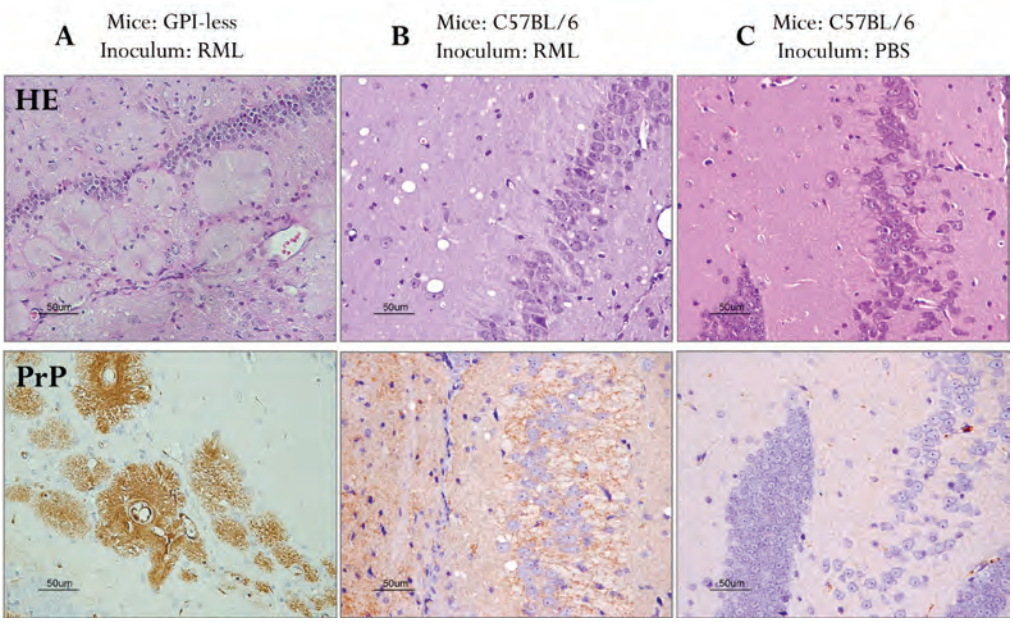

Figure 2.3. *Histopathological and immunohistochemical analyses. Sections are from the brain at the level of the hippocampus and each section was stained with haematoxylin and eosin (HE) or prepared for immunohistochemical analysis using the 6H4 antibody (PrP). Scale bars 50 µm.* ***A.*** *GPI-less mice inoculatedwith RML strain. In the HE hyaline deposits were observed, arranged radially around blood vessels. The deposits showed strong immunoreactivity to 6H4 antibody against prion protein. Most of the PrP immunoreactive deposits were perivascular although in some of them no central vessel was seen.* ***B.*** *Wild-type PrP mice (C57BL/6) inoculated with GPI-less PrP^{Sc}. In the HE, the image shows a moderate spongiosis. In immunohistochemical analysis there are deposits of PrPres with diffuse granular appearance. Amyloid plaques are not observed.* ***C.*** *Negative control. Wild-type PrP mice (C57BL/6) inoculated with PBS. HE slides do not present lesions. There is not immunoreactivity to 6H4 antibody against prion protein. It is possible to observed the blood vessel.*

Furthermore, to be absolutely sure that the material was an infectious protein, I tested whether these GPI-anchorless mice could replicate the scrapie agent. Then, ten wild-type PrP (C57BL/6) mice were inoculated with 20 µl of 2 % infected GPI-less brain homogenate. All of

them developed clinical scrapie and died within 154±15 days post-inoculation (Figure 2.2 B). Infected GPI-less brain homogenate inoculum behaves in a similar way to RML inoculum [12], which has typical incubation times of ~150 days in wt mice. Further, PrP^{Sc} was detected in brains of these second-passage wt animals and histopathology, performed by Enric Vidal (as seen above), showed typical RML lesion profile (Figure 2.3 B), a rather generalised spongyform appearance caused by vacuolation and the absence of amyloid plaques.

2.3 Isolation of PrP^{Sc}

A variety of studies were carried out with the PrP^{Sc}. Depending on the technique to be used, PrP^{Sc} was obtained by two different ways.

2.3.1 Brain homogenate

In some experiments, working with the purified protein is not crucial or even ideal; we can study directly the PrP^{Sc} from the brain. Therefore, for convenience and whenever the technique allows it, brain homogenate (unpurified protein) was used.

To prepare the brain homogenate, hamster and mouse infected brains were homogenized using a dounce homogenizer (Wheaton Industries Inc, NJ, USA), to 10 % (w/v) in phosphate buffered saline (PBS) and 5 % of sarkosyl. Furthermore, to clarify the homogenate it was treated with one pulse of sonication with a probe ultrasonic homogenizer (Cole Parmer Instrument CO., Chicago IL, USA).

2.3.2 Isolation of GPI-anchorless PrP^{Sc}

To analyze the protein with high-resolution techniques it is essential to isolate the PrP^{Sc}, because it is necessary a high grade of purity. The isolates, lacking glycans and GPI anchor (see above), were obtained from brains of infected GPI-anchorless mice.

GPI-anchorless PrP^{Sc} was isolated using a slightly modified version of the method of Baron GS. *et al.* [13] (Figure 2.5) based on the special property that anchorless PrPres is accumulated in large amyloid deposits. 10 % brain homogenate (w/v) in PBS was adjusted, to a final volume of 12 ml, to contain 50 mM Tris-HCl (pH 8.0), 137 mM NaCl and 2 % sarkosyl (TBSS) and incubated for 20 min at room temperature (RT). Nucleic acids were digested by treatment with Benzonase (25 U/ml) at 37 ºC for 30 min. The sample was centrifuged at 18,300 rpm, for 24 min at 20 ºC, in a Beckman Type 50.2 rotor. The supernatant was discarded; PrP^{Sc} and other detergent-insoluble material were in the pellet. After gently rinsing twice with TBSS, the pellet was resuspended, using the vortex, in a total volume of 5.6 ml of TBSS. Then, the material is digested with 10 µg/ml of PK at 37 ºC for 1 h. Protease digestion is terminated by addition of Pefabloc to 1 mM and incubated on ice for 10 min. Insoluble material, settled by gravity or visible in suspension, was removed by manual aspiration, with the end of a pipette tip, at any

stage of the procedure from herein. EDTA to 30 mM was added and incubated for 5 min at RT, after that NaCl to 1.7 M final concentration was added. Subsequently, the preparation was layered onto a sucrose cushion (1 M sucrose, 100 mM NaCl, 0.5 % sulfobetaine 3-14, 10 mM Tris-HCl (pH 7.4) at 20 °C) of 1/3 the volume of the sample and PrP^{Sc} was retrieved by centrifugation at 18,300 rpm, for 24 min at 4 °C, in a Beckman Type 50.2 rotor. After careful and complete removal of the supernatant and cleaning with cotton swabs the walls of the centrifugation tube, the pellet was resuspended in a total volume of 0.5 ml of 0.5 % sulfobetaine 3-14 in PBS. To wash the sample, it was briefly homogenized with a 0.5 ml dounce homogenizer (Wheaton Industries Inc, NJ, USA) and was recovered by centrifugation at 14,000 rpm (22,000 g) for 20 min at 4 °C in a microfuge, this washing step is repeated once more. Depending on the kind of the study, the final GPI-anchorless PrP^{Sc} pellet was resuspended in 100 µl of deionised water or in 20 µl of 6 M guanidine solution. The stock suspension thus prepared was stored at 4 °C. Its purity was assessed by SDS-PAGE with Coomassie blue staining and estimated to be 90 % (Figure 2.4). The yield of anchorless PrP^{Sc} was ~35 µg per brain, it was determined by BCA protein assay [14].

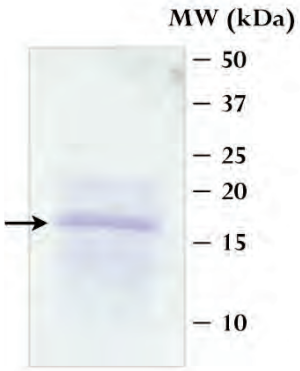

Figure 2.4. *Characterization of isolated GPI-anchorless PrP^{Sc}. 10 µl of sample were loaded and separated in a 15 % gel by SDS-PAGE. The purity was assessed by Coomassie blue staining. The molecular weight of the GPI-less PrP27-30 is ~16750 Da.*

For electron microscopy studies, I had to improve the GPI-anchorless PrP^{Sc} isolated method. Achieving a complete degradation of lipids was necessary because of lipids settle like a blanket covering the fibers; therefore disturbing the analysis of the PrP^{Sc} fibers by electron microscopy. To solve the problem, a final step was added to reach the complete degradation of lipids (Figure 2.5). The final pellet of purified PrP^{Sc} was resuspended in 100 µl of deionised water and was treated with lipase at 1 µg/ml, 2 h at 37 °C. To trap the fatty acids released by the lipase during the incubation, bovine serum albumin (BSA) was added to a final concentration of 10 mg/ml. As fatty acid laden-BSA is soluble, the sample was centrifuged at full-speed (22,000 g) for 20 min and the pellet, containing PrP^{Sc} fibers, was resuspended in 100 µl of deionised water. The sample was centrifuged again as above to eliminate completely the BSA. Finally, the pellet was resuspended in 100 µl of deionised water and sonicated three pulses at amplitude of 50 % with a probe ultrasonic homogenizer (Cole Parmer Instrument CO.,

Chicago IL, USA). With these steps, ultra clean and homogeneous GPI-less PrP^{Sc} fibers were obtained for optimal analysis (Figure 2.6).

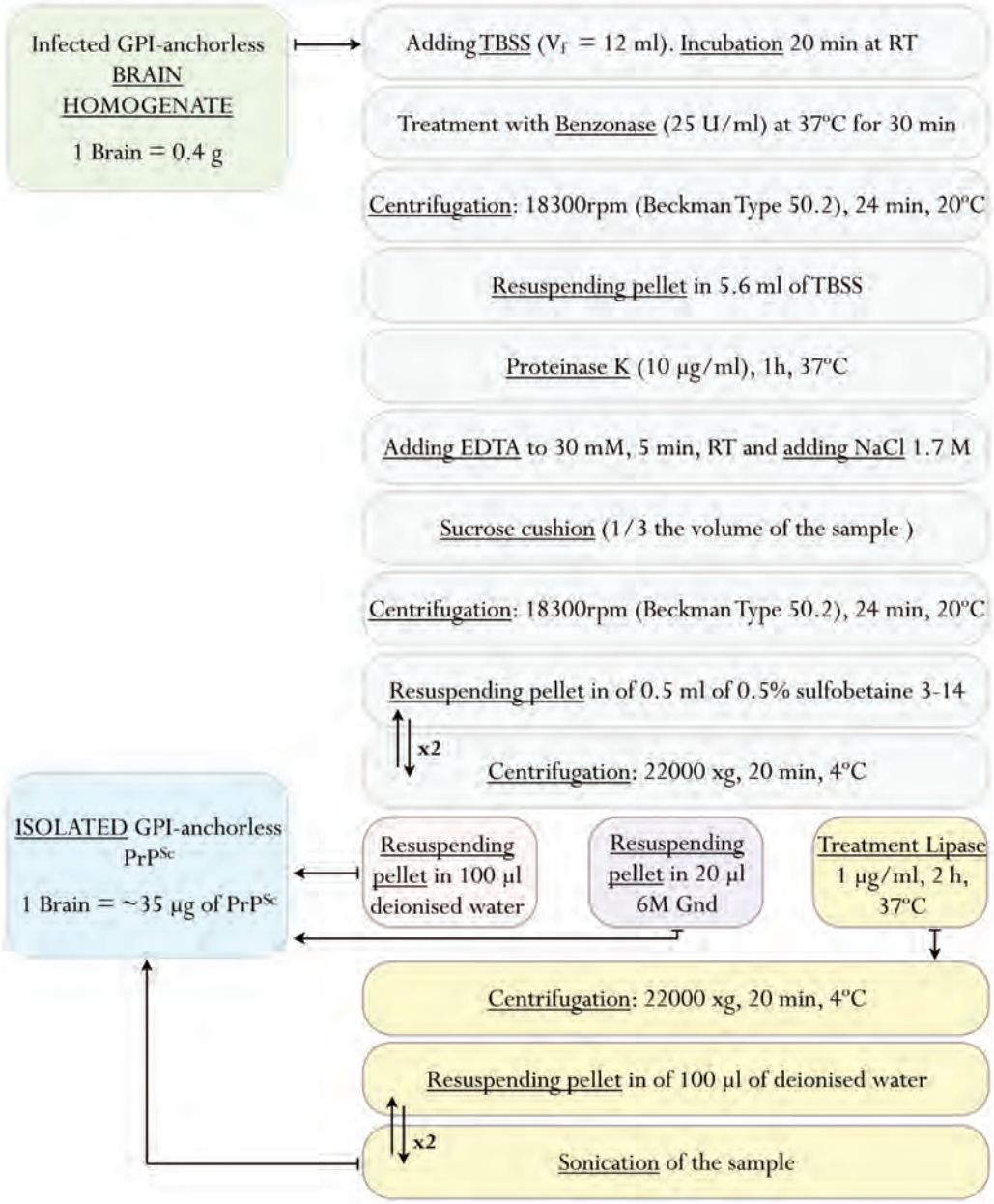

Figure 2.5. *Diagram of the isolation of GPI-anchorless PrP^{Sc}. Depending on the kind of study, the purification may proceed in three different ways until to have the isolated GPI-anchorless PrP^{Sc}.*

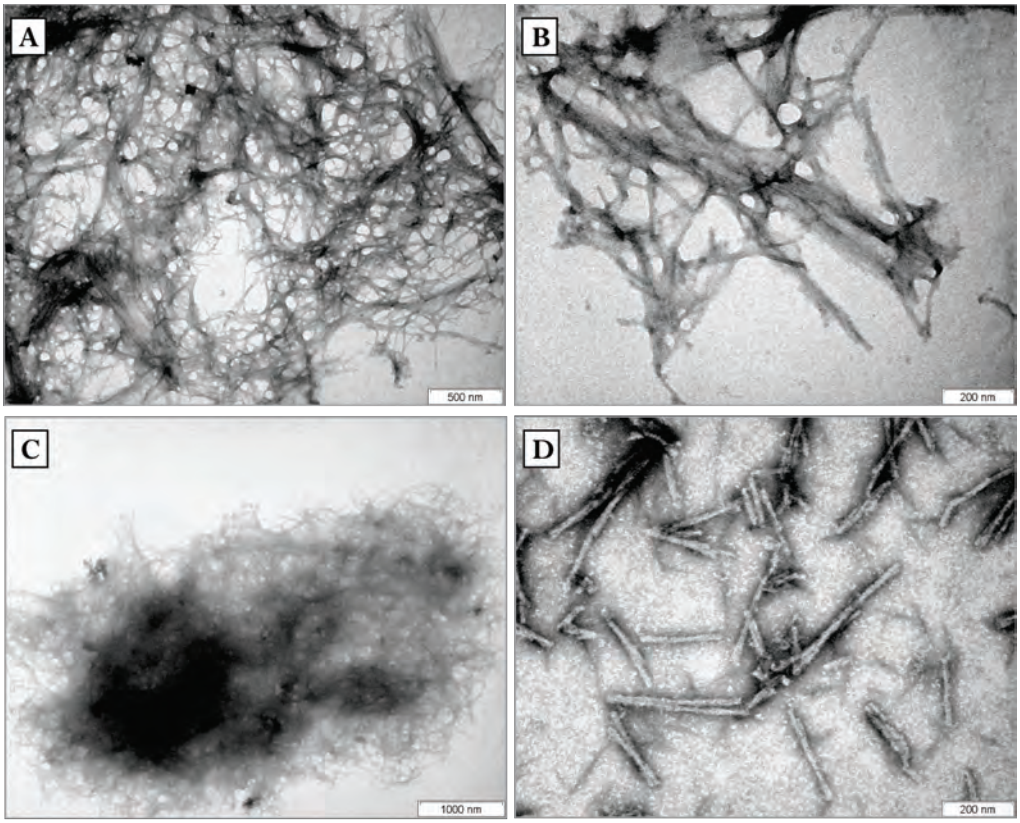

***Figure 2.6**: Transmission electron microscopy (TEM) images, comparing different ways to prepare anchorless scrapie fibers at the end of the isolation procedure. **A.** The isolated GPI-anchorless PrP^{Sc} was resuspended in 100 µl of deionised water. There are lot of fibers, but they are very crowded together and covered with what I believe to be lipidic material. **B.** The same sample was sonicated two pulses with a probe ultrasonic homogenizer. They are more scattered but still partially covered with gooey, putatively lipidic, material. **C.** The isolated GPI-anchorless PrP^{Sc} was treated with lipase and BSA. The image show a ball made up of fibers. **D.** The sample was sonicated three pulses to break up the ball. A lot of small very clean and homogeneous fibers were obtained.*

2.4 Concluding remarks

Currently, for the study of the prion structure it is necessary to induce the disease in laboratory animals, mainly in mice and hamsters, to obtain enough protein to work with. There is a considerable interest in the field to obtain artificially infectious prion proteins that mimic the same properties of natural prion strains, in large amounts. This objective has been encouraged since the publication of the article of Wang *et al.* [8]. Hence, despite the difficulty we are working to generate high-quality synthetic prions from recombinant protein.

In the meantime, transgenic mouse models have provided valuable insight on the prion diseases. GPI-anchorless PrP transgenic mice, expressing only anchorless PrP molecules, are very useful to study the role of the glycosylphosphatidylinositol in prion pathogenesis. Furthermore, due to the minimal amount of carbohydrates and the absence of the GPI, these mice are very valuable for the analyses of the effect of glycans and GPI anchor on PrPres structure [13] and to study the structure of prion itself [15]. Nevertheless there are very few studies that use the GPI-less animal model to find out more information about this atypical protein.

Different GPI-anchorless PrP^{Sc} isolation techniques have been described in the literature [13][16]. After several purification attempts to find the best-adapted method to our studies, I decided to use an adaptation of Baron *et al.* method. It was necessary to improve this purification system because in our microscopy studies, fibers have to be spotless, we cannot have any artefact disturbing the analytical process. I tried different strategies to clean the fibers without success, like washing with methanol/chloroform or heating. Finally, I decided to treat the isolated GPI-anchorless PrP^{Sc} with lipase from porcine pancreas, because it is an enzyme that catalyzes the hydrolysis of lipids. Then, the enzyme degraded all these lipid layers that covered up and interspersed between the fibers, obtaining the perfect sample to analyze by microscopy.

It can be foresee that the combination of these different ways to generate prion protein and the improved purification method will allow the application of new techniques and therefore the obtaining of new insights on the structure of PrP^{Sc}.

2.5 References

1. Legname G, Baskakov IV, Nguyen H-OB, Riesner D, Cohen FE, et al. (2004) Synthetic mammalian prions. Science 305: 673–676.

2. Colby DW, Giles K, Legname G, Wille H, Baskakov IV, et al. (2009) Design and construction of diverse mammalian prion strains. Proc. Natl. Acad. Sci. U.S.A. 106: 20417–20422.

3. Makarava N, Kovacs GG, Bocharova O, Savtchenko R, Alexeeva I, et al. (2010) Recombinant prion protein induces a new transmissible prion disease in wild-type animals. Acta Neuropathol. 119: 177–187.

4. Colby DW, Wain R, Baskakov IV, Legname G, Palmer CG, et al. (2010) Protease-sensitive synthetic prions. PLoS Pathog. 6: e1000736.

5. Makarava N, Kovacs GG, Savtchenko R, Alexeeva I, Budka H, et al. (2011) Genesis of mammalian prions: from non-infectious amyloid fibrils to a transmissible prion disease. PLoS Pathog. 7: e1002419.

6. Deleault NR, Harris BT, Rees JR, Supattapone S (2007) Formation of native prions from minimal components in vitro. Proc. Natl. Acad. Sci. U.S.A. 104: 9741–9746.

7. Barria MA, Mukherjee A, Gonzalez-Romero D, Morales R, Soto C (2009) De novo generation of infectious prions in vitro produces a new disease phenotype. PLoS Pathog. 5: e1000421.

8. Wang F, Wang X, Yuan C-G, Ma J (2010) Generating a prion with bacterially expressed recombinant prion protein. Science 327: 1132–1135.

9. Kimberlin RH, Walker C (1977) Characteristics of a short incubation model of scrapie in the golden hamster. J. Gen. Virol. 34: 295–304.

10. Chesebro B, Trifilo M, Race R, Meade-White K, Teng C, et al. (2005) Anchorless prion protein results in infectious amyloid disease without clinical scrapie. Science 308: 1435–1439.

11. Chesebro B, Race B, Meade-White K, LaCasse R, Race R, et al. (2010) Fatal transmissible amyloid encephalopathy: a new type of prion disease associated with lack of prion protein membrane anchoring. PLoS Pathog. 6: e1000800.

12. Chandler RL (1961) Encephalopathy in mice produced by inoculation with scrapie brain material. Lancet 1: 1378–1379.

13. Baron GS, Hughson AG, Raymond GJ, Offerdahl DK, Barton KA, et al. (2011) Effect of glycans and the glycophosphatidylinositol anchor on strain dependent conformations of scrapie prion protein: improved purifications and infrared spectra. Biochemistry 50: 4479–4490.

14. Raymond, G. J., and Chabry, J. (2004) Purification of the pathological isoform of prion protein (PrPSc or PrPres) from transmis- sible spongiform encephalopathy-affected brain tissue. In Techniques in Prion Research (Lehmann, S., and Grassi, J., Eds.) pp 16-26, Birkhauser Verlag, Basel, Switzerland.

15. Smirnovas V, Baron GS, Offerdahl DK, Raymond GJ, Caughey B, et al. (2011) Structural organization of brain-derived mammalian prions examined by hydrogen-deuterium exchange. Nat. Struct. Mol. Biol. 18: 504–506.

16. Sim VL, Caughey B (2009) Ultrastructures and strain comparison of under-glycosylated scrapie prion fibrils. Neurobiol. Aging 30: 2031–2042.

3

Limited proteolysis

Abstract

Limited proteolysis has proven to be a very useful tool to pinpoint flexible regions within scrapie prion protein (PrP^{Sc}), but the heterogeneity derived from carbohydrate and glysosylphosphatidylinositol (GPI) moieties has limited such analysis to the N-terminal half of the molecule (Sajnani et al, 2008 J. Mol. Biol. 382, 88-98). I have located all flexible, proteinase K (PK) susceptible regions of GPI-less PrP^{Sc}, which lacks such heterogeneity, by using limited proteolysis followed by Western blot and mass spectrometry analysis. Samples were treated with 25 µg/ml of PK, deglycosylated, subjected to Tricine-SDS-PAGE, and probed with antibody R1, which recognizes epitope Y_{225}-S_{230}. Seven bands have been detected with apparent MWs of approximately 17, 14.6, 13, 12, 10.2, 8 and 6.7 kDa. Subsequent analysis by MALDI provided the exact MWs of PK-resistant fragments, namely, 17148, 16726, 16371, 13606, 13463, 12173, 12041, 11171, 9687, 9573, 8358, 7436 and 6274. They correspond to N-terminal cleavages at positions G_{81}, G_{85}, G_{89}, A_{116}, G_{118}, M_{133}, S_{134}, G_{141}, N_{152}, M_{153}, Y_{162}, S_{169} and V_{179}, respectively. The first 9 cleavages, up to position 153, match very well with sites previously identified in wild type PrP^{Sc}. These results reinforce the hypothesis that the structure of PrP^{Sc} consists of a series of short highly PK-resistant β-sheet strands connected by short flexible loops and turns exhibiting higher sensitivity to PK. A sizeable C-terminal stretch of PrP^{Sc} is highly resistant to PK and therefore perhaps constituted by β-sheet secondary structure.

3.1 Introduction

Limited proteolysis is a useful and reliable method to probe the structure of native proteins. Despite the fact that it is a low-resolution technique; it provides comprehensive information about the peptide bond with respect to the fold of the protein. Then, it allows us to localize the more flexible areas and the possible α-helices and/or β-sheets.

In a previous study [1], the group I work with demonstrated the usefulness of combining limited proteolysis and mass spectrometry (MS) to obtain structural information about two strains of hamster PrP^{Sc}. Nevertheless, they were only able to analyze the N-terminal half of the protein, because of the high heterogeneity derived from the glycophosphatidylinositol (GPI) anchor and the carbohydrates contained in its C-terminal region, which complicates the interpretation of Western blots. In this study I have solved that problem working with GPI-anchorless PrP^{Sc} [2][3] that also is mainly expressed in the unglycosylated form, which further reduces its heterogeneity (see Chapter 2). Thereby, I could obtain novel knowledge about the whole structure of PrP^{Sc}.

GPI-less PrP^{Sc} made the accurate detection and location of flexible, PK-susceptible regions possible and PK-resistant fragments were analyzed by a Tricine-SDS-PAGE technique [4], that provides a superior resolution. Furthermore, PrP peptides were characterized by nano-LC-ESI (electrospray ionization)-Qq (double quadrupole)-TOF and MALDI (matrix-assisted laser desorption/ionization)–TOF (time of flight).

3.1.1 Limited proteolysis

Proteolysis is a hydrolytic reaction; it consists in the degradation of proteins by specific enzymes called proteases. Proteases have different functions in the biological systems such as removal of N-terminal methionine residues after translation, elimination of the signal sequence of peptides after their transport through a membrane, digestion of proteins from foods as a source of amino acids and conversion of inactive proteins (pro-proteins) into their final functional forms. In biochemistry, proteases have been used in numerous areas of study including sequencing, enzyme (in) activation, study of the structure of proteins and complete degradation.

Proteases, that could be sequence-specific or not have preference for any specific amino acid, cut a given bond that connects two amino acids in the string of amino acids known as a polypeptide. When used as a biochemical tool, proteolytic digestion is usually carried out under denaturing conditions, thus in the places where the amino acids residues satisfy the specificity requirements of the protease, the peptide bond is cut. This kind of proteolytic digestion is useful for determination of amino acid sequence and the creation of limit digest "map" for protein identification.

Limited proteolysis, another biochemical tool based on the used of proteases, is a good tool to find out conformational features of proteins because it provides information about the peptide

bonds regarding the fold of the protein. In this case, it is necessary to limit the reaction in some way, like the incubation time of enzyme, temperature, pH, ionic strength, using chemicals, or more typically, working in native conditions. Then, a non sequence-specific enzyme is used to cut with respect to fold (Figure 3.1). The paradigm of limited proteolysis is this: higher order structure and not primary sequence is the main determinant of the site of initial hydrolysis [5].

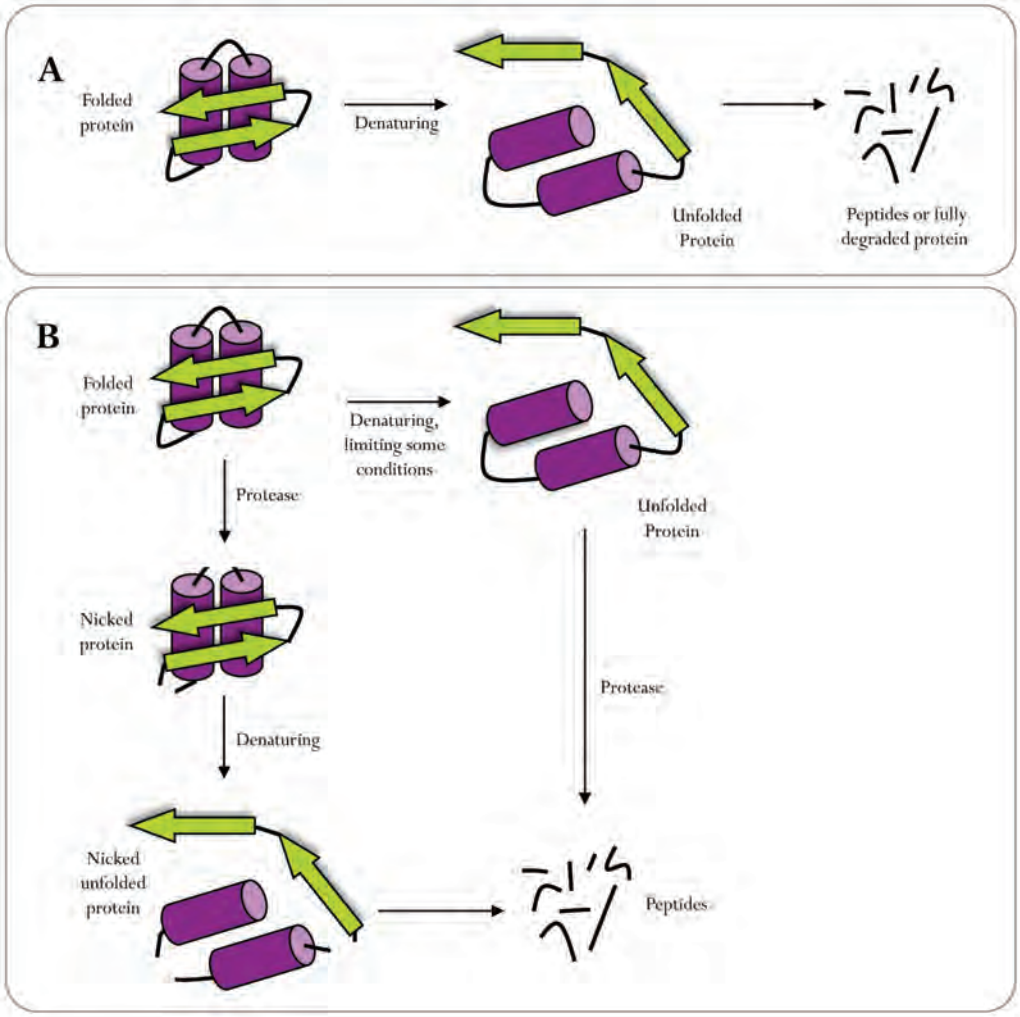

Figure 3.1. *Schematic view of proteolysis and limited proteolysis mechanism.* ***A.*** *Proteolysis takes place under denaturing conditions, every peptide bond are cut where the local amino acid sequence satisfies the specificity requirements of the protease.* ***B.*** *Limited proteolysis needs some restriction in the reaction: native conditions, incubation time, pH, chemicals, temperature, in this way the enzyme cut the peptide bonds with respect to the overall fold of the protein.*

There are three types of conformational determinants, which establish where the specific enzyme would cut: flexibility: the ability to unfold locally is critical for limited proteolysis to take place and areas with high segmental mobility are the better places; exposure: sites near to the surface undergo local unfolding more easily; local interactions: interactions such as hydrogen bonds, disulphide linkages and van der Waals interactions are not good for unfolding. Then, as loops are the most flexible areas; the partial unfolding in β-strands need to break too many inter-strand hydrogen bonds; and in the α-helix there are also similar restrictions that make unfavourable proteolysis in the middle of helices; it can be concluded that the proteolitic cleavage in native state proteins occurs preferentially within loops, more rarely within α-helix and on the other hand, β-strands are very resistant to proteolysis under limited conditions (Figure 3.2) [5].

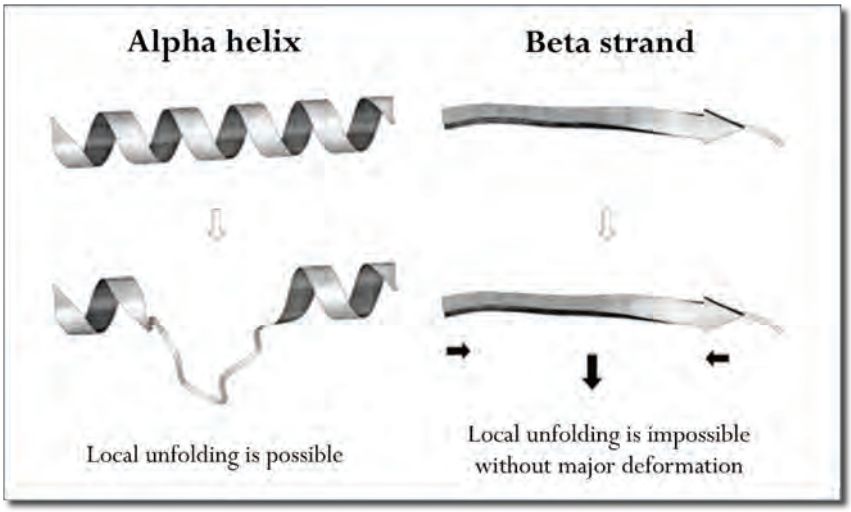

Figure 3.2. *Secondary structural models for local unfolding. It can occur in α-helix, but it is not possible within β-strand, hence, β-strands are very resistant to limited proteolysis. (Hubbard SJ (1998)* [5]*)*

PrP^{C} is very sensitive to proteolytic digestion and is completely degraded by proteinase K. Instead PrP^{Sc}, in native state, is partially resistant to proteases; the protease more commonly used for this reaction is the nonspecific proteinase K. The main fraction that remains intact after treatment with PK is a truncated form of PrP^{Sc} called PrP27-30, due to its size in SDS-PAGE [6][7]. This PK-resistant PrP^{Sc} fraction is composed of three different sub-fractions according to possible glycosilation states: di-, mono- and no- glycosylated. PrP27-30 is infectious and it continues to have the characteristics of a prion. To simplify the heterogeneity, PrP27-30 is treated with peptide-N-glycosidase F (PNGase F), this endoglycosidase releases the N-linked oligosaccharides and the three bands are converted into one, the non-glycosylated form, with a size of 19-21 kDa (Figure 3.3) [8].

Hence, limited proteolysis indicates that PrP^{Sc} has two domains, one PK-resistant core and one labile. The sensitive domain is located in the N-terminal region. This high sensitivity to proteases suggests that it is a very flexible area. Knowing that PrP^{C} is not resistant to proteases and comparing with PrP^{C} NMR studies that show it to contain a totally unstructured amino-terminal region [9], it is possible to conclude that this region of PrP^{Sc} remains unstructured. The border point between both domains is within the 78-103 region, it depends on the species; in Syrian Hamster PrP27-30 made up of amino acid residues ~90-231.

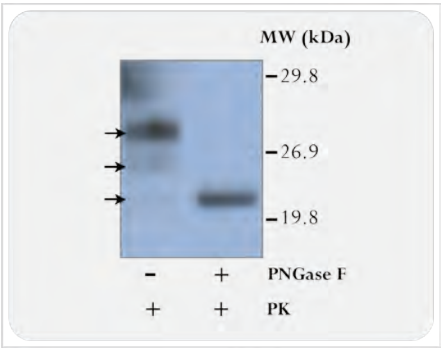

Figure 3.3. *Western blot of SHaPrP^{Sc}. Samples were treated with PK, followed by incubation in the absence (-) or presence (+) of PNGase F. PK-resistant PrP^{Sc} was detected by Western blot using a central region antibody 3F4 (epitope 109-112). In the sample treated with PK and without PNGase F the bands di-, mono- and no- glycosilated (arrows, from higher to lower size) can be observed. In the sample with PK and PNGase F appears only the no-glycosylated form of the protein.*

Over the years, several PrP^{Sc} limited proteolysis studies have reported minor PK-resistant fragments detected with C-terminal antibodies [10][11][12][13]. More recently, the group I work with provided more exhaustive information about limited proteolysis of PrP^{Sc} and these minor bands (Sajnani *et al* [1]). Sajnani *et al.* compared different N-terminal cleavage sites of two hamster PrP^{Sc} strains, 263K and Drowsy (Dy), that differ in the size of the PrP27-30 of 20/21 and 19 kDa respectively, incubation time, symptoms, and tropism for specific brain areas [1]. The cleavage sites generated by limited proteolysis were analyzed by mass spectrometry. But to use this technique, after treatment whit PK, it is necessary to further treat the PrP^{Sc} after denaturing it, with 2-nitro-5-thiocyanatobenzoic acid (NTCB) to cleave at the N-terminal side of cysteine 179 because the presence of the carbohydrate chains and GPI anchor introduce a high heterogeneity, then it would be is impossible to analyze the protein by mass spectrometry. Thereby, all analyzed peptides span from the residue x (amino-terminal) to 178. Sajnani *et al.* got different cleavage sites: the more N-terminal are 70, 74, 78, 82, 86, 90 and 92; the more internal are 117, 119, 135, 139 and 142 and 154 in 263K, for Dy are the same plus 101. Nevertheless the intensity of specific peaks between both strains is different [1].

These studies conclude that there are four susceptibility regions in $SHaPrP^{Sc}$: 23-86 (263K strain) 23-101 (Dy strain), 117-119, 131-142 and the region around 154. The amino-terminal half of PrP^{Sc} features a series of short PK-resistant stretches, presumably β-strands, interspersed

with short PK-sensitive stretches, likely loops and turns. But unfortunately, the structural information was largely limited to the N-terminal portion of the protein [1].

3.1.2 Tricine-SDS-PAGE

The peptides obtained by limited proteolysis, in the study of *Sajnani et al.* [1], could be detected by Western blot with C-terminal antibodies. Both strains of $SHaPrP^{Sc}$ were cut with different concentrations of PK and deglycosylated with PNGase F. This technique is useful because it provides information of most C-terminal region, beyond position 179. In WB an intense band appears of 20/21 kDa for 263K and 19 kDa for Dy that corresponds to a peptide beginning from around position 90. Furthermore there are other lower-molecular-weight bands but due to the limited resolution of the Glycine-SDS-PAGE electrophoretic technique, it was impossible to identify the exact size of these bands, except the band of ~16 kDa, which should correspond to the residue 117-119 (Figure 3.4).

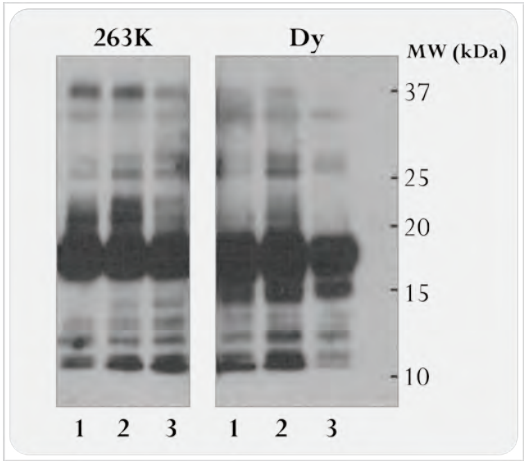

Figure 3.4. *Western blot of purified 263K and Dy PrP^{Sc}. Samples were treated with different concentrations of PK: 50, 200 and 1600 µg/ml (lane 1, 2 and 3, respectively) and subsequently, they were treated with PNGase F. Samples were resolved on Glycine-SDS-PAGE, and detected with a C-terminal antibody R1 (epitope 226-231). (Sajnani G et al. (2008)* [1]*)*

Therefore, to try to resolve with most resolution the PK-resistant peptides, I decided to optimize and use another high-resolution system of electrophoresis, called Tricine-SDS-PAGE.

Tricine-SDS-PAGE [4] is an SDS electrophoretic technique for separating proteins based on Tricine-Tris buffer system. Tricine-SDS-PAGE is commonly used to separate proteins in the mass range 1-100 kDa, especially for the resolution of proteins smaller than 30 kDa. The gels have a lower concentration of acrylamide, this facilitates the electroblotting. The sample buffer and the running conditions are special; they include high glycerol percentage sample buffer, high-ionic-strength running buffer, low voltage and correspondingly extended transfer times. Although, it is worth noting that the SDS-PAGE analysis is not an exact technique and the

peptide size is approximate, in the Tricine-SDS-PAGE the apparent sizes are more accurate. Further, I used three sets of overlapping MW markers: Peptide Molecular Weight (Sigma-Aldrich, St. Louis, MO, USA), Kaleidoscope Prestained Standard (BioRad, Hercules, CA, USA) and Novex Sharp Protein Standard (Invitrogen, Carlsbad, CA, USA), so as to be able to make mass assignments as accurate as possible.

3.1.3 Outline of experimental approach

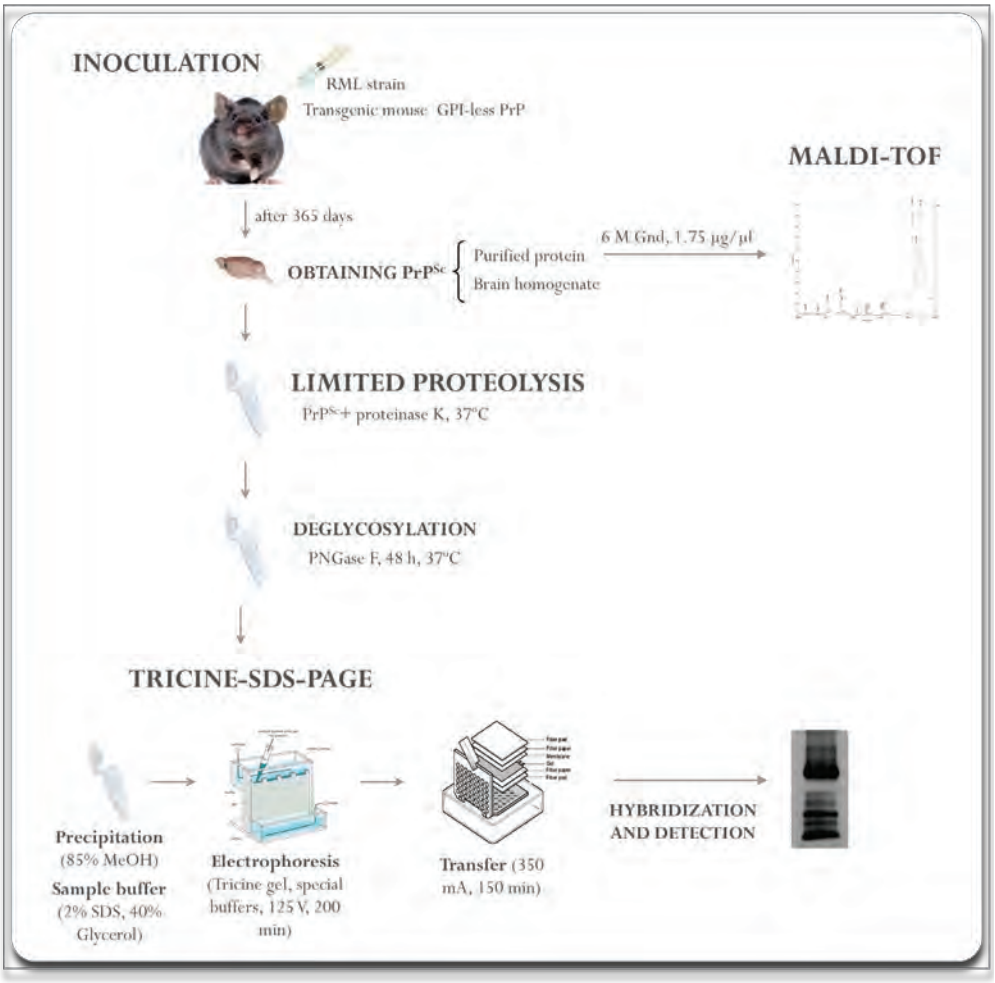

Figure 3.5. *Experimental design scheme. PrP^{Sc} is obtained from infected brains. Protein can be purified or can be used as brain homogenate. The isolated protein is resuspended in denaturing buffer and is analyzed by MALDI-TOF. The limited proteolysis experiment is carried out with the brain homogenate; sample is treated with proteinase K at different ratios or different incubation times, at 37 °C. Then, sample is deglycosylated and precipitated. Next, Tricine-SDS-PAGE technique is used to resolve the small peptides and finally by Western blot the different C-terminal fragments are detected.*

3.2 Studies on GPI-anchorless PrP^{Sc}

3.2.1 Identification of PK cleavage sites by Western blot

To resolve the different peptides formed after digestion with PK, in particular small ones, with the best possible resolution, I used a Tricine-SDS-PAGE technique [4]. I found that it was necessary to precipitate the sample before resuspending it in the high-glycerol sample buffer in order to get reproducible separations. GPI-anchorless PrP^{Sc} brain homogenate was treated with 25 μg/ml of PK; despite GPI-less PrP^{Sc} being mainly in the unglycosylated form, the sample was further deglycosylated with PNGase F, so as to eliminate any interference from glycosylated peptides when assigning molecular weight values to the peptides detected. N-terminal antibody #51, which recognizes epitope G_{92}-K_{100}, detected just one intense, wide band with an approximate MW of 17 kDa, (Figure 3.6, lane 1) which suggests that there are different cleavage points (hence the wide appearance of the band) around residue 89. Very importantly, the fact that only one band is detected by this antibody also means that there are no other C-terminally truncated fragments containing this epitope. In the Western blot probed with the W226 antibody (Figure 3.6, lane 2), which is specific for the W_{144}-N_{152} region, four bands with approximate MWs: 17, 14.6, 13 and 12 kDa were detected, suggestive of three additional cleavage points in the region between residues ~89 and 145. The C-terminal R1 antibody, which recognizes the epitope Y_{225}-S_{230} (Figure 3.6, lane 3), detected seven different bands with approximate MWs of 17, 14.6, 13, 12, 10.2, 8 and 6.7 kDa, suggestive of yet three additional cleavages resulting in N-terminal truncation around residues 149, 164 and 175.

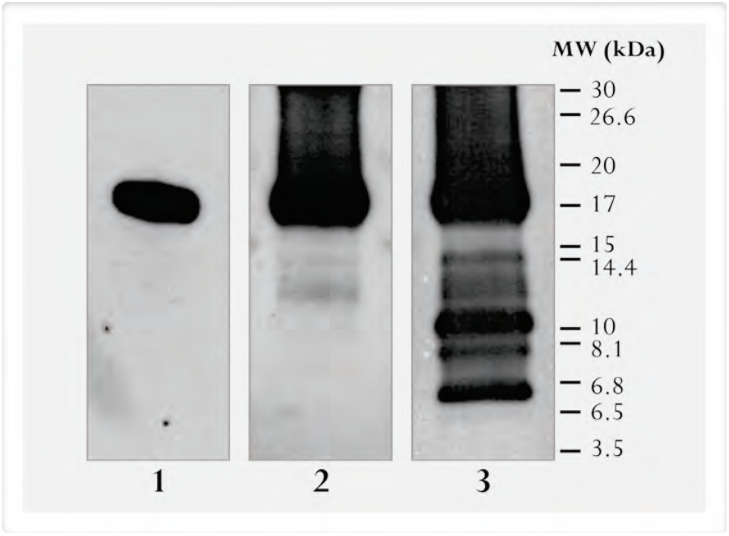

Figure 3.6. *PK-resistant fragments in brain homogenate from scrapie-infected GPI-anchorless tg mouse. Samples were treated with 25 μg/ml of PK and subsequently deglycosylated with PNGase F. Samples were resolved on Tricine-SDS-PAGE. PrP was detected with different monoclonal antibodies: lane 1: #51 (epitope 92-100); lane 2: W226 (epitope 144-152); lane 3: (epitope 225-230).*

3.2.2 Identification of PK cleavage sites by mass spectrometric detection

To get the exact masses from PK-resistant peptides, and therefore unequivocally indentify them, I used mass spectrometry technique. Then, since it is necessary to isolate the sample to avoid impurities, I needed to be sure that the PK-resistant fragments obtained from isolated PrP^{Sc} are similar to those obtained from brain homogenates. It was found to be the case (Figure 3.7), all the bands appear at the same molecular weight.

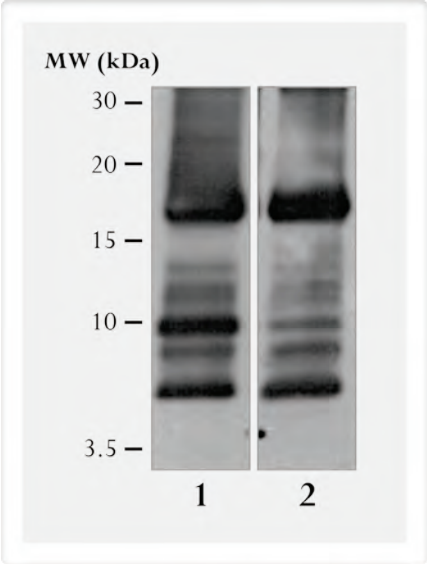

Figure 3.7. *PK-resistant fragments in brain homogenate (lane 1) and purified GPI-anchorless PrP^{Sc} (lane 2). Both samples were digested with proteinase K, 25 µg/ml and 10 µg/ml, respectively and treated with PNGase F. Samples were resolved on Tricine-SDS-PAGE gels and PrP was detected with the C-terminal R1 antibody, which recognizes the epitope 225-230.*

Firstly, samples were analyzed by nano-LC-ESI-Qq-TOF MS, which provides high mass accuracy, and two peaks were identified with exact molecular masses: 17148 Da and 16371 Da, which correspond to peptides Gly_{81}-Ser_{232} and Gly_{89}-Ser_{232}, respectively (Chapter 6 - appendix II). It should be noted that Ser_{232} is the C-terminus of GPI-less PrP^{Sc}, which features a stop codon after the triplet encoding this residue (see appendix I in Chapter 6 and [2]). However, despite several attempts the smaller peptides did not ionize well under the ESI conditions. Therefore, I decided to use MALDI-TOF as an alternative analytical method. Given that the mass range of PK-resistant peptides to be analyzed is very wide, spanning between 17 and 6 kDa, a complex calibration method covering the entire range was developed, and providing acceptable mass accuracy across it. For this purpose, an iterative calibration approach was used. First, insulin (m/z = 5733), ribonuclease A (m/z = 13682) and lysozyme (m/z = 14305) were used mixed with the sample, as internal standards, however, they suppressed some of the less abundant peaks in the spectrum. Therefore, they were used to calibrate a peak with a mass of

9573 Da, with which they did not interfere, corresponding to Met_{153}-Ser_{232} (Chapter 6 - appendix II). Then, the 9573, 16371 and 17148 Da peaks were used to calibrate the rest of peaks in the spectrum.

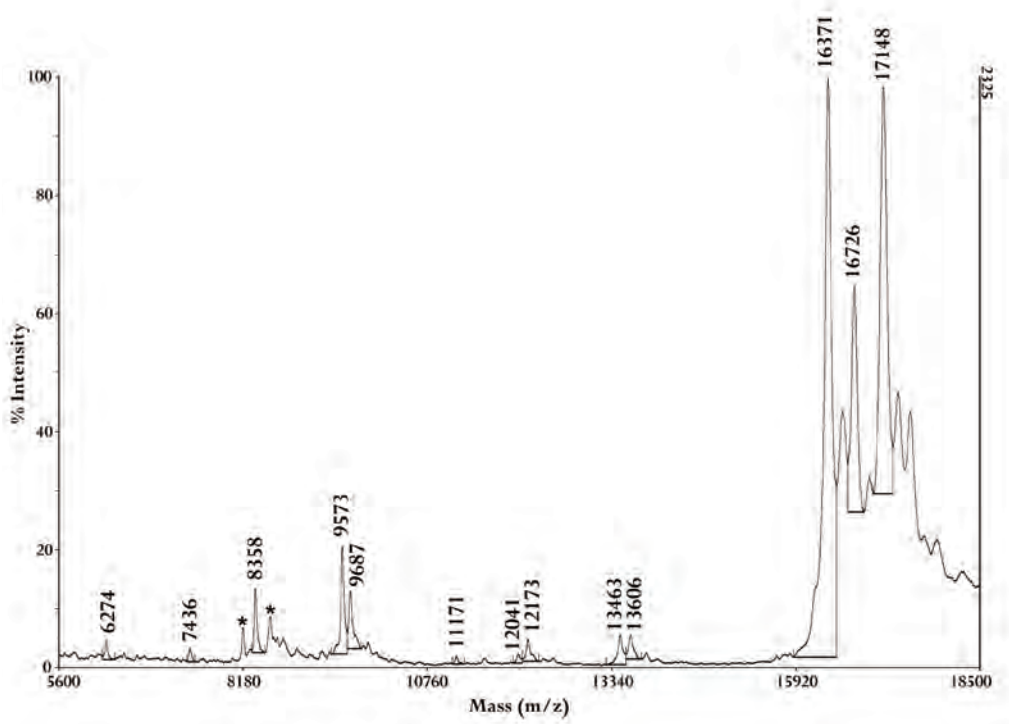

Figure 3.8. *MALDI spectrum of PK-treated GPI-anchorless PrP^{Sc} isolated from scrapie-infected GPI-anchorless mouse. During the process of isolation the sample was digested with 10 µg/ml of PK for 1 h, at 37 ºC. Purified GPI-anchorless PrP^{Sc} was resuspended in 20 µl of 6 M GndHCl, to a final concentration of 1.75 µg/µl. The sample was analyzed by MALDI-TOF, mixing 1 µL with 49 µL of sinapinic acid (SA) as matrix. Asterisks mark doubly-charged ions from peptides with m/z 16371 and 17148. Unmarked peaks could not be identified due to low resolution in the >16 kDa region.*

Figure 3.8 presents the MALDI-TOF spectrum. Thirteen peaks of different masses (*m/z*) were detected: 17148, 16726, 16371, 13606, 13463, 12173, 12041, 11171, 9687, 9573, 8358, 7436 and 6274. They match quite well with the bands identified by Western blot analysis (Table 3.I). Based on the theoretical molecular weight calculated from the sequence of the mouse PrP, using the GPMAW 6.0 software (Lighthouse, Odense, Denmark), ten of these peaks, correspond to peptides spanning from positions 81, 85, 89, 116, 118, 133, 134, 141, 152 and 153 to the C-terminus (Ser_{232}). Besides, three peaks corresponding to new cleavage points in the C-terminal region, at positions 162, 169 and 179, were detected. No peaks corresponding to C-terminally truncated peptides were found (Figure 3.6), in agreement with the presence of just one band being detected by antibody #51, which recognizes the amino-terminally located epitope G_{92}-K_{100}.

Table 3.I. *PK-resistant fragments in GPI-anchorless* PrP^{Sc}

WESTERN BLOT		MALDI-TOF			
Band	kDa	Peak (Da)	Theoretical mass (Da)	Cleavage point	Peptide
1	17	17148	17148	81	G_{81} - S_{232}
		16726	16729	85	G_{85} - S_{232}
		16371	16371	89	G_{89} - S_{232}
2	14.6	13606	13605	116	A_{116} - S_{232}
		13463	13463	118	G_{118} - S_{232}
3	13	12173	12172	133	M_{133} - S_{232}
		12041	12041	134	S_{134} - S_{232}
4	12	11171	11172	141	G_{141} - S_{232}
5	10.2	9687	9688	152	N_{152} - S_{232}
		9573	9574	153	M_{153} - S_{232}
6	8	8358	8358	162	Y_{162} - S_{232}
7	6.7	7436	7436	169	S_{169} - S_{232}
		6274	6278	179	V_{179} - S_{232}

3.2.3 Kinetics of PK digestion

Next, I carried out a study to addresses the question of observing the kinetic of appearance of the different PK-resistant bands observed by Western blot.

Infected brain homogenate was treated with 25 µg/ml of PK at 37 °C, for 0, 30, 60, 120, 180, 240, 300 and 360 minutes. Samples were deglycosylated and analyzed by Tricine-SDS-PAGE. Gradual disappearance of all PK-resistant bands was observed; however, the kinetics of disappearance was different for different bands. The intensities of the 17, 14.6, 13, 12, and 6.7 kDa bands decreased steadily over time, with faster relative decreases for 14.6, 13 and 12.

On the other hand, the 10.2 and 8 kDa bands, exhibited a much slower decrease in intensity. Thus, by 240 minutes the intensity of the 17 and 10.2 kDa bands equaled and by 360 minutes the intensities of the 17, 10.2 and 8 kDa bands were virtually similar (Figure 3.9).

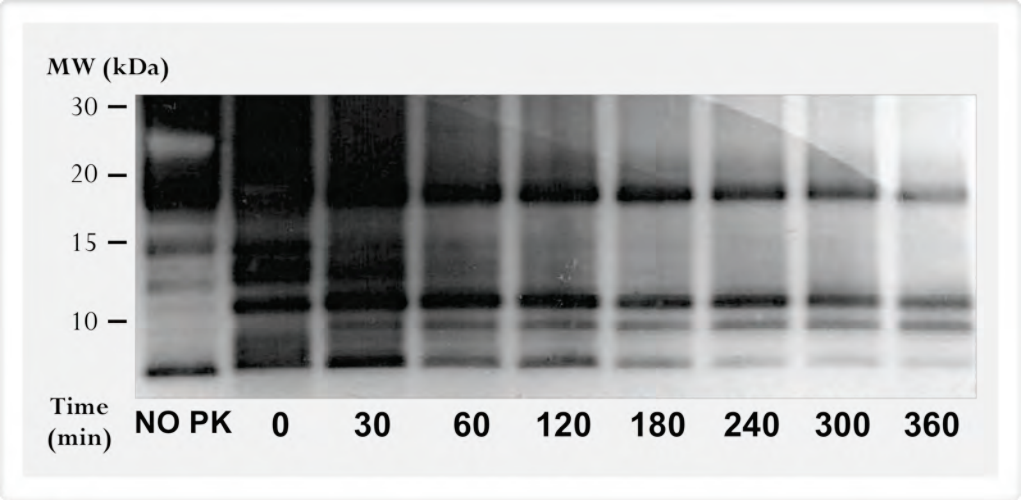

Figure 3.9. *Kinetic of PK digestion of PrP^{Sc} in scrapie-infected GPI-anchorless tg mouse brain homogenate. Samples were digested with PK (25 µg/ml) and the reaction stopped after 0, 30, 60, 120, 180, 240, 300 and 360 minutes. Samples were treated with PNGase F, subjected to Tricine-SDS-PAGE. After blotting, membrane was probed with R1 antibody (epitope 225-230).*

3.2.4 PK cleavage analysis after partial unfolding

In an attempt to determine the relationship of the resistant peptides to one another and to extend the map of PK-sensible cleavage sites of PrP^{Sc}, brain homogenate containing GPI-anchorless PrP^{Sc} was treated with different concentrations of guanidine before cleavage analysis. Kocisko *et al*. have shown that partial unfolding of PrP^{Sc} with up to 2.5-3 M guanidine is reversible upon dialysis [10]. GPI-less samples were treated with 0.5 M, 1 M, 2 M, 3 M or 4 M of guanidine for 1 h at 37 °C and then diluted to 0.4 M to reduce guanidine concentration before PK digestion at 25 µg/ml (Figure 3.10).

As the concentration of guanidine increases, the conformation of PrP^{Sc} is destabilized and the molecule is rendered increasingly susceptible to proteolytic digestion, however, the relative abundance of different PK-resistant bands changed conspicuously after treatment with different concentrations of guanidine. Beyond 1 M, the 10.2 and, to a lesser extent, 12 and 8 kDa bands, corresponding to peptides 152/153-232, 141-232, and 162-232 became predominant. Beyond 3 M guanidine, hardly any PK-resistant material was left (Figure 3.10). Of note, just as seen in the PK kinetic analysis, no new cleavage sites were detected. The apparent higher global intensity of all bands seen after treatment with 0.5 M guanidine, as compared to the 0 M guanidine sample, was reproducibly seen in repeated experiments. I interpret it as an effect of

guanidine to solubilize peptides that otherwise probably stick to the plastic walls of the eppendorf tube throughout the incubation period.

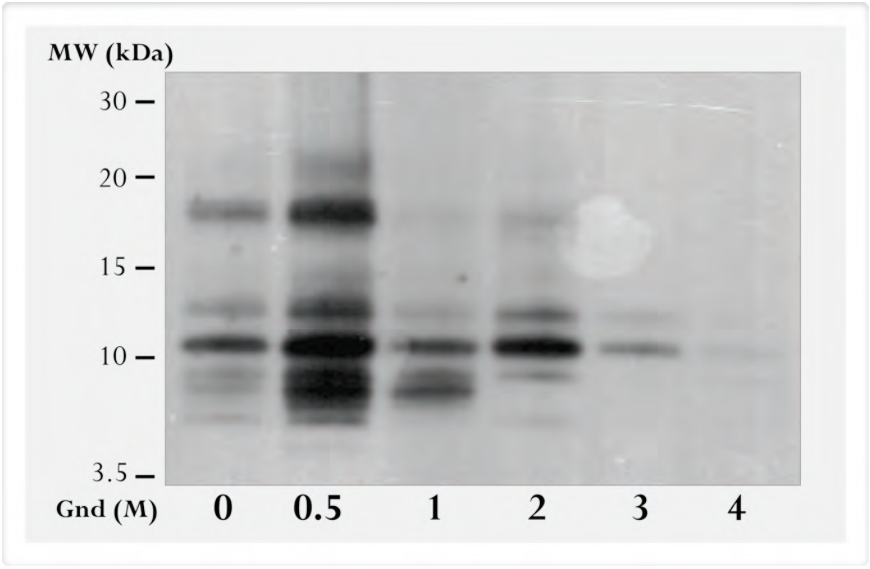

Figure 3.10. *Effect of guanidine-induced partial unfolding of GPI-anchorless brain homogenate PrP^{Sc} on its digestion by PK. Samples were treated with 0 M, 0.5 M, 1 M, 2 M, 3 M and 4 M of guanidine; then they were diluted to a final concentration of 0.4 M of guanidine and digested with 25 µg/ml of PK for 1 h at 37 ºC, and deglycosylated with PNGase F. Samples were resolved on Tricine-SDS-PAGE and PrP was detected with C-terminal R1 antibody (epitope 225-230).*

3.3 Studies on Syrian hamster PrP^{Sc} ($SHaPrP^{Sc}$)

3.3.1 Identification of PK cleavage sites in two strains of $SHaPrP^{Sc}$ by Western blot

In order to extend our previous study [1], studying the C-terminal region of the wild type PrP^{Sc}, PK-resistant fragments of $SHaPrP^{Sc}$ were resolved by Tricine-SDS-PAGE [4] system, obtaining a better resolution of the bands and predicting new cleavage points and then, new flexible areas.

I compared two hamster PrP^{Sc} strains, 263K and Drowsy (Dy) that differ in the size of their main PK resistant cores (PrP27-30), 20/21 and 19 kDa respectively, incubation time of the disease, clinical signs, and tropism for specific brain areas. 263K and Dy hamster PrP^{Sc} brain homogenates were treated with 50 µg/ml and 30 µg/ml of proteinase K, respectively, this difference in the PK concentrations is because Dy strain is more susceptible to digestion that 263K. Subsequently the samples were deglycosylated with PNGase F and were probed with three different antibodies. N-terminal antibody 3F4, which recognizes epitope 109-112 detected just one intense, wide band in both strains with an approximate MW of 20/21 an

19 kDa, respectively (Figure 3.11 A) which suggests that there are different cleavage points around residue 90 and excludes the presence of significant amounts of doubly (N-, and C-terminal) cut bands. The Western blot probed with the W226 antibody (Figure 3.11 B), which is specific for the 145-153 region, presents a different pattern in both strains, although this difference could be attributed to the affinity of the antibody. In 263K two bands were observed, with an approximate MW: 20/21 and 17 kDa, however, three bands were detected in Dy, with an approximate MW of 19, 17 and 15 kDa, suggestive of additional cleavage points in the region between residues ~89 and 153. It is known that the 17 kDa band corresponds with the residue 117-119 [1]. The C-terminal R1 antibody, which recognizes the epitope 226-231 (Figure 3.11 C), detected six different bands with an apparent MW of approximately 20/21 or 19, 17, 15, 14, 10.6 and 6.5 kDa, suggestive of there are several cleavage points in the C-terminal region beyond residue 154. It is worth noting that the pattern is the same in both strains, although the intensities between bands are different.

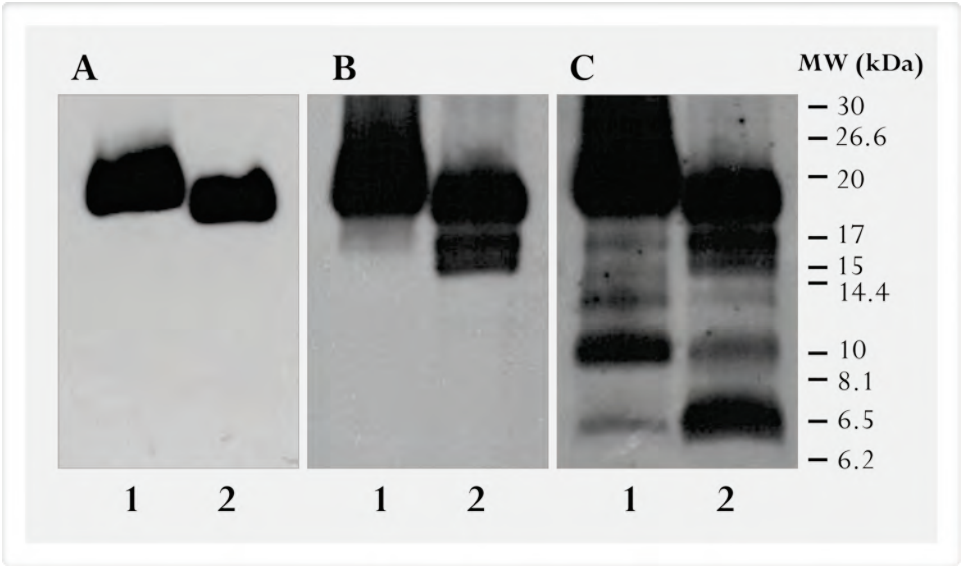

Figure 3.11. *PK-resistant fragments in brain homogenate from 263K (lane 1) and Dy (lane 2) scrapie-infected hamster. Samples were treated with 50 µg/ml and 30 µg/ml of PK, respectively, and subsequently deglycosylated with PNGase F. Samples were resolved on Tricine-SDS-PAGE and PrP was detected with different monoclonal antibodies.* ***A.*** *N-terminal 3F4 antibody (epitope 109-112).* ***B.*** *W226 antibody (epitope 145-153) and* ***C.*** *C-terminal R1 antibody (epitope 226-231).*

Given that 20-19 kDa band corresponds to the predominant $G_{86/90}$-S_{231} peptide, whose mean MW is ~16.2 kDa, the apparent mass contribution of the glycophosphatidylinositol (GPI) anchor is ~3.3 kDa. We assume that all bands correspond to peptides containing GPI, because the C-terminal antibody used (R1) recognizes the residues 226-231. Then, subtracting 3.3 Da to all the bands, masses of bands higher than 10.6 kDa fit with cleavage sites at previously identified flexible stretches [1]: the band of 17 kDa would correspond with the residue 117

and/or 119, 15 kDa bands with the residue 135 and/or 139, and the band of 14 kDa with the 142 residue. I also observed another susceptibility C-terminal region make up for the 10.6 and 6.5 kDa bands; subtracting the GPI, their mass would be 7.3 and 3.2 kDa, then these bands would correspond to cleavages around positions N_{170} and M_{206}, respectively.

On the other hand, with respect to the difference between strains, we confirm that Dy PrP^{Sc} is overall more susceptible to digestion that 263K. Nevertheless, the same cleavage points appear in both, except for the most amino terminal region. Thus they must have very similar tertiary structures.

To sum up, these PK-cleavage points analyzed by WB have to get with cautions because this is not an accurate technique and it is not sure whether these PK-resistant peptides have the GPI moiety. Then, I can only get clues to understand better other results. However, it should be noted that there are several similarities with the results obtained from the GPI-anchorless PrP^{Sc}. The cleavage points of the bands higher that 10.6 kDa, in addition to being consistent with those seen in the previous study [1], also fit perfectly with the residues observed in the GPI-less PrP^{Sc} (as will be explained in the conclusions). Nevertheless, the two C-terminal cleavage sites are not in agreement with the GPI-anchorless PrP^{Sc} flexible stretches, but it is impossible to conclude whether the reason is because some bands in $SHaPrP^{Sc}$ do not have the GPI anchor and/or correspond with other different cleavage points.

I have to mention that several attempts to resolve the GPI issue were made, unsuccessfully. Until I could work with the GPI-anchorless PrP^{Sc}, trying to find out with certainty if the bands had the GPI or not, it was a matter of utmost importance; it was necessary to obtain accurate data and design other sort of experiments. Some of my experiments consisted of different strategies. I tried to remove the GPI with 48 % of aqueous hydrofluoric acid, a solution that has been reported to cut the GPI in the phosphodiester bond [14], which would lead to an easily observable electrophoretic migration difference in the bands previously containing GPI. However, this strategy did not work in my hands. Another attempt was carried out with the *Streptococcus agalactiae* CAMP factor that binds to GPI-anchored proteins, thereby biotinylated CAMP factor, kindly provided by Michael Palmer from the University of Waterloo, Ontario, Canada, was used to probe the blots, followed by probing with HRP-labelled avidin-peroxidase as a secondary antibody to recognize what bands had the GPI anchor [15]. This approach was also unsuccessful because I obtained an awful background impossible to solve and only non-specific bands were detected, even in the negative control.

3.3.2 Identification of PK cleavage sites in PK-sensitive $SHaPrP^{Sc}$ ($sPrP^{Sc}$) by Western blot

In 1998 Safar *et al*. reported the existence of a subset of PrP^{Sc} molecules that are completely degraded by PK, which hence were termed, PK-sensitive PrP^{Sc} ($sPrP^{Sc}$) [16]. Tzaban *et al*. later demonstrated for the first time that prion-infected tissues contain $sPrP^{Sc}$ molecules that form low molecular weight aggregates [17]. In the last years, a method of isolation of the PK-sensitive

PrP^{Sc} fraction by centrifugation was developed by the group in which I work, and it was also shown that $sPrP^{Sc}$ has PMCA converting activity [18]. It was concluded that $sPrP^{Sc}$ is a conformer made up of smaller multimers, whereas PrPres is formed by larger aggregates.

However a question still unresolved was raised: are $sPrP^{Sc}$ and $rPrP^{Sc}$ two populations with different conformations or simply different sized multimers with the same conformation?. To address this question and help to draw conclusions in this study, SHa $sPrP^{Sc}$, provided by Miguel A. Pastrana from our laboratory [18], was further characterized by limited proteolysis coupled to Tricine-SDS-PAGE technique. SHa $sPrP^{Sc}$ was obtained from total $SHaPrP^{Sc}$ by differential centrifugation at an intermediate speed. Furthermore it has to be noted that $sPrP^{Sc}$ has a partial resistance to lower concentrations of PK (Figure 3.12).

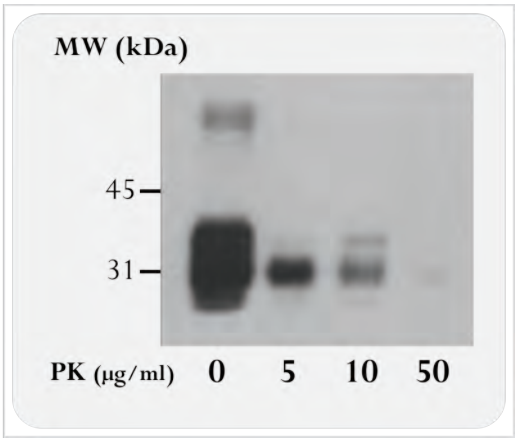

Figure 3.12. *Partial PK resistance of $sPrP^{Sc}$. $sPrP^{Sc}$ was treated with increasing concentrations of PK at 37 ºC for 1 h and analyzed by Wester blot, using 3F4 antibody (epitope 109-112). (Pastrana MA et al. (2006) [18])*

There are evident similarities of the PK-cleavage pattern between sensitive and total PrP^{Sc} when comparing the digested samples by Western blot assay using a C-terminal antibody, R1 (epitope 226-231) after PK-treatment and deglycosylation (Figure 3.13). Besides the intense band corresponding to cleavages around position 90, 6-7 additional lower molecular weight bands are seen in both cases. Furthermore, the relative intensities of some of the bands vary between $sPrP^{Sc}$ and total PrP^{Sc}. The main band centered at 19-20 kDa smears a bit more into the 20-21 kDa region in the $sPrP^{Sc}$ sample, the 17 kDa band is more intense in total PrP^{Sc}, bands around 15, and finally, bands at 10 and 6 kDa are more intense in $sPrP^{Sc}$, but the overall pattern is very similar. Additionally, comparing the pattern of total and sensitive PrP^{Sc} with the resistant PrP^{Sc} of 263K strain (Figure 3.11 C, lane 1), it can be observed that the bands are essentially the same, being the main band and the 10.6 kDa band the most intense of all.

Therefore, limited proteolysis studies on the $sPrP^{Sc}$ fraction of 263K indicate that, as in total and resistant PrP^{Sc}, the sensitive fraction is also composed of alternating PK-resistant stretches interspersed with PK-susceptible stretches. The relatively small variations in intensity of some

of the PK-resistant bands detected by SDS-PAGE (Figure 3.13), could be interpreted as corresponding to differences in accessibility of the PK-resistant stretches involved, but the global emerging picture is one of a shared basic structural organization. Of note, $sPrP^{Sc}$ was shown to be infectious by Sajnani G *et al*. These studies on infectivity and structural characteristics of $sPrP^{Sc}$ have been recently published [19] (see Chapter 6, appendix IV - list of publications).

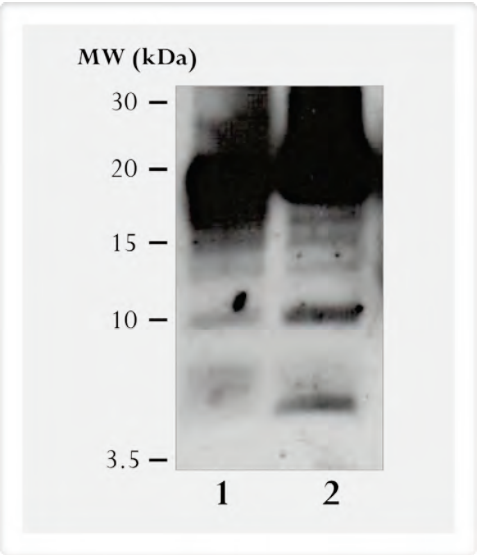

Figure 3.13. *Limited proteolysis of $sPrP^{Sc}$, 263K strain. Isolated total PrP^{Sc} (lane 1) and isolated $sPrP^{Sc}$ (lane 2) were treated with 50 and 5 µg/ml of PK, respectively and subsequently, were treated with PNGase F. Samples were resolved on Tricine-SDS-PAGE gels and C-terminal R1 antibody was used to detect the PrP, which recognizes the epitope 226-231 (hamster nomenclature).*

3.4 Conclusions

I provide here new experimental data that offer insights of the structure of PrP^{Sc}. By subjecting GPI-less PrP^{Sc} to limited proteolysis coupled to mass spectrometry and high-resolution Tricine-SDS-PAGE, I was able to obtain a complete map of relative susceptibility to PK of the entire GPI-less PrP^{Sc} sequence. In particular, I was able to analyze the C-terminal area of the PrP^{Sc}, hitherto unknown as regards its susceptibility to PK.

Thirteen peptide fragments corresponding to a minimum of five and a maximum of eight regions of susceptibility were identified in the GPI-less PrP^{Sc} molecule: 23-89, 116-118, 133-141, 152-153 and the most C-terminus region 162-179 (Table 3.I and Figure 3.14). This study agrees very well with previous research from the group in which I work (Sajnani *et al.* [1]) which allowed to obtain structural information only on the N-terminal half of the protein in two strains of wt $SHaPrP^{Sc}$, due to the high heterogeneity arising from the GPI anchor and the

carbohydrate moieties. The results provided in the present study are in good agreement with the previous ones, matching four areas of susceptibility identified in SHaPrP^{Sc}: 23-101 (extreme proteolytic susceptibility), 117-119, 131-142, and the region around 154 (SHaPrP numbering). In the present study three additional PK cleavage points beyond position 154 were found, at residues 162, 169 and 179.

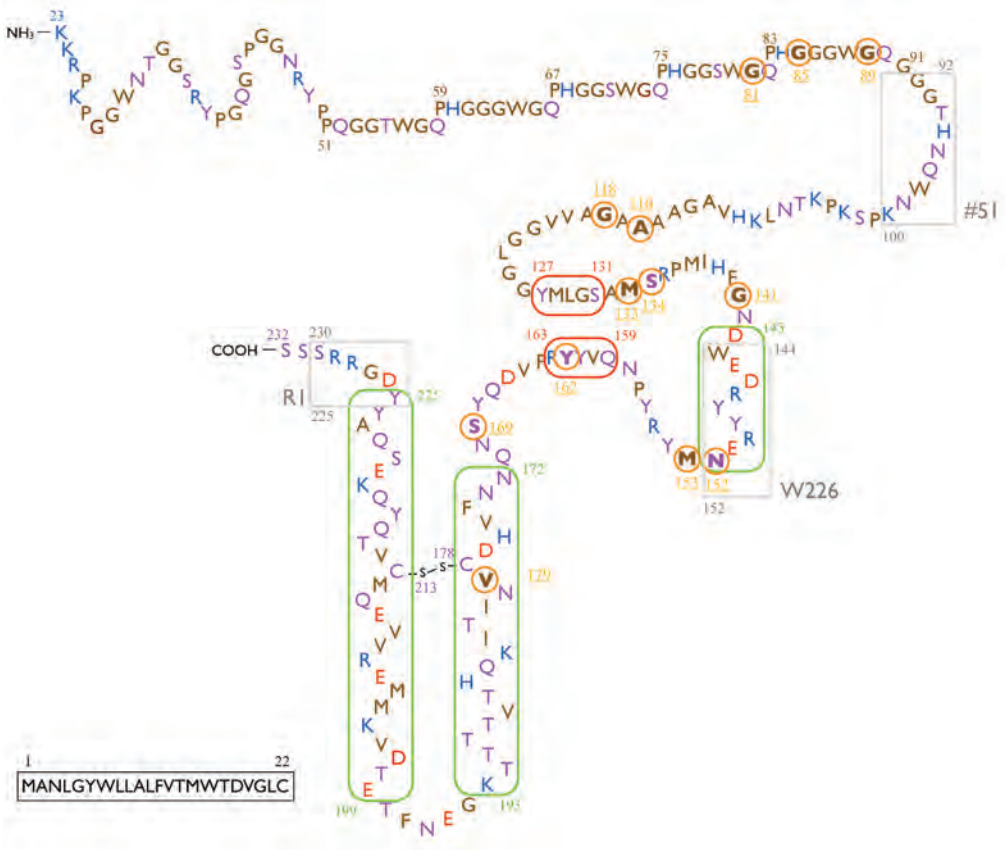

Figure 3.14: *Schematic representation of the sequence of mouse GPI-anchorless PrP. The epitopes of the antibodies #51 (GGTHNQWNP), W226 (WEDRYYREN), and R1 (YDGRRS) are indicated with grey squares. The positions of the two β-sheets (β-sheet 1 and β-sheet 2) in PrP^{C} are indicated with a red square and the three a-helices (a-helix A, a-helix B, and a-helix C) in the same conformer, are marked with green squares. The PK cleavage sites at 81, 85, 89, 116, 118, 133, 134, 141, 152, 153, 162, 169, and 179 are surrounded with orange circles. The N-terminus starts at position 23 (K) as a result of the cleavage of a 22 amino acid signal peptide. The C-terminus is position 232 (S). Amino acid colour code: negatively charged (acidic): red; positively charged (basic): blue; neutral hydrophilic: purple; neutral hydrophobic: brown. (Adapted from Dumpitak C* [20]*)*

Furthermore, it is important to note that I did not find evidence of any PK-resistant peptide with an N-terminus beginning beyond position 179; I believe this is not a consequence of technical limitations, as the Tricine-based SDS-PAGE electrophoretic separation method allows

identification of peptides as small as 3.5 kDa (Figure 3.6, lane 3). This means that either this region is completely resistant to proteinase K, or no stable PK-resistant cores remain if PK cleaves beyond that point.

In the study, the presence of only one band in the WB probed with antibody #51, which recognizes epitope G_{92}-K_{100}, excludes the existence of significant amounts of PK-resistant C-truncated peptides in the samples. This conspicuous absence of C-terminally truncated peptides suggests two possibilities. PK, as all proteases, cleaves at flexible, accessible regions, particularly those not featuring extensive H-bonding, i.e, loops [1][5]. Therefore, either after the nick has been produced at a "floppy" region, the N-terminal side is rendered unstable and it is further degraded by PK as it unwinds, or, more likely, the entire N-terminal region, up to the position at which resistance starts, was, at a given point, in a partially unfolded state in a fraction of PrP^{Sc} subunits. In consequence, the N-termini of PK-resistant peptides likely signal the beginning of stretches of rigid, tightly packed, extensively H-bonded stretches (probably β-sheet rich segments), while the sequence stretch immediately preceding such termini are likely to correspond to flexible stretches (loops and turns) connecting them.

Treatment of GPI-less PrP^{Sc} with PK for increased periods of time showed different kinetics for the different PK-resistant PrP^{Sc} fragments (Figure 3.9). The behaviour of the band of 17, 10.2 and 8 kDa (G_{81}, M_{153}, S_{162}-S_{232}) is particularly relevant as their intensities, at 360 minutes, are similar. This further suggests that different PK-resistant fragments are not from different subpopulations of GPI-less PrP^{Sc}, instead they are derived from a larger common GPI-less PrP^{Sc} peptide.

I extended the limited proteolysis studies by partially unfolding PrP^{Sc} with different concentrations of guanidine. In the present study, as the concentration of guanidine increased, so did susceptibility of PrP^{Sc} to proteolytic digestion, as expected. At 4 M of guanidine complete degradation of PrP^{Sc} occurred (Figure 3.10). Nevertheless, at guanidine concentrations between 0.5 M and 3 M abundant PK-resistant fragments remain. These are the same ones seen in the absence of guanidine, *i.e.,* no new cleavage sites appear. However, the relative intensity of bands changes substantially. With increasing concentrations of guanidine (1-3 M), the predominant band is the 10.2 kDa one (152/153-232) and, to a lesser extent, the 12 and 8 kDa. These results mirror those of the PK time course (see above), that is, all of the bands are derived from the progressive N-terminal digestion of a progenitor peptide. In their original report, Kocisko *et al.* identified in $SHaPrP^{Sc}$ partially unfolded with guanidine, a highly stable PK-resistant core starts before position 143 and continues to the C- terminus [10]. Sajnani *et al.* also detected a resistant $SHaPrP_{Sc}$ core starting at position 139/142 [1].

To sum up, I present experimental constraints that expand the knowledge about the structure of the PrP^{Sc}, in the form of a complete map of susceptibility of the prion protein to PK. In agreement with, and expanding previous data [1], this present studies support the hypothesis that the structure of PrP^{Sc} consists of a series of short highly PK-resistant β-sheet strands connected by short flexible loops and turns exhibiting higher sensitivity to PK. The PK

susceptibility map presented here allows the identification of possible β-strand stretches making up the cross-β spine of PrP^{Sc}. Further, the data suggest that a sizeable C-terminal stretch of PrP^{Sc} is highly resistant to PK and therefore perhaps constituted by β-sheet secondary structure.

3.5 Experimental

Animals - Transgenic homozygous GPI-anchorless PrP mice (tg44(+/+)) were intracerebrally inoculated at age of six weeks with 20 µl of 2 % RML-infected brain homogenate. At 365 days post inoculation, mice, which did not show any scrapie-associated signs, were culled and their brains immediately harvested, rinsed in PBS, and stored at -80 °C until use (for more detailed information see Chapter 2).

Preparation of brain homogenates and isolation of GPI-anchorless PrP^{Sc} - Mouse brain homogenates, 10 % w/v, were prepared in PBS, 5 % sarkosyl, using a dounce homogenizer (Wheaton Industries Inc, NJ, USA), followed by one pulse of sonication to clarify the homogenate, with a probe ultrasonic homogenizer (Cole Parmer Instrument CO., Chicago IL, USA).

GPI-anchorless PrP^{Sc} was isolated using the method of Baron GS. *et al*. [21]. During the purification, total PrP^{Sc} was treated with 10 µg/ml of proteinase K. The final GPI-anchorless PrP^{Sc} pellet was resuspended in 100 µl of deionised water or in 20 µl of 6 M guanidine solution. The stock suspension thus prepared was stored at 4 °C. The yield of anchorless PrP^{Sc} was ~35 µg per brain (for more thorough information see Chapter 2).

Limited proteolysis - Aliquots of brain homogenate (10 % in PBS, 5 % Sarkosyl) were digested with PK (Sigma-Aldrich, St. Louis, MO, USA) in 20 mM Tris-HCl pH 8.5, at different ratios, at 37 °C for 1 h unless otherwise stated. Digestion was stopped by addition of Pefabloc (Fluka, Buchs, Switzerland) to a final concentration of 2 mM. Deglycosylation was carried out with 2 µl of PNGase F solution (New England Biolabs, Ipswich, MA, USA) at 37 °C for 48 h, according to the manufacturer's instructions.

Digestion with PK after partial unfolding with GdnHCl - Brain homogenate samples were partially unfolded by treatment with different concentrations of GndHCl (0 to 4 M), as previously described [1][10]. Brain homogenate samples (5 µl) were mixed with an equal volume of GndHCl aqueous solution to attain the desired final GndHCl concentration of and then incubated at 37 °C for 1 h. Samples were then further diluted with 20 mM Tris-HCl pH 8.5 to a final concentration of 0.4 M GndHCl. Samples were then treated with 25 µg/ml of PK for 1 h at 37 °C, and the digestion stopped by adding Pefabloc to a final concentration of 2 mM. Protein was precipitated by addition of ice-cold methanol to a final concentration of 85 %, and the resulting pellets were resuspended in 9 µl of deionized water, and deglycosylated with PNGase F as described above.

Tricine-SDS-PAGE and Western Blot analysis - Samples were precipitated with ice-cold 85 % MeOH and pellets boiled for 10 minutes in 10 µl of tricine sample buffer (BioRad, Hercules, CA, USA) with 2 % (v/v) of β-mercaptoethanol as reducing agent. Electrophoresis was carried out using 10-20 % Tris-Tricine/ Peptide Precast gels (BioRad, Hercules, CA, USA), in the Criterion System (BioRad, Hercules, CA, USA). The cathode buffer was Tris-Tricine-SDS buffer 1 X (Sigma-Aldrich, St. Louis, MO, USA) and the anode buffer, 1 M Tris-HCl pH 8.9. Electrophoresis was performed at constant voltage (125 volts) for 200 minutes, on ice.

Electroblotting was carried out at a constant intensity of 350 mA, for 150 minutes, onto Immobilon-P transfer membrane, PVDF, 0.45 µm (Millipore, Billerica, MA, USA), at cold conditions. Membranes were probed with the following monoclonal antibodies recognizing different mouse and hamster PrP epitopes: mAb #51 (a gift from Lothar Stitz, Friedrich Loeffler Institut, Tübingen, Germany), which recognizes mouse residues 92-100, undiluted; 3F4 (Dako, Glostrup, Denmark) that recognizes hamster residues 109-112 at 1:5000 dilution; W226 (a gift from Lothar Stitz, Friedrich Loeffler Institut, Tübingen, Germany), which recognizes residues 144-152, at 1:5000 dilution, and R1 (a generous gift from Hanna Serban, UCSF), which recognizes residues 225-230, at a 1:5000 dilution. Peroxidase-labelled anti-mouse (GE Healthcare, Little Chalfont, UK) or anti-human antibodies (Thermo Fisher Scientific, Rockford, IL, USA) were used as the secondary antibodies, both at a 1:5000 dilution. Blots were developed with ECL-plus reagent (GE Healthcare, Little Chalfont, UK). Three sets of partially overlapping MW markers: Peptide Molecular Weight (Sigma-Aldrich, St. Louis, MO, USA), Kaleidoscope Prestained Standard (BioRad, Hercules, CA, USA) and Novex Sharp Protein Standard (Invitrogen, Carlsbad, CA, USA) were run in each analysis to calibrate the MW of bands.

Mass spectrometry - GPI-anchorless PrP^{Sc}, whose purification procedure involves treatment with 10 µg/ml PK for 1 h at 37 °C (see above), was resuspended in 20 µl of 6 M GndHCl, to a final concentration of 1.75 µg/µl. As GPI-less PrP^{Sc} is mainly in the unglycosylated form it was not necessary to remove the carbohydrates with PNGase F. NanoLC/ESI/MS analysis was done with an Applied Biosystems (AB SCIEX, Framingham, MA) model QStar Pulsar equipped with a Proxeon Biosystems (Odense, Denmark) nanoelectrospray source. Samples were loaded automatically onto a C-18 trap cartridge and chromatographed on a reversed-phase column (Vydac Everest 238EV5.07515, 75 mm x 150 mm) fitted with a coated spray tip (FS360-50-5-CE; New Objective, Inc.). A nanoflow LCsystem (Dionex, Sunnyvale, CA) with autosampler, column switching device, loading pump, and nanoflow solvent delivery system was used. Elution solvents were A (0.5 % acetic acid in water) and B (0.5 % acetic acid in 80 % acetonitrile/20 % water). Samples were eluted at 250 nL/min with the following binary gradient profile: 8 % B at 0 min to 80 % B in a 30 min linear gradient, held at 80 % B for 5 min, then back to 8 % B for 15 minutes. The QStar Pulsar was externally calibrated daily with human [Glu1]-fibrinopeptide B.

In parallel, the same sample was analyzed by MALDI-TOF, mixing 1 µL with 49 µL of sinapinic acid (SA) as matrix, consisting of 10 mg/mL SA dissolved in 30 % ACN with 0.3 % TFA. 0.5 µL were deposited using the dried-droplet method onto a 384 Opti-TOF MALDI plate (Applied Biosystems, Foster City, CA, USA). MALDI analysis was performed in a 4800 MALDI-TOF/TOF analyzer (Applied Biosystems, Foster City, CA, USA). MS spectra were acquire in linear mode with a Nd:YAG, 355 nm wavelength laser, and averaging 500 laser shots. The ions were accelerated by 20 kV in source. The two peaks observed and identified by nanoLC-ESI-TOF (16371 Da and 17148 Da, corresponding to PrP fragments 89-232 and 81-232, respectively), along with insulin (8 µg/mL, Sigma-Aldrich, St. Louis, MO), ribonuclease A (120 µg/mL, Sigma-Aldrich, St. Louis, MO) and lysozyme (100 µg/mL, Sigma-Aldrich, St. Louis, MO) were used as internal calibrants. Masses were matched to PrP fragments with the help of GPMAW 6.0 software (Lighthouse, Odense, Denmark).

3.6 References

1. Sajnani G, Pastrana MA, Dynin I, Onisko B, Requena JR (2008) Scrapie prion protein structural constraints obtained by limited proteolysis and mass spectrometry. J. Mol. Biol. 382: 88–98.

2. Chesebro B, Trifilo M, Race R, Meade-White K, Teng C, et al. (2005) Anchorless prion protein results in infectious amyloid disease without clinical scrapie. Science 308: 1435–1439.

3. Chesebro B, Race B, Meade-White K, LaCasse R, Race R, et al. (2010) Fatal transmissible amyloid encephalopathy: a new type of prion disease associated with lack of prion protein membrane anchoring. PLoS Pathog. 6: e1000800.

4. Schägger H (2006) Tricine-SDS-PAGE. Nat Protoc 1: 16–22.

5. Hubbard SJ (1998) The structural aspects of limited proteolysis of native proteins. Biochim. Biophys. Acta 1382: 191–206.

6. Bolton DC, McKinley MP, Prusiner SB (1982) Identification of a protein that purifies with the scrapie prion. Science 218: 1309–1311.

7. McKinley MP, Bolton DC, Prusiner SB (1983) A protease-resistant protein is a structural component of the scrapie prion. Cell 35: 57–62.

8. Parchi P, Zou W, Wang W, Brown P, Capellari S, et al. (2000) Genetic influence on the structural variations of the abnormal prion protein. Proc. Natl. Acad. Sci. U.S.A. 97: 10168–10172.

9. Prusiner SB (1998) Prions. Proc. Natl. Acad. Sci. U.S.A. 95: 13363–13383.

10. Kocisko DA, Lansbury PT, Caughey B (1996) Partial unfolding and refolding of scrapie-associated prion protein: evidence for a critical 16-kDa C-terminal domain. Biochemistry 35: 13434–13442.

11. Bartz JC, Bessen RA, McKenzie D, Marsh RF, Aiken JM (2000) Adaptation and selection of prion protein strain conformations following interspecies transmission of transmissible mink encephalopathy. Journal of Virology 74: 5542–5547.

12. Zou W-Q, Capellari S, Parchi P, Sy M-S, Gambetti P, et al. (2003) Identification of novel proteinase K-resistant C-terminal fragments of PrP in Creutzfeldt-Jakob disease. J. Biol. Chem. 278: 40429–40436.

13. Zanusso G, Farinazzo A, Prelli F, Fiorini M, Gelati M, et al. (2004) Identification of distinct N-terminal truncated forms of prion protein in different Creutzfeldt-Jakob disease subtypes. J. Biol. Chem. 279: 38936–38942.

14. Notari S, Strammiello R, Capellari S, Giese A, Cescatti M, et al. (2008) Characterization of truncated forms of abnormal prion protein in Creutzfeldt-Jakob disease. J. Biol. Chem. 283: 30557–30565.

15. Lang S, Xue J, Guo Z, Palmer M (2007) Streptococcus agalactiae CAMP factor binds to GPI-anchored proteins. Med. Microbiol. Immunol. 196: 1–10.

16. Safar J, Wille H, Itri V, Groth D, Serban H, et al. (1998) Eight prion strains have PrP(Sc) molecules with different conformations. Nat. Med. 4: 1157–1165.

17. Tzaban S, Friedlander G, Schonberger O, Horonchik L, Yedidia Y, et al. (2002) Protease-sensitive scrapie prion protein in aggregates of heterogeneous sizes. Biochemistry 41: 12868–12875.

18. Pastrana MA, Sajnani G, Onisko B, Castilla J, Morales R, et al. (2006) Isolation and characterization of a proteinase K-sensitive PrPSc fraction. Biochemistry 45: 15710–15717.

19. Sajnani G, Silva CJ, Ramos A, Pastrana MA, Onisko BC, et al. (2012) PK-sensitive PrP Is Infectious and Shares Basic Structural Features with PK-resistant PrP. PLoS Pathog. 8: e1002547.

20. Dumpitak C (2003) Untersuchungen zu Struktur und Funktion von Polysacchariden und alterungsassoziierten Proteinmodifikationen bei Prionen. Dissertation. Düsseldorf: Heinrich-Heine-Universität.

21. Baron GS, Hughson AG, Raymond GJ, Offerdahl DK, Barton KA, et al. (2011) Effect of glycans and the glycophosphatidylinositol anchor on strain dependent conformations of scrapie prion protein: improved purifications and infrared spectra. Biochemistry 50: 4479–4490.

4

Electron microscopy

Abstract

Prion protein has the property to polymerize into amyloid fibers. Taking advantage of this feature, we used different electron microscopy (EM) techniques, from low-resolution to three-dimensional reconstruction of the PrP^{Sc} fibers. As the previous studies of this thesis, GPI-anchorless PrP^{Sc} was used, because it provides the cleanest possible sample, without losing the natural properties of the wild-type PrP^{Sc}. We have obtained dimensions and morphological information about the prion protein protofilaments. Fibers have a no regular helical pattern and are made up for two protofilaments intertwined, with no regular crossover distance. 3D reconstruction of 2D cryomicroscopy (cryo-EM) images of the fibers also shows two protofilaments coiling around a common axis. Moreover, there are 2-2.5 nm repetition densities along the axis, suggesting each of these is a stacked monomer of PrP^{Sc}. These axial densities are also evident in reconstructed tomograms obtained by cryo-EM tomography of fiber samples. Another important measure is a 4.8 Å reflection presents in the Fast Fourier Transform (FFT), characteristic of the cross-β structure. A high-resolution image of cryo-EM also shows clearly the 4.8 Å reflection of the spacing between the beta repeat strands that are stacked like a "ladder". These measurements of the scrapie fibers should lead to develop a real model of the prion structure.

4.1 Introduction

Electron microscopy (EM) is a technique developed in the 1930s, based on a beam of electrons to create a magnified image of the specimen rather than a beam o light, achieving higher magnifications and a greater resolution. EM has become in a powerful technique to observe the ultrastructure of a wide range of biological and inorganic samples.

Furthermore, currently there are different types of EM methods that use several signals arising from the interaction of the electron beam with the sample to obtain information about structure, morphology and composition.

Electron microscopy techniques have been very useful for studying the ultrastructural features of prions. In 1981, using transmission electron microscopy (TEM), abnormal fibrillary structures in subfractions of synaptosomal preparations from scrapie affected mice and hamster were observed. These fibers were designated "scrapie-associated fibrils (SAFs)" from scrapie affected mice and hamster [1]. Later, those fibers were also observed in CJD brain fractions [2]. At the same time, Prusiner SB *et al.*, after the purification process of scrapie prions based on centrifugation, could observe that the purified preparations contained numerous rod-shaped particles, measuring 10-20 nm in diameter and 100-200 nm in length. These rods were aggregates of prions and are not fundamental particles themselves; they were termed "prion rods" [3][4].

Knowing these properties of polymerization and aggregation of the PrP^{Sc}, into heterogeneous amyloid fibers, more studies were performed. Nevertheless the presence of fibers or amyloid plaques was not always observed; Godsave *et al.* demonstrated by cryo-inmunogold EM that brain sections from scrapie infected mice do no contain any significant PrP^{Sc} fibers [5]. Then, it was concluded that the fiber formation is dependent of the purification method, which is characterized by consecutives steps of ultracentrifugation, protease and detergent treatment [6][7]. On the other hand, GPI-anchorless PrP^{Sc}, produced in mice expressing PrP lacking the GPI anchor, is deposited as amyloid plaques into the brain [8].

A recent study using TEM and atomic force microscopy (AFM) has compared PrP27-30 fibers from GPI-anchorless and wild type mice infected with different scrapie strains and the authors obtained dimensions and morphological information about the protofilaments. They have observed that fibers are generally 100-150 nm in length, 4-5 nm in wide and are intertwined. Furthermore, they concluded there are variations in the different strains, ME7 and 22L fibrils contained thinner protofilaments, 22L fibrils preferred left-handed twists, and 22L fibril periodicities averaged 106 nm per half-turn, compared with 64 and 66 nm for RML and ME7 fibrils, respectively [9].

Despite these comprehensive studies, the structure of PrP^{Sc} is still poorly understood. Nonetheless, in the last few years, some great technological breakthroughs have significantly contributed to improve the resolution of the different EM techniques. Besides, the

computational developments in conjunction to emerging technologies in EM instrumentation, and novel sample preparations have allowed us to find out in detail new measurements and insights on the structure of the PrP^{Sc}.

4.1.1 Outline of experimental approach

In these studies, each technique and each result is related to the previous one. They are independent studies, but only with them together it has been possible to reach a three-dimensional reconstruction of the PrP^{Sc}. Therefore, this chapter is arranged according to this idea.

It should also be noted that in this chapter I am going to write in plural, because of the described studies have been performed by several researchers from different laboratories and several fields of knowledge. Without their help and experience it would have been impossible to approach this project.

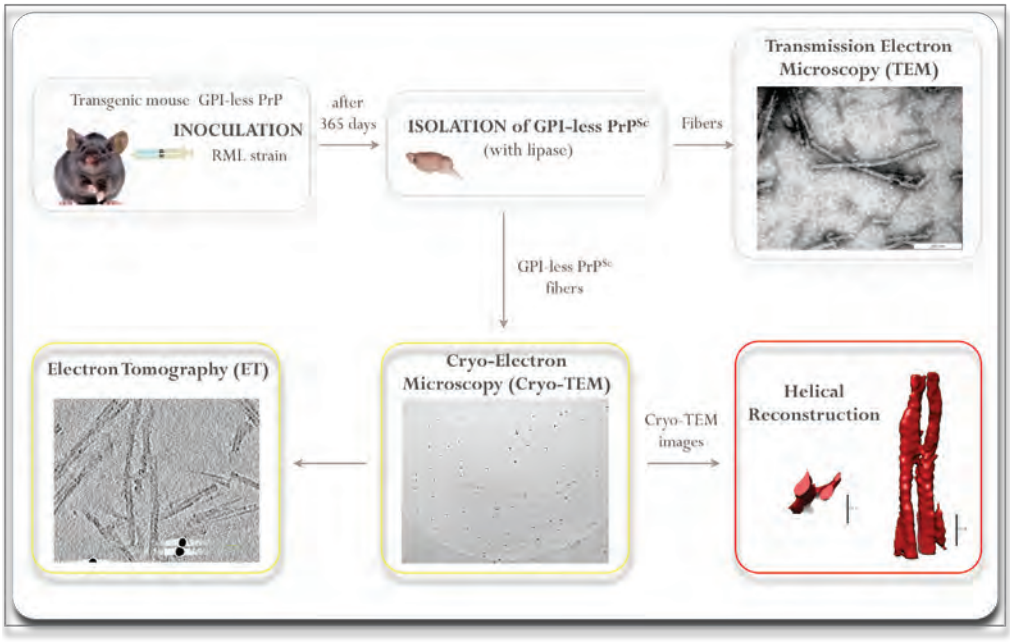

Figure 4.1. *Experimental design scheme. GPI-less PrP^{Sc} is obtained from RML infected brains of tg mice expressing the GPI-anchorless PrP. The protein is purified and the quality of the fibers is checked by TEM. When the perfect sample is got, the fibers are analyzed by cryo-TEM. Next, to obtain the 3D reconstruction, the 2D projection images obtained by cryo-EM are subjected to helical reconstruction; alternatively, vitrified samples are subjected to electron tomography, and 3D reconstructions are obtained by weighed back projection technique.*

Studies were carried out with the GPI-less PrP^{Sc} from scrapie infected tg mice expressing GPI-anchorless PrP; the used EM techniques require the cleanest and most homogeneous fibers of PrP^{Sc} available. For the time being this is achievable with the anchorless PrP^{Sc} material, since

GPI-less PrP^{Sc} fibers preformed in the brain of scrapie-infected mice are easy to isolate using mild centrifugation yielding very pure samples. Please refer to chapter 2 for a more detailed discussion.

4.2 Transmission electron microscopy (TEM)

Transmission electron microscopy (TEM) involves a high voltage electron beam emitted by a cathode and focused by magnetic lenses. The electron beam that has been partially transmitted through the very thin specimen carries information about the structure of the specimen. The image is magnified by a series of magnetic lenses and it is recorded by an imaging recording system.

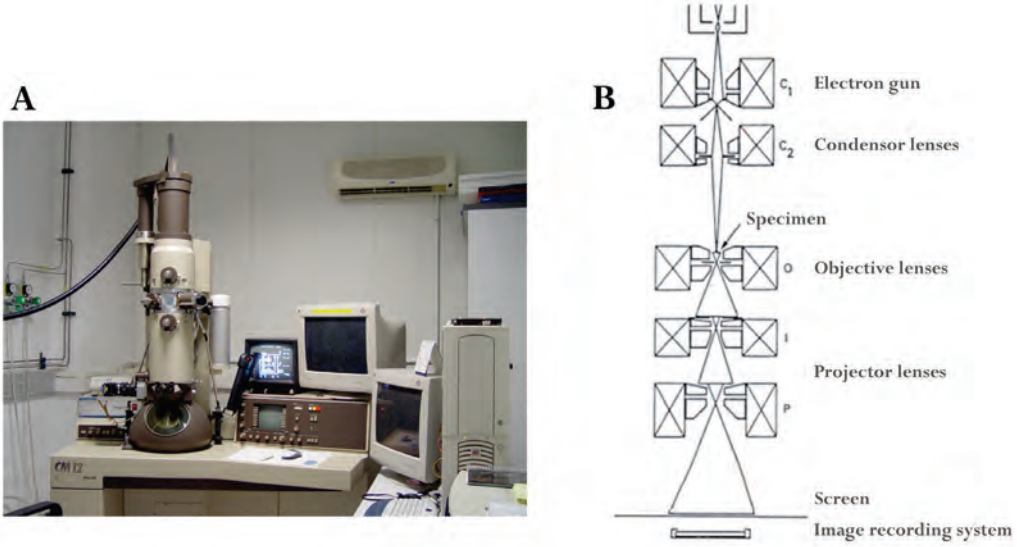

Figure 4.2. *Transmission electron microscopy.* ***A.*** *Transmission electron microscope Philips CM-12. The images are recorded with a MEGA VIEW-II DOCU camera (University of Santiago de Compostela (USC), Galicia, Spain).* ***B.*** *Layout of optical components in a basic TEM. The components are located in a vacuum system, in which the electrons travel.*

TEM has a limit of resolution of 2 nm. But in the life sciences, the specimen preparation limits the resolution of what we can see in the electron microscope, rather than the microscope itself. The sample should be negative stained, a method in which the specimen is dried and embedded in a layer of electron-dense heavy metal salts to scatter imaging electrons and thus give contrast between different structures, since most biological materials are nearly "transparent" to the electron beam. Then, transmission electron microscopes produce two-dimensional, black and white images.

4.2.1 Results of TEM

In this group of experiments, the first aim was to monitor the appearance and quality of GPI-less PrP^{Sc} as different modifications to the isolation method were introduced. An ideal sample is, for our purposes a specimen free of bacteria, lipids, other kind of impurities and/or artefacts that might hamper our studies. Furthermore, the more scattered that fibers are, the better, given that the ideal situation for cryo-EM tomography and helical reconstruction from 2D images is one in which individual fibers are available. This is very difficult to achieve, given the tendency of PrP^{Sc} fibers to clump together, particularly under centrifugation, a necessary step to isolate them (Figure 4.3).

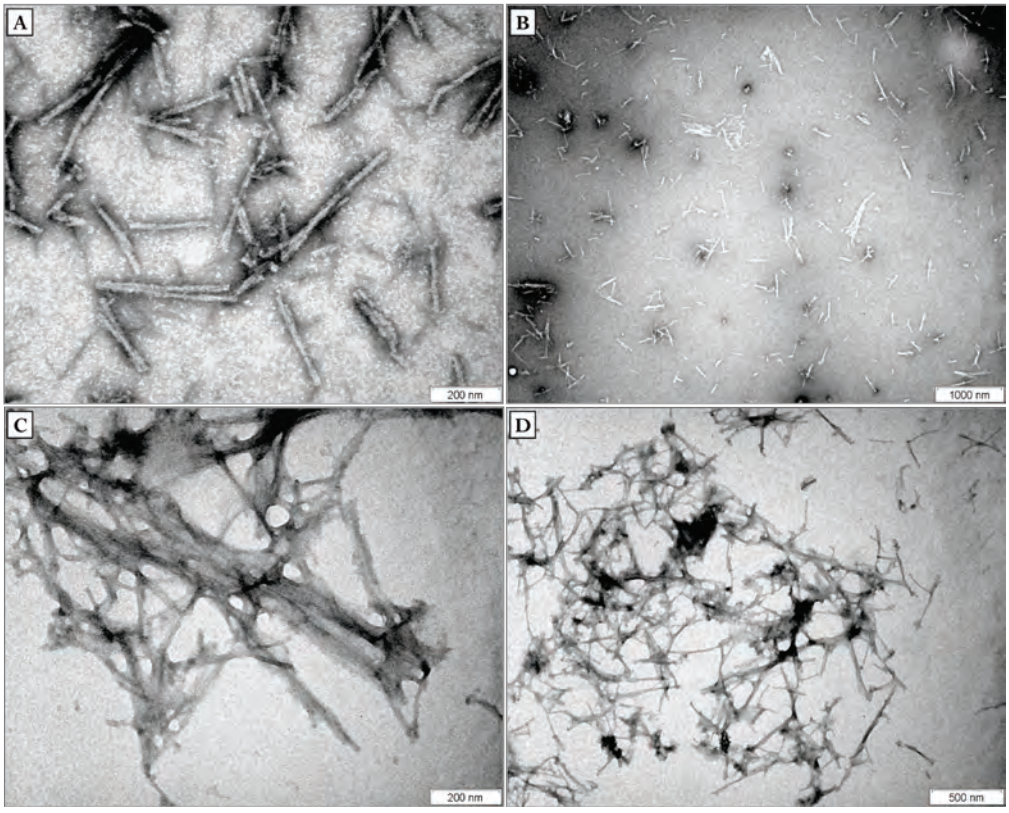

***Figure 4.3**. TEM images of GPI-anchorless PrP^{Sc} fibers. They were analyzed with the transmission electron microscope Philips CM-12 (University of Santiago de Compostela (USC), Galicia, Spain). **A-B.** Good preparations. They are clean and homogeneous. The scale bar is 200 nm and 1000 nm, respectively. **C-D.** Bad samples. Fibers are covered by lipids and junk. The scale bar is 200 nm and 1000 nm, respectively**. All samples were stained with uranyl acetate.*

All isolation methods described in the literature were not good enough for the EM surveys [9][10], because of the isolated protein was still having a lot of lipids covering the fibers. I found out a technique to achieve a complete degradation of lipids during the process of isolation of the GPI-less PrP^{Sc}. That step was to treat the sample with lipase; it is an enzyme that catalyzes the hydrolysis of lipids (see Chapter 2 - isolation of GPI-anchorless PrP^{Sc}). Then, ultra clean and homogeneous GPI-less PrP^{Sc} fibers are obtained for optimal analysis (Figure 4.3 A and B).

TEM is the best method to observe whether the fibers have achieved the quality required to be further analyzed by cryo-EM technique, because the preparation of the sample is very simple, the results are obtained very fast and the microscope is easy to use. Nevertheless, there is a disadvantage; the negative staining could cause possible distortions of the molecules resulting from the staining/drying procedure; this is why definitive measurements were not made, and the technique was just used as a quality control.

Anyway, I had the possibility to analyze the best samples by a more powerful transmission electron microscope at 200 kV but more complicated to use. It was possible to observe with clarity the fiber morphology and how they are intertwined. Sometimes can be seen two twisted fibers and the tendency to form lateral aggregates (Figure 4.4). Although TEM data are not definitive, some measurements were made; the intertwined fibers have 10 nm width, and each protofilament has a wide of 4-5 nm, in agreement with previous studies [9].

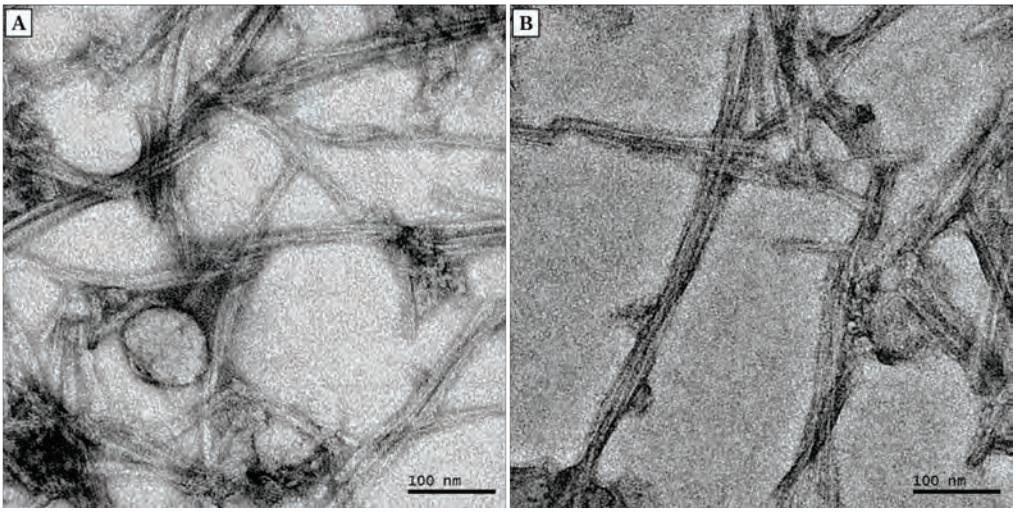

Figure 4.4**. TEM images of GPI-anchorless PrP^{Sc} fibers. They were analyzed with the transmission electron microscope LIBRA 200 FE OMEGA (University of Santiago de Compostela (USC), Galicia, Spain).* ***A-B. *Both are good preparation. The scale bar is 100 nm. All samples were stained with uranyl acetate.*

4.3 Cryo-transmission electron microscopy (Cryo-TEM)

Cryo-transmission electron microscopy (cryo-TEM) or electron cryomicroscopy is a kind of TEM where the sample is studied at cryogenic temperatures. Inside of an automated vitrification robot, a drop of the sample is pipetted onto a grid coated with a thin carbon film previously glow discharged; the grid is rapidly plunged into liquid ethane to form vitreous ice and then imaging the frozen film using an electron microscope. The specimen is maintained continuously below -170 °C during storage and also during imaging in the electron microscope to prevent the formation of ice crystals [11]. This technique produces many images of the same specimen in different orientations (Figure 4.5).

The cryo-TEM images of a protein molecule have much lower contrast than a negative stain and have a lot of noise. However for 3D reconstructions of macromolecules, vitrification of the unstained specimen is the method of choice, due to fact that this technique preserves the specimen virtually free of artefacts, so the morphology and chemistry of the observed sample bears a close resemblance to its *in vivo* state.

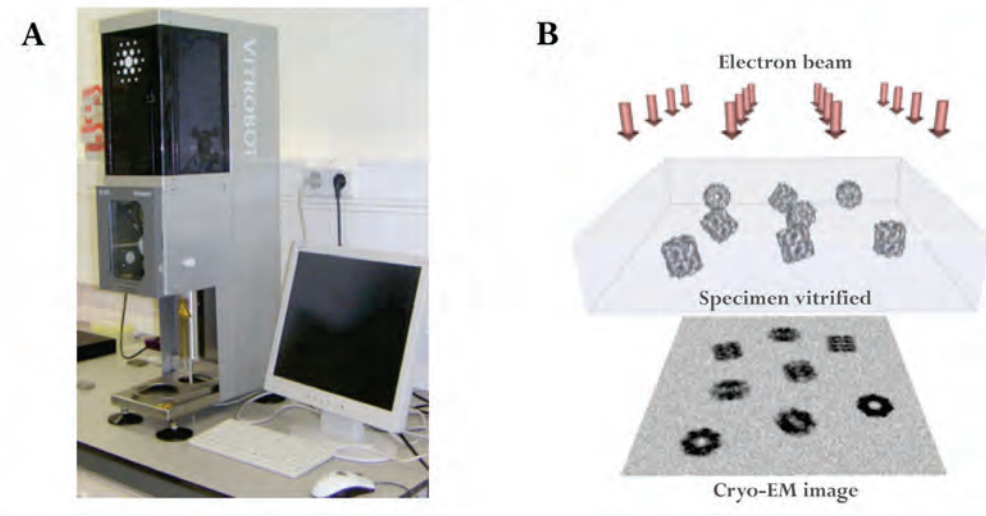

***Figure 4.5**. Cryo-transmission electron microscopy. **A.** Vitrification robot "Vitrobot™ Mark III" (FEI Co., Eindhoven, The Netherlands). **B.** Schematic representation of cryo-TEM imaging.*

4.3.1 Results of cryo-TEM

To continue the studies on the structure of the PrP^{Sc}, the best GPI-less PrP^{Sc} samples obtained in my laboratory were sent to the Dr. Matthijn Vos, from FEI Company, Eindhoven, The Netherlands. He analyzed the samples by cryo-transmission electron microscopy to find out more ultrastructural information of the scrapie prion protein in native conditions and with more

powerful microscopes. Note that with cryo-TEM, we will obtain images that allow us to use computational methods to develop an atomic model of the PrP^{Sc}.

After the meticulous preparation of the sample embedded in a thin layer of vitreous ice, it was loaded into a electron microscope and the GPI-less PrP^{Sc} fibers were analyzed using low electron dose, to avoid the radiation damage; the whole grid was screened for areas with suitable ice. The recorded low-magnification images showed clearly a high amount of prion fibers and the most important feature, that can be observed, is that the sample keeps clean and homogeneous (Figure 4.6). Then, the study can continue with confidence.

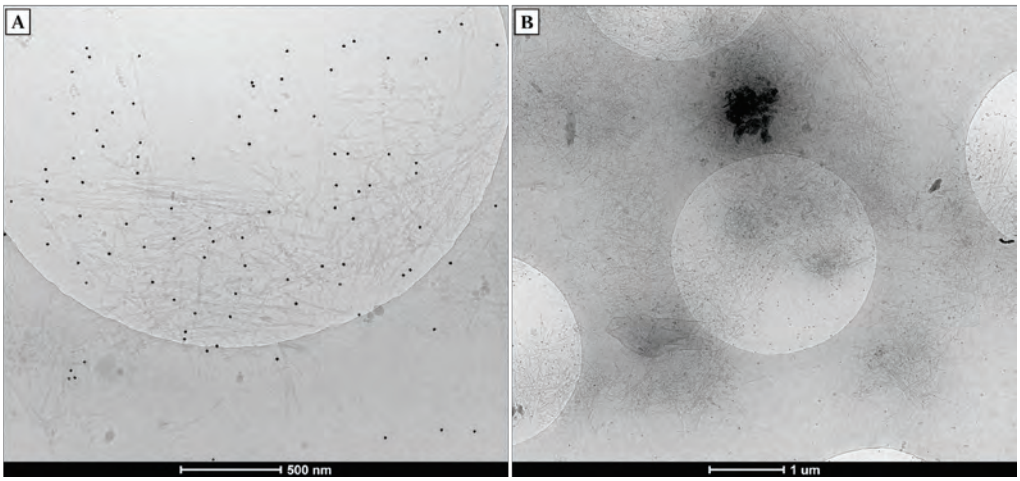

Figure 4.6. *Low magnification cryo-EM images of GPI-less PrP^{Sc} fibers. The sample was analyzed with the Titan Krios™ microscope and Falcon I direct electron detector (FEI Co., Eindhoven, The Netherlands).* ***A.*** *Scale bar is 500 nm.* ***B.*** *Scale bar is 1 µm. The visible dots are fiduciary gold that serves as references for later studies.*

In high-resolution cryo-TEM images of the GPI-less PrP^{Sc}, after closer examination was observed that the fibers are made up of two thinner protofilaments. Furthermore, their Fast Fourier Transform (FFT), automatically calculated along the length of a fiber, that can be used to determine repeating features in an image, showed a specific 4.8 Å reflection, which indicates a β-sheet stacking along the fiber direction (Figure 4.7).

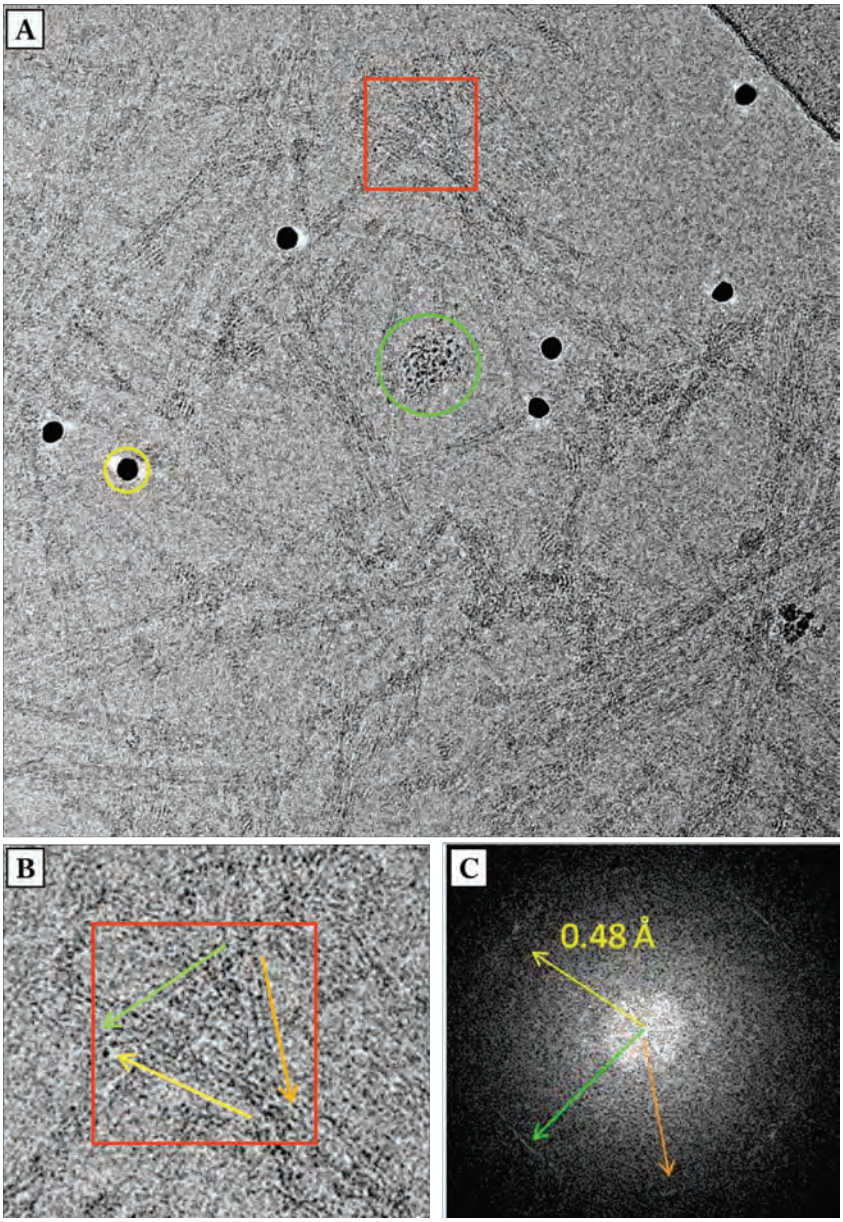

Figure 4.7. *High-resolution cryo-TEM images of GPI-less PrP^{Sc} fibers. The sample was analyzed with the Titan Krios™ TEM and Falcon II direct electron detector (FEI Co., Eindhoven, The Netherlands).* ***A.*** *Overview clearly showing the prion fibers. The yellow circle shows the fiducial gold that has been added for tomography studies. Green circle marks ferritin, which is always present in small quantities after isolation of the PrP^{Sc} from the brain.* ***B.*** *Enlargement of the indicated squared red area in A, showing the smaller fibers by three arrows.* ***C.*** *Fast Fourier Transform (FFT) of the indicated red area in B, showing the 0.48 nm hydrogen bond distance. Note that all three directions indicated with the yellow, green and orange arrow show strong signals in the FFT.*

As it has been explained above, the vitrified fibers have different orientations in the ice, and then we can observe many images of the same experimental object (fiber in this case) in different positions. In some lucky instances, we were able to locate fibers that were in an optimal focal plane throughout a sufficient distance; so as to generate images in which individual β-strands stacked along the fiber longitudinal axis were clearly seen (Figure 4.8). This is a remarkable result that has been reported before only in one instance for fibers formed by a short amyloid beta peptide [12].

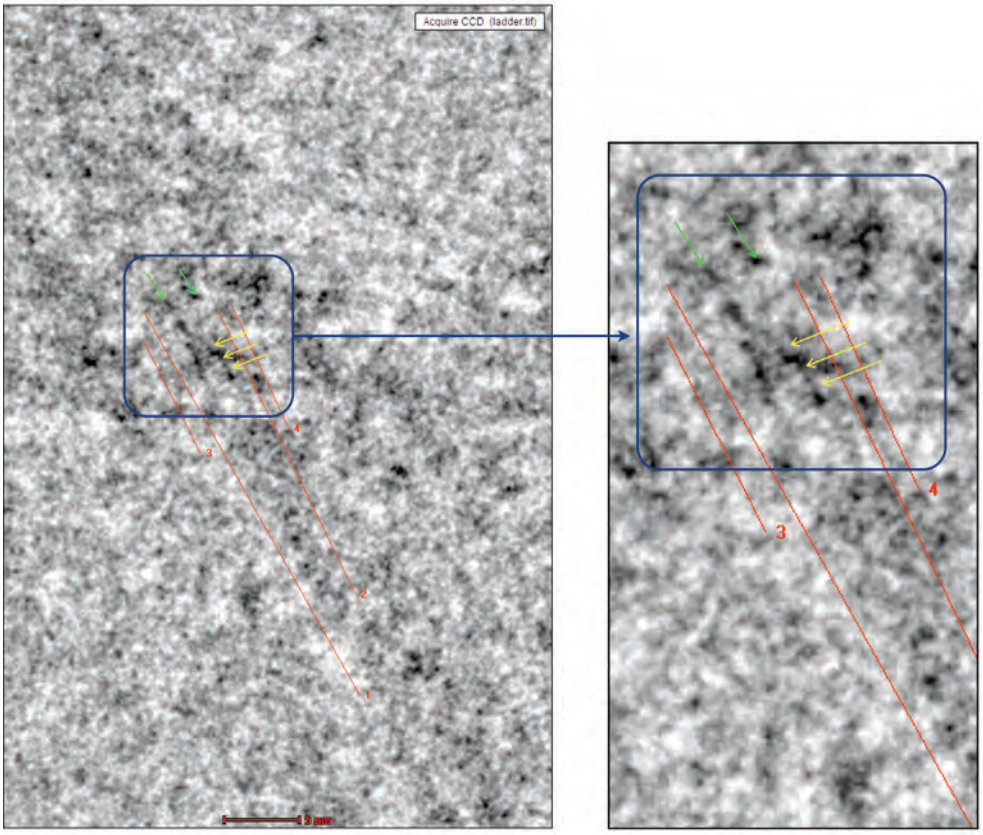

Figure 4.8. *High-resolution cryo-TEM images of GPI-less PrP^{Sc} fibers. The image was acquired with Titan Krios™ microscope and Falcon II direct electron detector (FEI Co., Eindhoven, The Netherlands). The green arrows show the beginning of two parallel protofilaments. The yellow arrows indicate the 0.5 nm periodicities within the fibers. The other red lines are just for reference to acquire the image. The scale bar is 5 nm.*

4.4 Cryo-TEM tomography (Cryo-ET)

Electron tomography (ET) is a technique for obtaining detailed 3D structures of unique objects from tilted 2D images. In this approach, with an electron microscope, a beam of electrons is passed through the sample and multiple images are recorded serially at different tilt angles of the

stage and they are computationally combined to generate a density map or tomogram of the imaged specimen. The recording of electron tomographic tilt series is fully automated. ET in combination with the preparation technique based on cryo-conditions (cryo-ET), that provides the best possible structural preservation of the sample, is a promising approach to find out comprehensively insights of the macromolecular architecture of complexes [13][14].

Nevertheless, there are some disadvantages that make difficult the interpretation of electron tomograms. First, the tomographic tilt series are collected from the same specimen area, and then the electron dose has to be very low to avoid radiation damage. This problem limits the resolution of the tomogram or it can exhibit a lot of noise. However, the noise can be reduced by denoising data processing algorithms. Second, the tilt range spans from ± 60-70 degrees, depending of the technical limitations of the electron microscope. This results in a 'missing wedge' of data reflecting the incomplete sampling of the full tilt range, so there are uncertainties about structural detail of the reconstructed density map. This last problem is solved by recording dual-tilt axis tilt series. Despite these problems, electron tomography has made stunning progress [14][15].

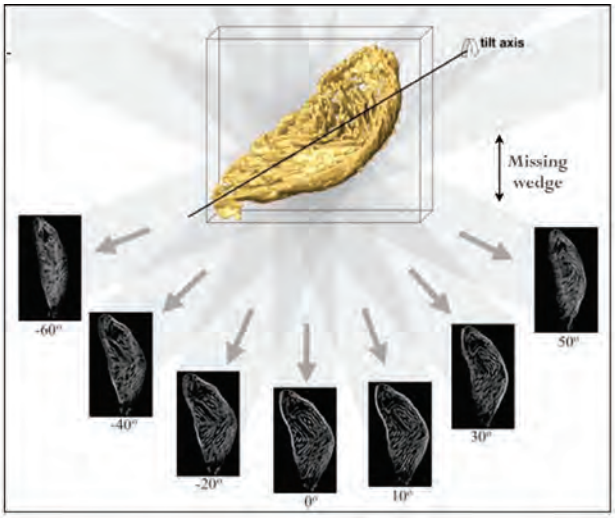

Figure 4.9. *Principle of tomography. Projections of the specimen were recorded from different directions by tilting the specimen holder. (Fernández J.J (2012) [14])*

4.4.1 Results of cryo-ET

Using the suitable samples of GPI-less PrP^{Sc} analyzed by cryo-TEM, at low-dose cryo-tomography, tilt series from -70º to +70º were recorded and subsequently reconstructed to a 3D volume. To facilitate alignment of the image stack before reconstruction of the cryo-electron tomograms, 15 nm fiducial gold particles were added into the sample to be used as electron dense markers, so they are used for further fine alignment of the images, also called image stack. Next, in order to obtain high resolution structures the contrast transfer function

must be corrected (CTF), it means that the aberrations caused by the lenses of the microscope and from the defocus used in imaging have to be corrected. Finally, the tomographic reconstruction was made by the weighted backprojection (WBP), this standard method consists in that the specimen mass is projected back into the volume to be reconstructed (Figure 4.9). This last process is repeated for all the projection images, therefore the 3D mass of the sample is reconstructed from a series of 2D projection images [14]. In our studies, all those steps were made by Dr. Matthijn Vos (from FEI Company, Eindhoven, The Netherlands).

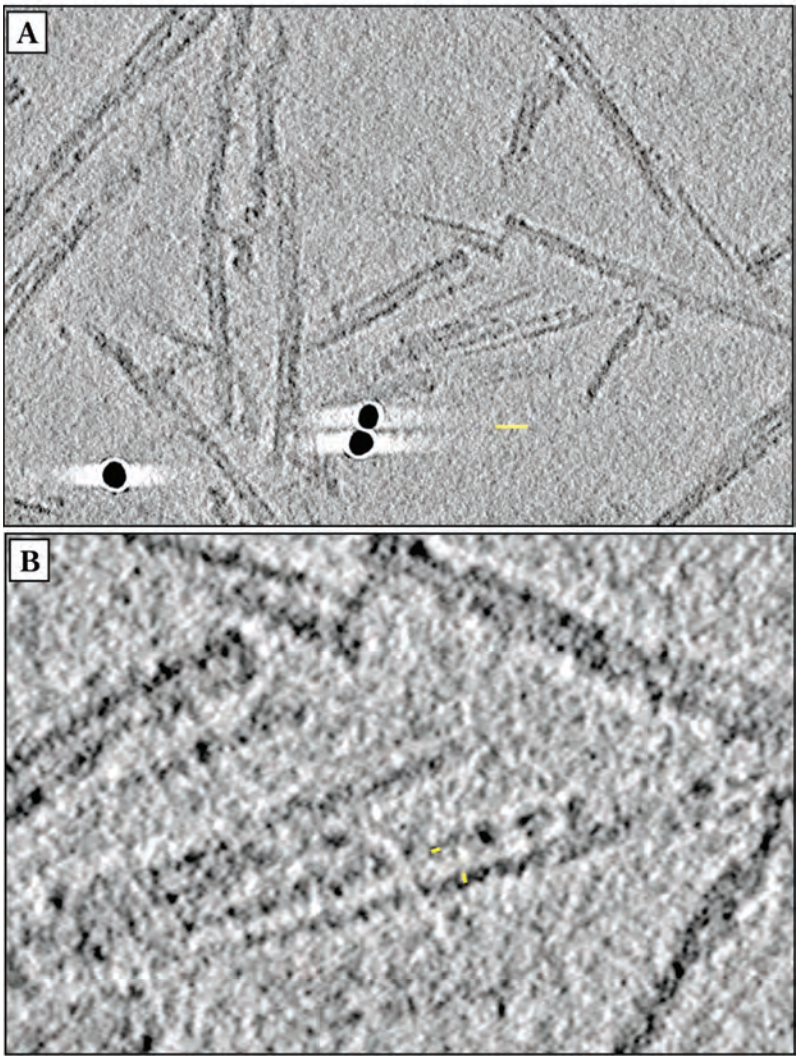

Figure 4.10. *Slices in the XY plane of a tomogram of GPI-less PrP^{Sc} fibers. The images were taken with Titan Krios™ microscope and Falcon I direct electron detector (FEI Co., Eindhoven, The Netherlands).* ***A.*** *The dark balls are fiducial gold with a size of 15 nm. The yellow line represents a 15 nm scale bar.* ***B.*** *High-magnification image. The yellow lines are showing the 2 nm axial densities into the fibers.*

3D reconstructions can be visualized by means of visualization software in the form of an .avi file, which shows different side views of the 3D volume as the point of view progresses along a given axis. Such file is attached or available upon request (ester.vazquez@usc.es). Instead, we have obtained XY slices of the total reconstructed 3D volume in which is possible to discern the molecular shape of the typical PrP^{Sc} fibers (Figure 4.10). These clearly show two intertwined protofilaments, as electrondense parallel tracks, each about 3 nm wide, separated by a lucent space. Furthermore high-magnification images show a repetition of discontinuous axial ~2 nm densities (Figure 4.10 B). These might be the individual stacked PrP^{Sc} subunits.

At the same time, different software applications are been used to generate a projected view of the surface of the 3D object (surface rendering). We have not produced such projections from the original tomogram; rather, they have been obtained after submitting the tomogram to the averaging technique known as "subtomogram averaging". These studies are in a very preliminary stage, and then still there are much work to do to reach definitive conclusions.

4.5 Helical reconstruction

Helical reconstruction is an image processing method that can be used for generating three-dimensional models of near-atomic resolution from data acquired by cryo-TEM. This method is used when the structure of interest forms a natural helix. Since the helix is a recurring structure with a very well defined pattern, the repeating pattern of the helix can be exploited to solve the structure. In this case, no alignment of the particles is needed, since the individual positions of subunits within the helix are clearly defined by the shape of the helix. The process of helical reconstruction is largely automated, but it is really complex [16][17]. The specimen is reconstructed in 3D from cryo-EM images, without the need for tomography, therefore the method avoids the missing wedge in Fourier space due the limitations on tilting. A right helical symmetry should give a stable converged reconstruction [16][17].

It is necessary to mention that PrP^{Sc} does not have a real helical symmetry. Then the process applied to our protein is slightly different to the generalized helical reconstruction used in samples with a regular symmetry.

To begin the three-dimensional reconstruction of the prion protein, the contrast of the cryo-EM image is inverted and low pass filtering is applied, obtaining an averaged projection image. The process continues with a particle segmentation of the “helical particle” in overlapping segments, using the graphical program Boxer (which is a program in the EMAN package). Boxer will automatically generate a series of particle boxes along the helix length; the boxed segments and their coordinates have to be saved. After, to create and refine the reconstruction, the SPIDER software has to be configured with all the constraints, such as the name and path of the stack, number of boxed images in the stack, dimensions, in-plane angles, etc., and the 3D reconstruction is generated using back projection. The 3D image can be observed and manipulated in the Chimera software.

4.5.1 Results of helical reconstruction

To carry out the helical reconstruction technique, cryo-EM micrographs were sent to the Dr. Howard S. Young, Dr. Ludovic Renault and Dr. Holger Wille, from the University of Alberta, Edmonton, Canada.

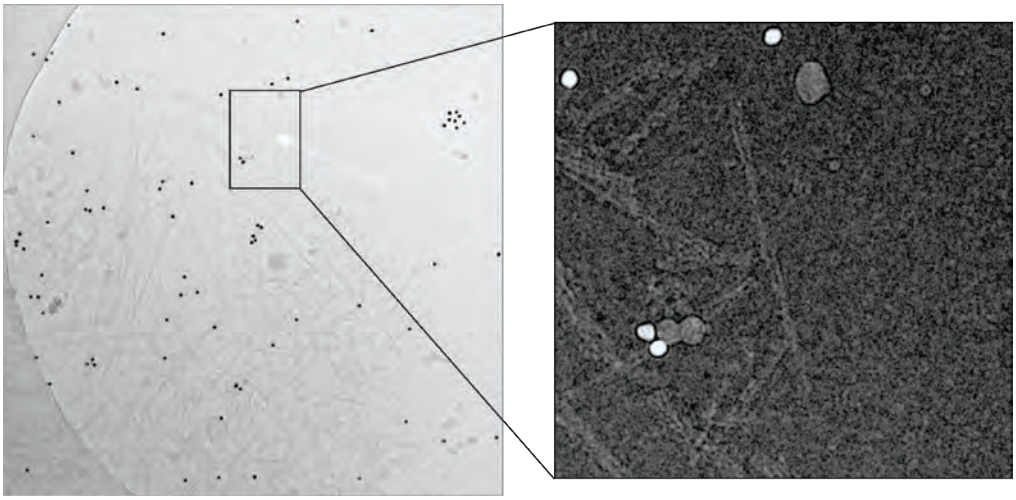

Figure 4.11. *Cryo-TEM image of GPI-less PrP^{Sc} fibers. In the left image, the white arrow pointed the fiber chosen for the helical reconstruction. The right image is a magnification of the same fiber with the contrast inverted.*

An initial 3D reconstruction of an individual fibril is presented. In the first steps of the procedure, a fibril was chosen to reconstruction and the contrast of the cryo-EM image is inverted (Figure 4.11).

The 3D volume is clearly made up by two protofilaments twisting around one another (Figure 4.12). It is possible to observe a finer rippling along the length of the protofilaments; this is a 24 Å (2.4 nm) repetition.

It is necessary to clarify that, as the subtomogram averaging, these helical reconstructions are preliminary results. We have to make the helical reconstruction of a lot of cryo-EM images of GPI-less PrP^{Sc} fibers, until to get the definitive 3D model of the PrP^{Sc}. Although, it is possible to disclose that these results are fitting with those obtained until now, by subtomogram averaging.

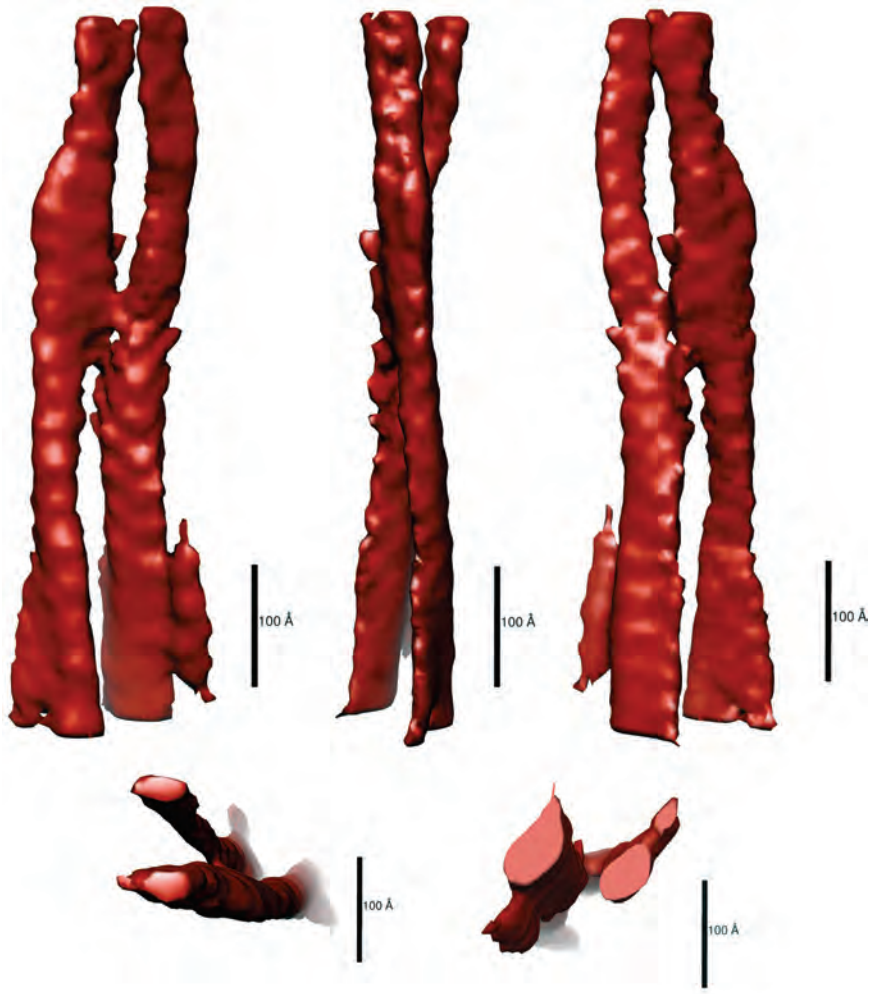

Figure 4.12. *3D reconstruction of a GPI-less PrP^{Sc} fiber. The red surface images are different views of the structure. The bottom images are the top (left) and the bottom (right) views. The scale bar is 100 Å.*

4.6 Conclusions

In this study, we used different electron microscopy techniques to acquire information on GPI-less PrP^{Sc} fibers global architecture, protofilament substructure and even location of the cross-β structure within fiber.

Our current interpretation, after thorough analysis of the results is that the basic fiber is made up of two intertwined protofilaments (Figures 4.10 and 4.12), each ~3-5 nm of wide. This range of width is due to the diameter of each protofilament is variable, as it can be see in the

helical reconstruction (Figure 4.12, bottom images). The shape is not circular, it is like a tear of about 2 nm at its narrowest and about 5 nm at its widest. There are repetitions of ~2 nm along the axis (Figures 4.10 B and 4.12), this could be interpreted that each density forms one monomer of PrP^{Sc}, so 2-2.5 nm axial densities might be individual stacked PrP^{Sc} subunits. Furthermore, it is possible to observe that there is no regular crossover distance. Cryo-TEM studies have provided a significant result, the presence of 4.8 Å reflection in FFT, indicating a β-sheet stack along the fiber direction (Figure 4.7); even due to the chance of two fibers were together in the same focal plane, we can see that these 0.5 nm repetitions are stacked like a "ladder" (Figure 4.8). However, no other reflections are observed indicating a head to tail uniform stacking of the basic units.

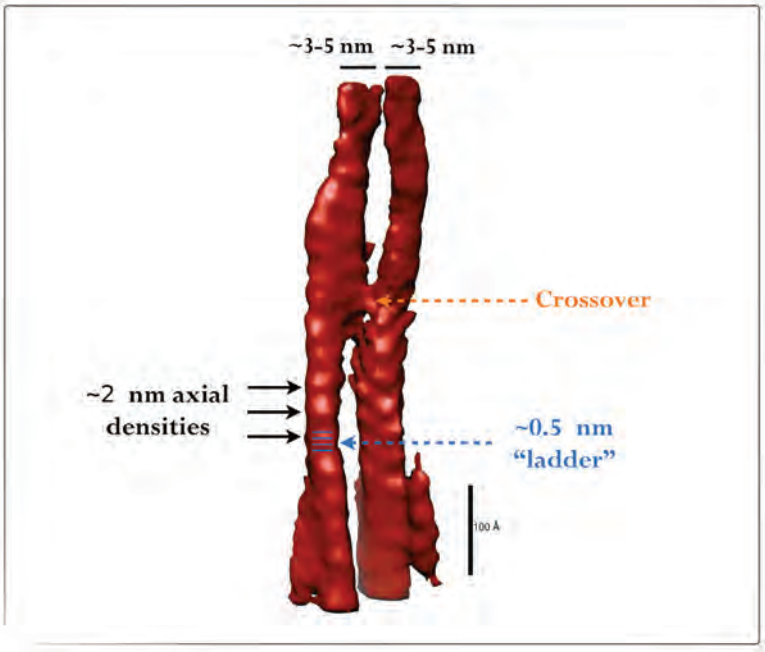

Figure 4.13. *Representation of all data together, in the 3D helical reconstruction of GPI-less PrP^{Sc} fiber. Scale bar 100 Å.*

The mammalian prion turns out to be very similar as HET-s prion protein from the filamentous fungus *Podospora anserina*, as both show densities along the backbone [18]. The HET-s densities are spaced ~1 nm apart while the PrP^{Sc} densities are a double length (2-2.5 nm). Moreover HET-s prion stacked monomers consist of solenoids featuring 2 rungs made up of β-strands. In turn, PrP^{Sc} has probably to be made up out of 4 rungs (see discussion in next chapter). Looking at the density profile the loop of the prion basic fiber is flatter in structure than the HET-s loop. The HET-s fiber is simple, while the PrP^{Sc} almost exclusively bundles 2 protofilaments. Just like HET-S the individual fiber is torqued in the form of a twisted ribbon. For the PrP^{Sc} structure two of these ribbons are intertwined.

4.7 Experimental

Isolation of GPI-anchorless PrP^{Sc} - GPI-anchorless PrP^{Sc} was isolated using a modified version of the method of Baron GS *et al*. [10]. During the purification, total PrP^{Sc} was treated with 10 µg/ml of proteinase K. The final pellet of purified PrP^{Sc} was resuspended in 100 µl of deionised water and was treated with lipase at 1 µg/ml and bovine serum albumin (BSA) to a final concentration of 10 mg/ml, 2 h at 37 °C. The sample was centrifuged (in the microfuge) at full-speed for 20 min and the pellet was resuspended in 100 µl of deionised water. The sample was centrifuged again as above to wash completely the BSA. Finally, the pellet was resuspended in 100 µl of deionised water and sonicated three pulses at amplitude of 50 % with a probe ultrasonic homogenizer (Cole Parmer Instrument CO., Chicago, IL, USA). The stock suspension thus prepared was stored at 4 °C. In some cases to avoid bacteria, 0.1 % sodium azide is added to the sample (for more information see Chapter 2).

Transmission electron microscopy - 10 µl of sample was applied to carbon-coated 400 mesh cupper (Ted Pella Inc., Redding, CA, USA), for 2 min. After, the grid with the sample was washed in two different drops of distilled water. Sample was then stained for 2 min with 2 % uranyl acetate (Electron Microscopy Science, Hatfield, PA, USA) and most of the liquid is removed from the drop by blotting with a piece of filter paper. Samples were viewed at 100 kV in a Philips CM-12 transmission electron microscope (FEI Co., Eindhoven, The Netherlands); digital images were taken with an MEGA VIEW-II DOCU camera system and were analyzed with the software SIS NT DOCU. In parallel, a selected number of samples were analyzed using LIBRA 200 FE OMEGA electron microscope (Carl Zeiss Inc.); the sample was view at 200 kV.

Cryo-transmission electron microscopy - Samples (3 µl) were mixed with a gold fiducial solution (15 nm gold particle size), for feature tracking during the reconstruction procedure and applied to glow-discharged Quantifoil grids (R2/2 Quantifoil Jena) within the Vitrobot™ Mark IV (FEI Company, Eindhoven, The Netherlands) where the environmental chamber was kept at relative humidity of 100 % and temperature of 22 °C. Excess liquid was blotted away with filter paper using an automatic blotting device within the Vitroblot and immediately the grids were plunge-frozen in liquid ethane. The grids were transferred to a Titan Krios™ transmission electron microscope equipped with Falcon direct electron detector (FEI Co., Eindhoven, The Netherlands), operating at 300 kV, under low-dose conditions (20 electrons per Å2) at liquid nitrogen temperatures.

Cryo-TEM tomography - The samples prepared in the above section were also used for low-dose cryo-TEM tomography. Tomograms of selected areas were obtained from -70 to +70 degrees with a 1.5 degree tilt increment. The Titan Krios™ microscope (FEI Co., Eindhoven, The Netherlands) operated at 300 kV, under low-dose conditions (50 electrons per Å2) at liquid nitrogen temperatures. The tilted images were aligned and reconstructed with the FEI inspect3D software (FEI Co., Eindhoven, The Netherlands).

Helical reconstruction - Dr. Howard S. Young, Dr. Ludovic Renault and Dr. Holger Wille, from the University of Alberta, Edmonton, Canada, carried out this technique. Results are still preliminary.

4.8 References

1. Merz PA, Somerville RA, Wisniewski HM, Iqbal K (1981) Abnormal fibrils from scrapie-infected brain. Acta Neuropathol. 54: 63–74.

2. Merz PA, Somerville RA, Wisniewski HM, Manuelidis L, Manuelidis EE (1983) Scrapie-associated fibrils in Creutzfeldt-Jakob disease. Nature 306: 474–476.

3. Prusiner SB, McKinley MP, Bowman KA, Bolton DC, Bendheim PE, et al. (1983) Scrapie prions aggregate to form amyloid-like birefringent rods. Cell 35: 349–358.

4. McKinley MP, Braunfeld MB, Bellinger CG, Prusiner SB (1986) Molecular characteristics of prion rods purified from scrapie-infected hamster brains. J. Infect. Dis. 154: 110–120.

5. Godsave SF, Wille H, Kujala P, Latawiec D, DeArmond SJ, et al. (2008) Cryo-immunogold electron microscopy for prions: toward identification of a conversion site. J. Neurosci. 28: 12489–12499.

6. Meyer RK, McKinley MP, Bowman KA, Braunfeld MB, Barry RA, et al. (1986) Separation and properties of cellular and scrapie prion proteins. Proc. Natl. Acad. Sci. U.S.A. 83: 2310–2314.

7. McKinley MP, Meyer RK, Kenaga L, Rahbar F, Cotter R, et al. (1991) Scrapie prion rod formation in vitro requires both detergent extraction and limited proteolysis. Journal of Virology 65: 1340–1351.

8. Chesebro B, Trifilo M, Race R, Meade-White K, Teng C, et al. (2005) Anchorless prion protein results in infectious amyloid disease without clinical scrapie. Science 308: 1435–1439.

9. Sim VL, Caughey B (2009) Ultrastructures and strain comparison of under-glycosylated scrapie prion fibrils. Neurobiol. Aging 30: 2031–2042.

10. Baron GS, Hughson AG, Raymond GJ, Offerdahl DK, Barton KA, et al. (2011) Effect of glycans and the glycophosphatidylinositol anchor on strain dependent conformations of scrapie prion protein: improved purifications and infrared spectra. Biochemistry 50: 4479–4490.

11. Wang L, Sigworth FJ (2006) Cryo-EM and single particles. Physiology (Bethesda) 21: 13–18.

12. Requena JR (2009) Structure of mammalian prions. Future Virology 4: 295–307.

13. Lučić V, Förster F, Baumeister W (2005) Structural studies by electron tomography: from cells to molecules. Annu. Rev. Biochem. 74: 833–865.

14. Fernandez J-J (2012) Computational methods for electron tomography. Micron 43: 1010–1030.

15. Baumeister W, Steven AC (2000) Macromolecular electron microscopy in the era of structural genomics. Trends Biochem. Sci. 25: 624–631.

16. Meng X, Zhao G, Zhang P (2011) Structure of HIV-1 capsid assemblies by cryo-electron microscopy and iterative helical real-space reconstruction. J Vis Exp.

17. Egelman EH (2007) The iterative helical real space reconstruction method: surmounting the problems posed by real polymers. Journal of Structural Biology 157: 83–94.

18. Mizuno N, Baxa U, Steven AC (2011) Structural dependence of HET-s amyloid fibril infectivity assessed by cryoelectron microscopy. Proc. Natl. Acad. Sci. U.S.A. 108: 3252–3257.

5

Discussion

Abstract

In this chapter, I have taken all the data obtained in this thesis to make a final common discussion. It is very interesting to analyze all results as a whole, and observe how each piece of the puzzle fits perfectly, in order to develop a new structural model of the PrP^{Sc}. I believe that the results presented in this thesis are an advance in the knowledge of prion protein. Our future perspectives are to refine the results obtained by the 3D reconstruction methods and attempt to get more data with other electron microscopy techniques, to generate a three-dimensional model with the highest possible resolution hitherto achieved.

Despite the difficulty to obtain substantial information on the structure of the PrP^{Sc}, in this thesis a large amount of experimental data were obtained, allowing the development of a new structural model.

GPI-anchorless PrP^{Sc} fibrils have a width of 3-5 nm ([1] and Chapter 4 of this thesis). During our electron microscopy studies we have observed ~2-2.5 nm densities along the fibril axis, showing each monomer of PrP^{Sc}. Also a 4.8 Å reflection was detected, indicating a cross-β along the fiber direction. These constraints mean that each PrP^{Sc} monomer must be coiled in such a way as to fit approximately 144 residues (~G_{89}-S_{232}) into this width while maintaining the observed high proportion of β-sheet secondary structure [2][3][4].

In order to do so, the PrP^{Sc} monomers must necessarily adopt a multilayer architecture. Such architecture is observed in SH3 fibers [5] or the HET-s fungal prion domain [6]. The HET-s prion domain packs 72 residues (218-289) into two windings of three β-strands each, alternating with turns and loops [6]. Wille *et al.* have concluded that PrP^{Sc} fibrils are composed of four rungs of β-strands, based on their interpretation of fiber X-ray diffraction patterns [7]. Accordingly, each rung of the GPI-anchorless PrP^{Sc} monomer would be comprised of ~36-37 residues.

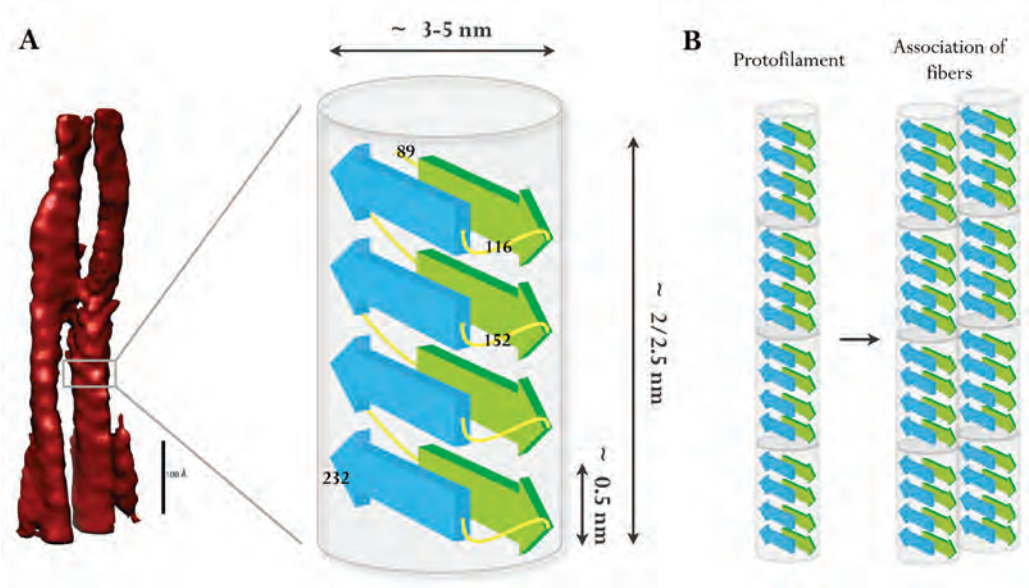

Figure discussion. *Cartoon of the structure of PrP^{Sc} (the shape and connection of the elements are arbitrary).* ***A.*** *Monomer of PrP^{Sc} is represented. Electron microscopy studies suggest that each monomer has a length of ~2-2.5 nm, and it is made up of four-rung separated ~0.5 nm, indicating a cross-β motif. Limited proteolysis reveals a number of cleavage sites, corresponding to loops connecting β-strands.* ***B.*** *Protofilament cores adopt a cross-β structure to form the fibers, stacking the monomers of PrP^{Sc}. Association between fibrils is the most common conformation of the fibers.*

The information emerging from limited proteolysis indicate that, positions N_{152}-M_{153} lie near the middle of the G_{85}-S_{232} sequence, and, therefore, it is tempting to speculate that they might be located at an exposed position at the border between rungs. This might explain why the N_{152}-S_{232} and/or M_{153}-S_{232} fragment emerges as the most conspicuous PK-resistant fragment after prolonged treatment with PK or partial unfolding with guanidine (Figures 3.9 and 3.10). Positions A_{116}-G_{118} might be the border between the two most amino-terminal rungs (approximately G_{85}-A_{115} and A_{119}-E_{151}). On the other hand, the results presented are partially inconsistent with the specific location assigned by Govaerts *et al.*, using threading algorithms, to residues K_{100}-P_{104} and E_{145}-R_{163}, placed in loops and not rungs [8]. Our experimental data suggest that the stretches formed by residues K_{100}-P_{104}, N_{142}-E_{151}, and Y_{154}-Y_{161}, are PK-resistant, *i.e.*, likely part of a β-strand rung that is stabilized by extensive H-bonding (Figure 3.6 and Table 3.I). However, due to the limitation of the techniques it is not possible to describe how many β-sheets are forming each rung. Still, the most likely it is that each rung is made up minimum of three β-sheets, but there could be more or even impossible to detect other cleavage points because of the conformation between rungs.

In summary, our data support a PrP^{Sc} structure consisting of a four-rung solenoid with a central β-strand-rich core; from which a series of highly PK-resistant β-sheet strands intersperse with PK-sensitive short flexible loops and turns. Furthermore, the region comprising ~V_{179} to the C-terminus of PrP^{Sc} is probably composed primarily of β-sheet, as it is highly resistant to PK. The data obtained from this GPI-anchorless PrP^{Sc} work is consistent with our previous results (263K and Dy strains) and those of other researchers using $SHaPrP^{Sc}$. Furthermore our results are consistent with those observed for human CJD PrP^{Sc}, which suggests that the myriad human, hamster and mouse prions share a common basic structure.

References

1. Sim VL, Caughey B (2009) Ultrastructures and strain comparison of under-glycosylated scrapie prion fibrils. Neurobiol. Aging 30: 2031–2042.

2. Caughey BW, Dong A, Bhat KS, Ernst D, Hayes SF, et al. (1991) Secondary structure analysis of the scrapie-associated protein PrP 27-30 in water by infrared spectroscopy. Biochemistry 30: 7672–7680.

3. Baron GS, Hughson AG, Raymond GJ, Offerdahl DK, Barton KA, et al. (2011) Effect of glycans and the glycophosphatidylinositol anchor on strain dependent conformations of scrapie prion protein: improved purifications and infrared spectra. Biochemistry 50: 4479–4490.

4. Smirnovas V, Baron GS, Offerdahl DK, Raymond GJ, Caughey B, et al. (2011) Structural organization of brain-derived mammalian prions examined by hydrogen-deuterium exchange. Nat. Struct. Mol. Biol. 18: 504–506.

5. Jiménez JL, Guijarro JI, Orlova E, Zurdo J, Dobson CM, et al. (1999) Cryo-electron microscopy structure of an SH3 amyloid fibril and model of the molecular packing. EMBO J. 18: 815–821.

6. Wasmer C, Lange A, Van Melckebeke H, Siemer AB, Riek R, et al. (2008) Amyloid fibrils of the HET-s(218-289) prion form a beta solenoid with a triangular hydrophobic core. Science 319: 1523–1526.

7. Wille H, Bian W, McDonald M, Kendall A, Colby DW, et al. (2009) Natural and synthetic prion structure from X-ray fiber diffraction. Proc. Natl. Acad. Sci. U.S.A. 106: 16990–16995.

8. Govaerts C, Wille H, Prusiner SB, Cohen FE (2004) Evidence for assembly of prions with left-handed beta-helices into trimers. Proc. Natl. Acad. Sci. U.S.A. 101: 8342–8347.

6

Appendices

Abstract

In this last chapter, four appendices are included with the aim of better understanding of this thesis. The first appendix is the explanation about the inconsistency between the sequence described of the GPI-anchorless tg mice in the original article (Chesebro B. et al. (2005)) and the description of this sequence in my studies. In the second appendix the ESI-TOF spectra of the two exact mass peaks detected and later used as internal standards, and the MALDI-TOF spectra obtained during the calibration process with insulin, ribonuclease A and lysozyme are shown. The appendix 3 summarizes the main abbreviations used in this document. The fourth appendix is a compilation of the publications and participation in conferences, during the period of my thesis.

APPENDIX I

Explanation of the GPI-anchorless tg mice sequence (23-232)

GPI-anchorless PrP transgenic mice were generated by Chesebro *et al*. (Chesebro B, Trifilo M, Race R, Meade-White K, Teng C, *et al*. (2005) Anchorless prion protein results in infectious amyloid disease without clinical scrapie. *Science* 308: 1435-1439). After a thorough explanation of how they constructed the transgenic mice, in the supplementary material, removing the GPI signal sequence; it is described that this PrP lacks the GPI anchor, but has the same amino acids (23-231) as wild-type PrP after removal of the signal peptide (SP) and the C-terminal signal sequences.

However, in the course of my mass spectrometry studies, an incoherence was detected. I have come to conclude that the sequence of PrP^{Sc} in these animals ends as: R_{229}-S-S-S_{232}. This seems to be inconsistent with the description of the PrP provided in the original Science paper of Bruce Chesebro.

It was critical to solve the dilemma, inasmuch as it is relevant to the conclusions of my studies. But since there are some uncertainties regarding the numbering of mouse vs. hamster or human PrP sequences, I may have misinterpreted that description. Then, I decided to ask directly Bruce Chesebro. Very kindly, he has replied (e-mail communication) that: "I have reviewed the details of the generation of our anchorless PrP construct. In fact, I think our description of this clone was in error as described in the supplement to our 2005 Science paper. The oligo used to make this mutation should have encoded R-S-S-S-stop at the PrP C-terminus (DNA=....AGA TCC AGC AGC TGA....). We did originally sequence the DNA of the original subclone where this oligo was inserted into PrP and confirmed this DNA sequence. It is confusing because Serine in encoded by two very different codons here, TCC and AGC. In summary, the stop codon is in place of residue 233, not 232 as we reported in 2005, and your protein data would appear to be correct"

Everyone who is knowledgeable or has read the article of Bruce Chesebro, could have appreciated this inconsistency in my thesis; then it is the reason and the explanation why I described that GPI-anchorless PrP transgenic mice express a PrP^{Sc} with a 23-232 amino acid sequence.

APPENDIX II

Calibration of the GPI-anchorless PrP^{Sc} MALDI-TOF spectrum

Nano-LC-ESI-Qq-TOF MS

Dr. Christopher J. Silva and Dr. Irina Dynin, from Western Regional Research Center, USDA, carried out this experiment. The spectra of the two peaks identified by ESI-TOF are showed. As it is explained in the chapter 3, these obtained peaks with exact MWs: 17148 and 16371 were used to calibrate the entire spectrum of the GPI-anchorless PrP^{Sc}. The experimental procedure is explained in chapter 3.

PEAK of 17148 Da

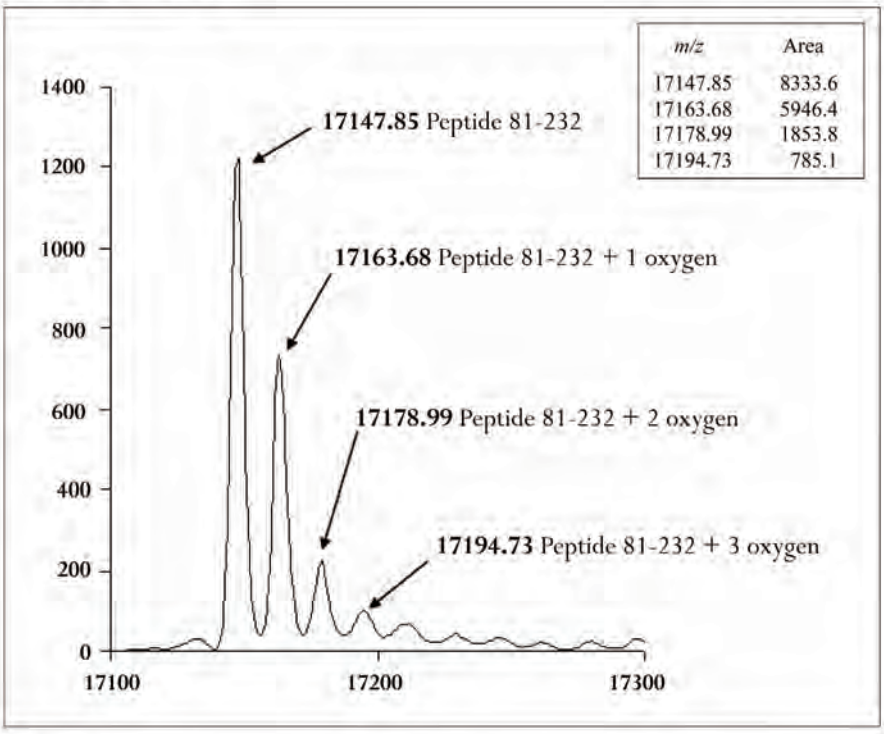

Peptide 81-232:
GQPHGGGWGQGGGTHNQWNKPSKPKTNLKHVAGAAAAGAVVGGLGGYMLGSAMSR
PMIHFGNDWEDRYYRENMYRYPNQVYYRPVDQYSNQNNFVHDCVNITIKQHTVTTTT
KGENFTETDVKMMERVVEQMCVTQYQKESQAYYDGRRS

Predicted molecular weight: 17147.91 Da
Difference between predicted and observed: 0.1 Da

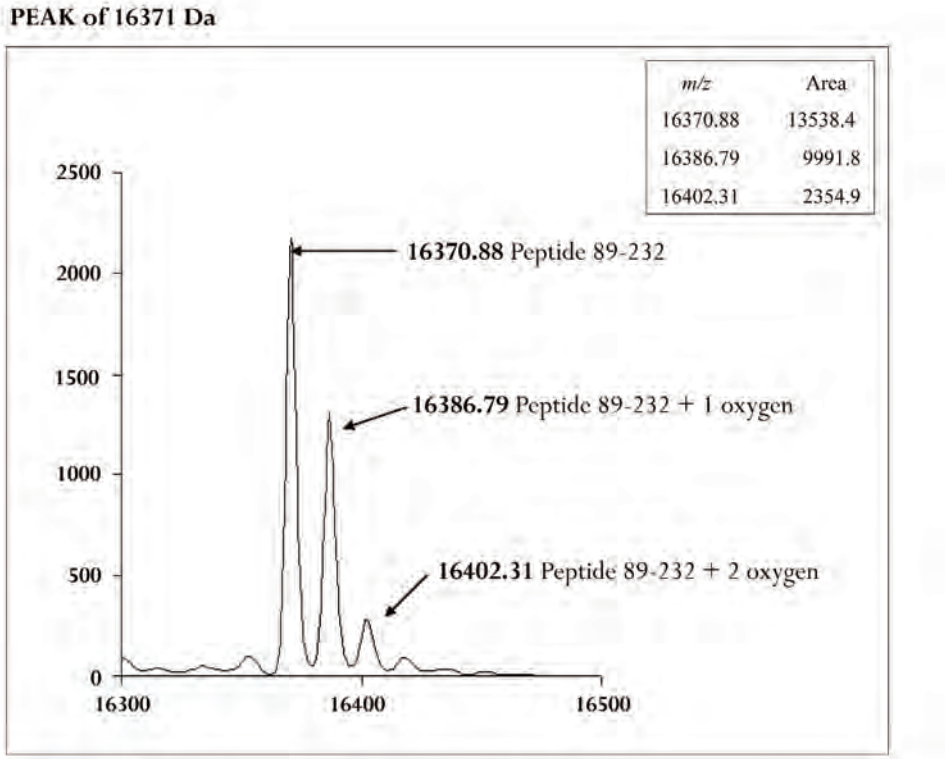

Peptide 89-232:
GQGGGTHNQWNKPSKPKTNLKHVAGAAAAGAVVGGLGGYMLGSAMSRPMIHFGNDW
EDRYYRENMYRYPNQVYYRPVDQYSNQNNFVHDCVNITIKQHTVTTTTKGENFTETDV
KMMERVVEQMCVTQYQKESQAYYDGRRS

Predicted molecular weight: 16371.11 Da
Difference between predicted and observed: 0.2 Da

MALDI-TOF

Dr. Jana Alonso, from Proteomics Unit, IDIS, Santiago de Compostela (Spain) has accomplished this experiment. The different spectra obtained during the iterative calibration process of the GPI-less PrP^{Sc} are reported. The signals of the internal standards overlapped the sample peaks, then, the known peaks of the GPI-less PrP^{Sc} (those obtained by ESI-TOF: 17148 and 16371 Da) and together with each of the different standards (insulin (m/z = 5733), ribonuclease A (m/z = 13682) and lysozyme (m/z = 14305)) were taken as reference to adjust the rest of peaks. It was possible to calibrate the 9573 Da peak. The experimental procedure is explained in chapter 3.

- **Spectrum of GPI-less PrP^{Sc} + insulin + ribonuclease A +lysozyme**

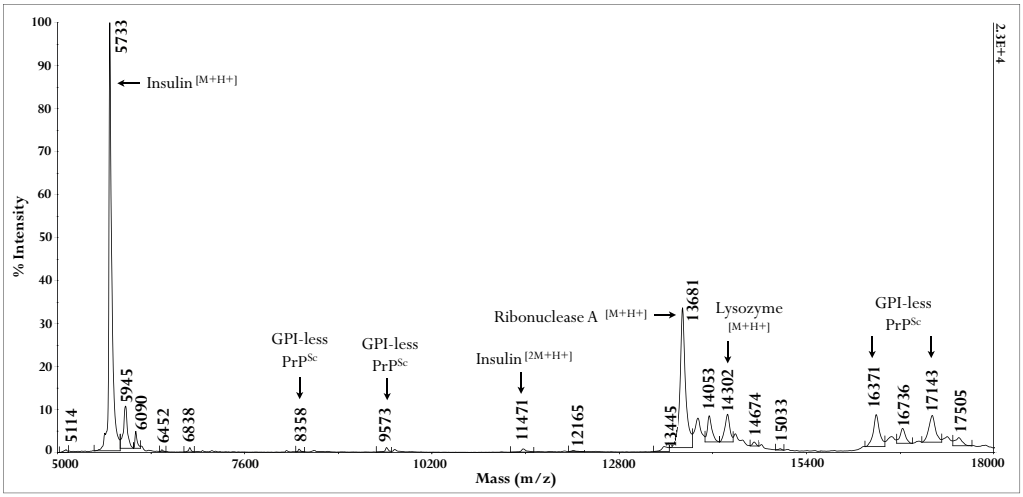

- **Spectrum of GPI-less PrP^{Sc} + insulin**

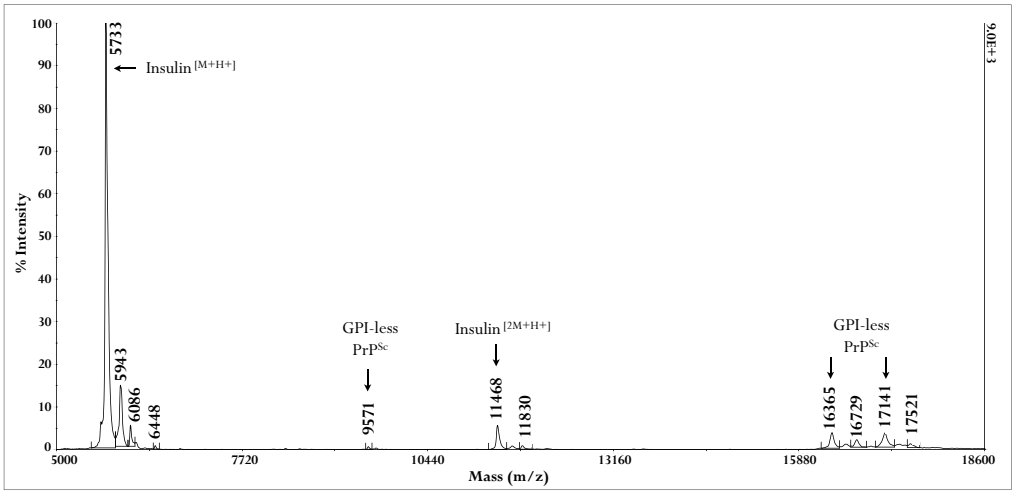

- **Spectrum of GPI-less PrP^{Sc} + ribonuclease A**

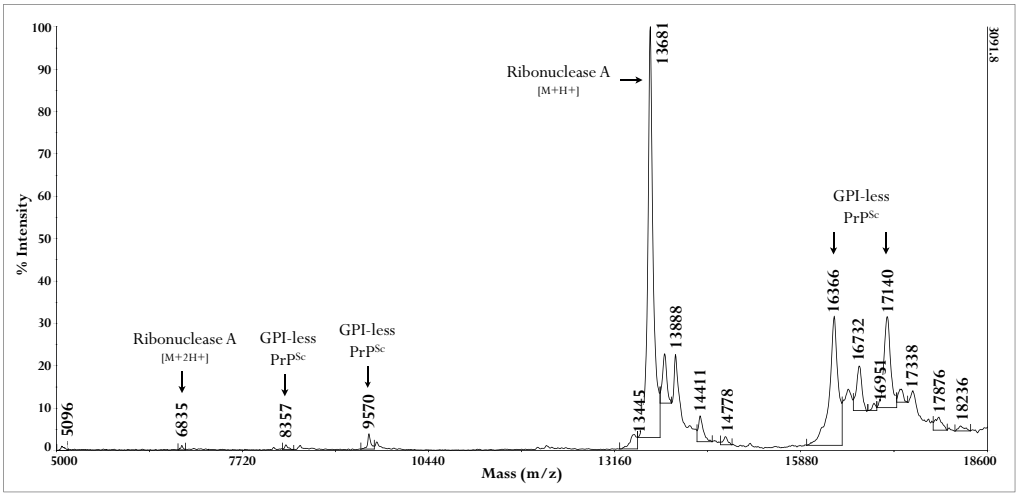

- **Spectrum of GPI-less PrP^{Sc} + lysozyme**

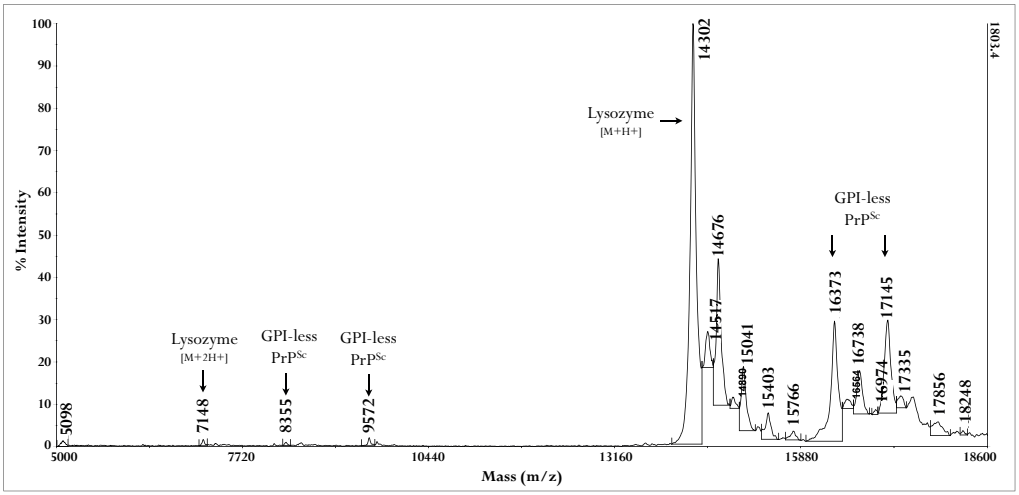

APPENDIX III

List of abbreviations

- 2D: two-dimensional.
- 3D: three-dimensional.
- Ab: antibody.
- ACN: acetonitrile.
- Ac_2O: acetic anhydride.
- AFM: atomic force microscopy.
- BS^3: bis(sulfosuccinimidyl) suberate.
- BSA: bovine serum albumin.
- BSE: bovine spongiform encephalopathy.
- CFT: contrast transfer function.
- CJD: Creutzfeldt-Jakob disease.
- vCJD: variant CJD.
- Cryo-TEM: cryo-transmission electron microscopy or electron cryomicroscopy.
- Cryo-ET: cryo-electron tomography.
- CWD: chronic wasting disease.
- Dy: drowsy strain.
- EDTA: ethylenediaminetetraacetic acid.
- EM: electron microscopy.
- ET: electron tomography.
- FFI: fatal familial insomnia.
- FFT: fast fourier transform.
- FSE: feline spongiform encephalopathy.
- FTIR: fourier transform infrared spectroscopy.
- GndHCl: guanidine hydrochloride.
- GPI: glycosylphosphatidylinositol.
- GPI-less: GPI-anchorless.
- GSS: Gerstmann-Sträussler syndrome.
- HE: haematoxylin and eosin.
- HGH: human growth hormone.
- H/D: hydrogen-deuterium exchange.
- IHC: immunohistochemical.
- IR: infrared spectroscopy.
- KO: knock out.
- MALDI-TOF: matrix-assisted laser desorption/ionization-time of flight.
- MBM: meat and bone meal.
- MeOH: methanol.
- MS: mass spectrometry.
- MW: molecular weight.
- nano-LC-ESI-Qq-TOF: electrospray ionization-double quadrupole-time of flight.

- NMR: nuclear magnetic resonance.
- NTCB: 2-nitro-5-thiocyanatobenzoic acid.
- PBS: phosphate buffered saline.
- PCR: polymerase chain reaction.
- PK: proteinase K.
- PMCA: protein misfolding cyclic amplification.
- PNGase F: peptide-N-glycosidase F.
- Prnp: prion protein gene.
- PrP: prion protein.
- bPrP: bovine prion protein.
- hPrP: human prion protein.
- MoPrP: mouse prion protein.
- PrP^{C}: cellular prion protein.
- PrP^{Sc}: scrapie prion protein.
- $PrP^{Sc}106$: miniprion.
- recPrP: recombinant prion protein.
- $sPrP^{Sc}$: protease-sensitive prion protein.
- PrP27-30 or PrPres: protease-resistant prion protein.
- RML: strain of mouse. Rocky Mountain laboratory.
- SA: sinapinic acid.
- SAFs: scrapie associated fibrils.
- SHaPrP: hamster prion protein.
- SDS-PAGE: sodium dodecyl sulfate-polyacrylamide gel electrophoresis.
- SP: signal peptide.
- TEM: transmission electron microscopy.
- TFA: trifluoroacetic acid.
- tg: transgenic.
- tg44+/-: transgenic heterozygous GPI-anchorless PrP mice.
- tg44 -/-: transgenic homozygous GPI-anchorless PrP mice.
- TME: transmissible mink encephalopathy.
- TNM: tetranitromethane.
- TSE: transmissible spongiform encephalopathy.
- WB: Western blot.
- WBP: weighted backprojection.
- Wt: wild-type.

APPENDIX IV

List of publications/Participation in conferences

Articles submitted

Vázquez-Fernández E, Alonso J, Pastrana MA, Ramos A, Stitz L, Vidal E, Dynin I, Petsch B, Silva CJ and Requena JR. ***Structural organization of mammalian prions as probed by limited proteolysis***. Under revision, PLoS One (2012).

Articles published

Sajnani G, Silva CJ, Ramos A, Pastrana MA, Onisko BC, Erickson ML, Antaki EM, Dynin I, Vázquez-Fernández E, Sigurdson CJ, Carter JM, Requena JR. ***PK-sensitive PrP is infectious and shares basic structural features with PK-resistant PrP***. PLoS Pathog. 2012;8(3):e1002547.

Gong B, Ramos A, Vázquez-Fernández E, Silva CJ, Alonso J, Liu Z, Requena JR. ***Probing structural differences between PrP(C) and PrP(Sc) by surface nitration and acetylation: evidence of conformational change in the C-terminus***. Biochemistry. 2011 Jun 7; 50(22):4963-72.

Studies selected for oral presentation

Fernández-Borges N, Vázquez-Fernández E, Rodríguez-Elezgarai S, Parra B, Alonso J, Di Bari MA, Sánchez-Martín M, Eraña H, Harrathi C, Gayosso M, Vidal E, Pumarola M, Agrimi U, Mayoral T, Nonno R, Andreoletti O, Requena JR and Castilla J. ***Highly infectious recombinant prions - A new challenge for understanding how prions work***. International Conference "Prion 2012", Amsterdam, The Netherlands.

Vázquez-Fernández E, Ramos A, Alonso J & Requena JR. ***Probing the structure of GPI-less PrP^{Sc} by limited proteolysis***. II National Prion Conference (2011), Madrid, Spain.

Fernández-Borges N, Parra B, Rodríguez-Elezgarai S, Vidal E, Sánchez-Martín M, de Castro J, Vázquez-Fernández E, Pumarola M, Requena JR, Mayoral T and Castilla J. ***Lessons from nature: prion resistant species and their mechanisms***. II National Prion Conference (2011), Madrid, Spain.

Sajnani G, Pastrana MA, Ramos A, Dynin I, Vázquez-Fernández E, Onisko B, Requena JR. ***Limited proteolysis of PK-sensitive PrP^{Sc} further supports a structure featuring beta sheet stretches interspersed with loops/turns for PrP^{Sc}***. International Conference "Prion 2008", Madrid, Spain.

Poster communications

Vázquez-Fernández E, Alonso J, Pastrana MA, Ramos A, Stitz L, Vidal E, Dynin I, Silva CJ and Requena JR. ***Probing the structure of GPI-anchorless PrP^{Sc} by limited proteolysis***. International Conference "Prion 2012", Amsterdam, The Netherlands.

Harrathi C, Eraña H, Rodríguez-Elezgarai S, Vázquez-Fernández E, Fernández-Borges N, Requena JR and Castilla J. ***Landing in a new recombinant prion world***. II National Prion Conference (2011), Madrid, Spain

Fernández-Borges N, Vázquez-Fernández E, Rodríguez-Elezgarai S, Gong B, Parra B, Alonso J, Requena JR and Castilla J. ***In vitro prion transmission studies. A switch to a recombinant PrP^{Sc} world***. International Conference "Prion 2011", Montreal, Canada.

Vázquez-Fernández E, Sajnani G, Ramos A and Requena JR. ***Further characterization of flexible regions of PrP^{Sc} by limited proteolysis***. I National Prion Conference (2010), Bilbao, Spain.

Vázquez-Fernández E, Sajnani G, Ramos A and Requena JR. ***Further characterization of flexible regions of PrP^{Sc} by limited proteolysis***. International Conference "Prion 2010", Salzburg, Austria.